Microsegregation in Manganese Steels

by

Altan Türkeli

Thesis submitted in fulfilment of the degree of
Doctor of Philosophy at the Department of Metallurgy
of the University of Sheffield

August 1989

FIGURES

Figure 1

Columnar and equiaxed solidification of a pure substance (7)

Figure 2

Constitutional undercooling in alloys (7)

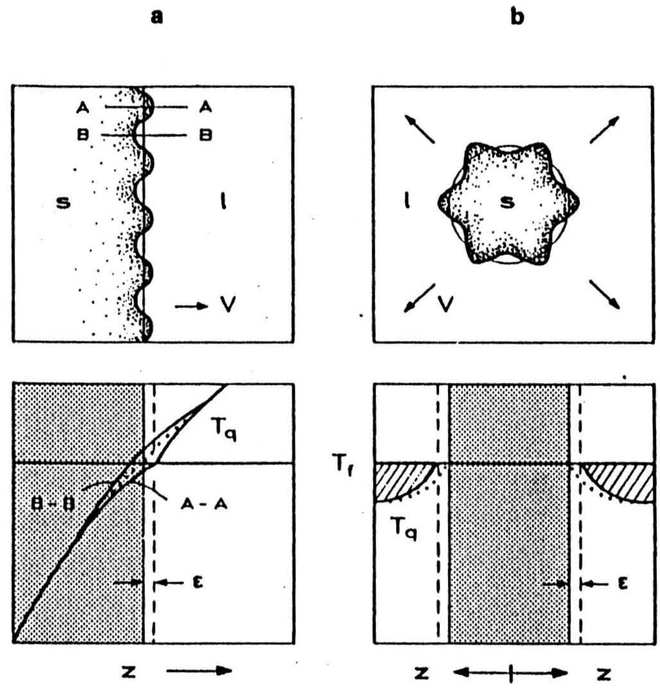
a
b
A
A
B
B
s
l
V
l
s
V
T_f
T_q
B - B
A - A
ε
z
T_f
T_q
ε
z
z

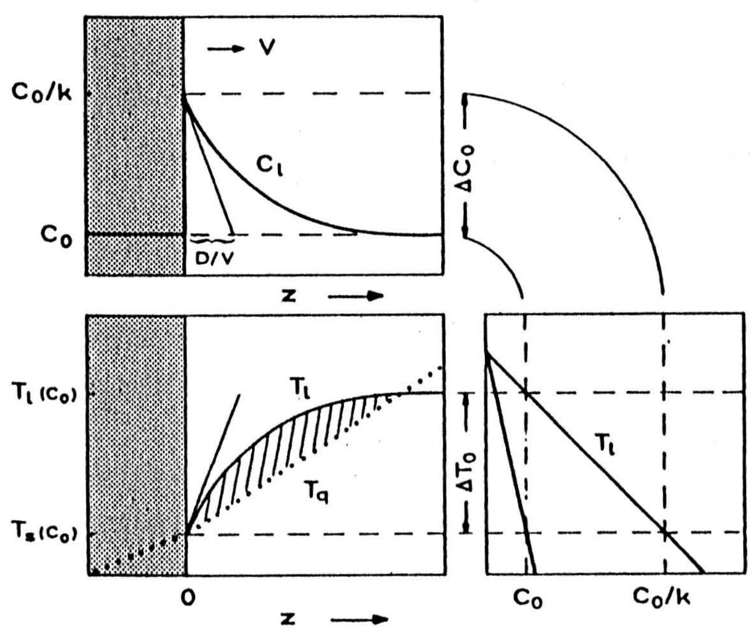
C_0/k
V
C_l
C_0
D/V
z
ΔC_0
T_l (C_0)
T_l
T_q
T_s (C_0)
0
z
ΔT_0
T_l
C_0
C_0/k

Figure 3

Results of Nash and Glicksman for dendrite tip radius and growth velocity (solid circle), related to graphs of V and r from Ivantsov, modified Ivantsov and Temkin (18)

Figure 4

Dependence of tip radius (R) and primary arm spacing (λ_1) on the dendrite growth velocity (V). (7)

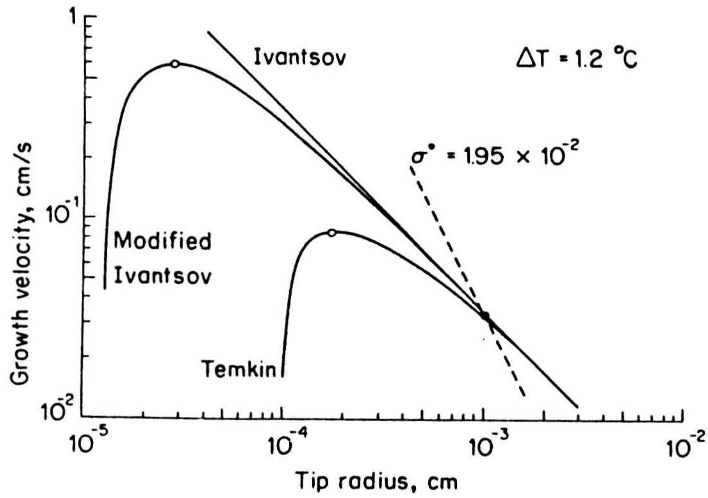

Ivantsov
ΔT = 1.2 °C
σ* = 1.95 × 10⁻²
Modified Ivantsov
Temkin
Growth velocity, cm/s
Tip radius, cm
1
10⁻¹
10⁻²
10⁻⁵
10⁻⁴
10⁻³
10⁻²

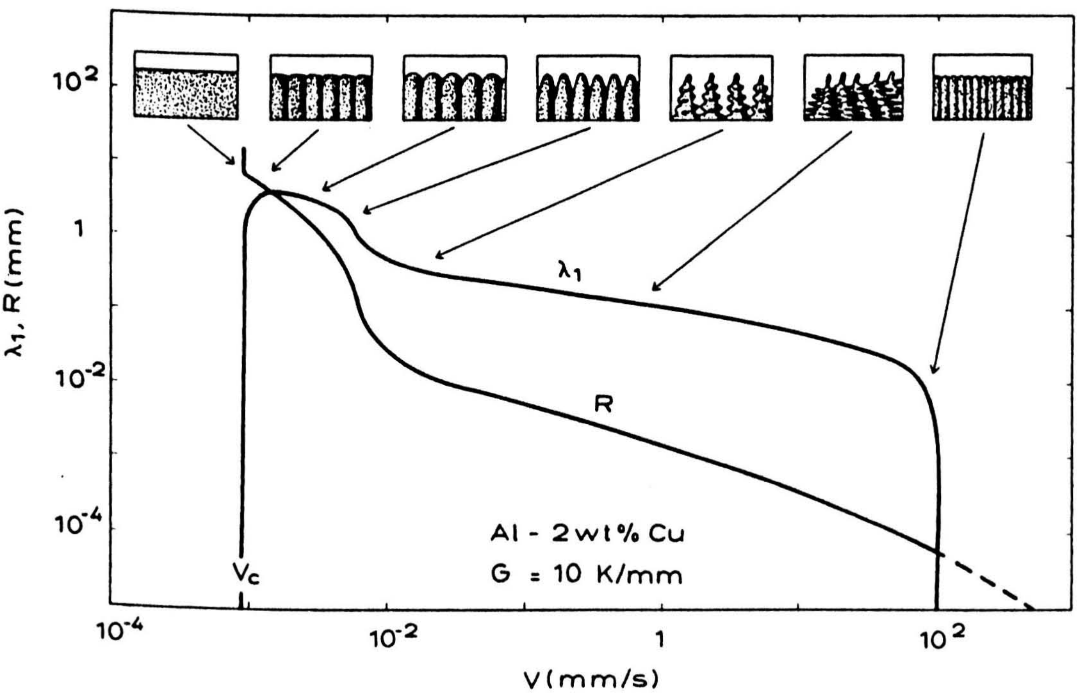

λ₁
R
Al - 2wt% Cu
G = 10 K/mm
Vc
λ₁, R(mm)
V(mm/s)
10²
1
10⁻²
10⁻⁴
10⁻⁴
10⁻²
1
10²

Figure 5

Comparison of the Kurz-Fisher and Hunt theories of primary spacing with the experimental data in succinonitrile- 5.5 mol pct. acetone system. Temperature gradient = 67 K/cm (30)

Figure 6

A quantitative comparison of the thermal gradient dependence of the primary arm spacings with the theoretical predictions for the directionally solidified alloys. (50)

a) Pb- 8 pct Au, V = 10 mm/sec

b) Pb- 3 pct Pd, V = 1.2 mm/sec

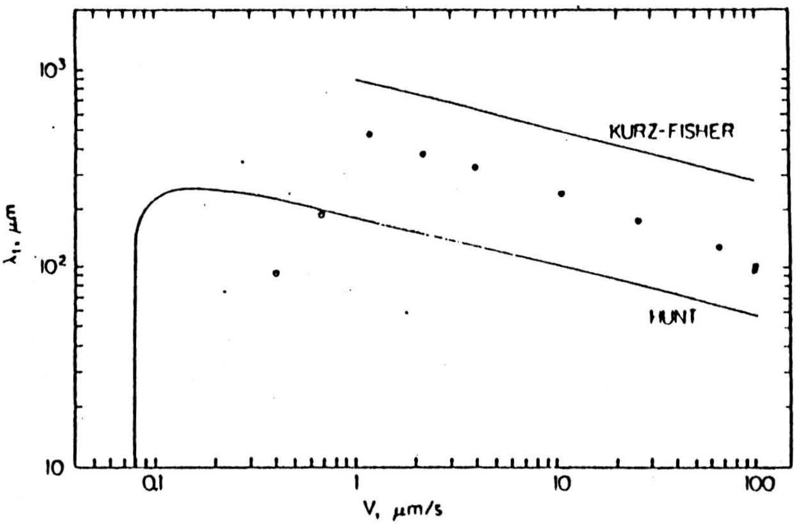

KURZ-FISHER
HUNT
λ₁, μm
V, μm/s

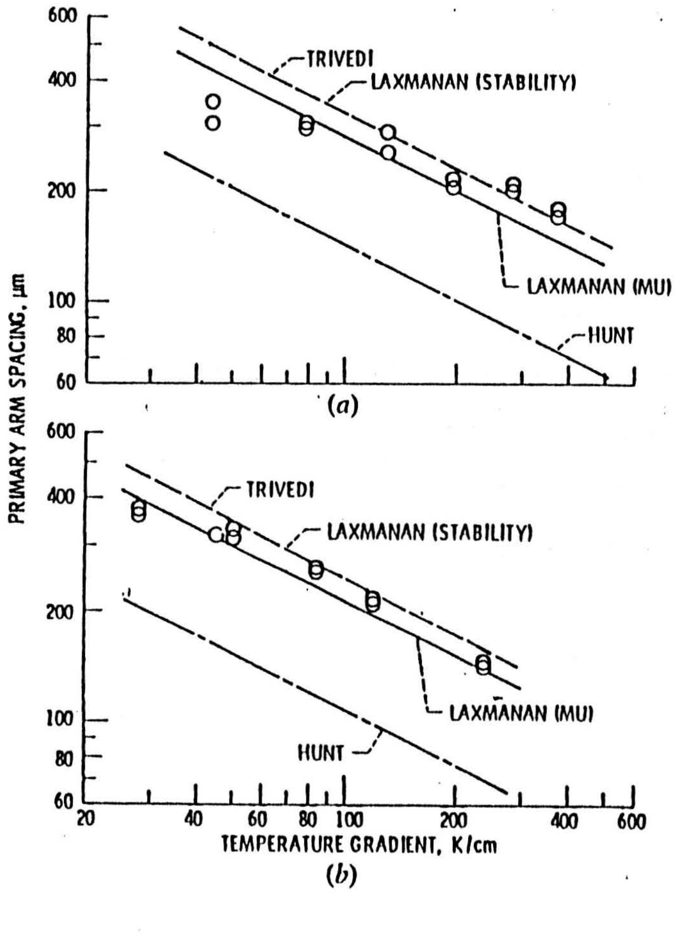

TRIVEDI
LAXMANAN (STABILITY)
LAXMANAN (MU)
HUNT
PRIMARY ARM SPACING, μm
TEMPERATURE GRADIENT, K/cm

(a)

(b)

Figure 7

Secondary dendrite arm spacings as a function of cooling rate in commercial steels containing from 0.1 to 0.9 % C (54)

Figure 8

Secondary dendrite arm coarsening mechanisms (ripening) (51)

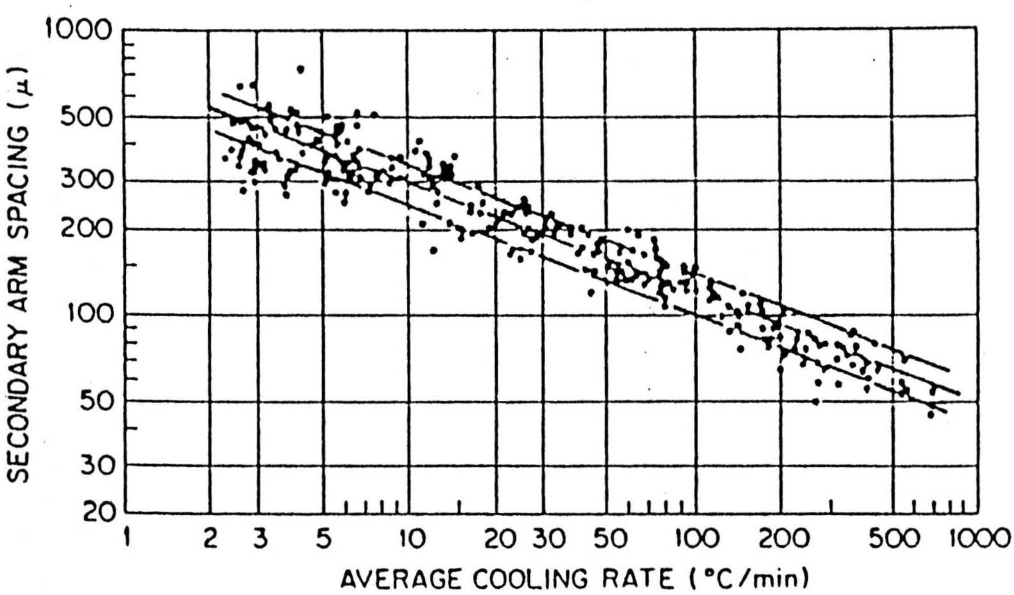

SECONDARY ARM SPACING (μ)
1000
500
300
200
100
50
30
20
1
2
3
5
10
20
30
50
100
200
500
1000
AVERAGE COOLING RATE (°C/min)

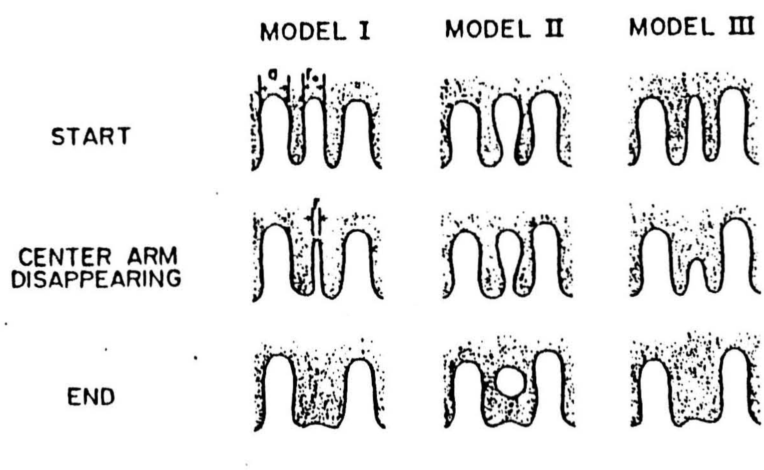

MODEL I
MODEL II
MODEL III
START
CENTER ARM DISAPPEARING
END

Figure 9

Schematic diagram showing the coalescence model (42)

λ_2 is the secondary dendrite arm spacing

r_A is the radius of curvature of the root of the interdendritic region

r_B is the radius of curvature of the dendrite tip

l is the length of a dendrite

Figure 10

Comparison between experimental secondary dendrite arm spacings and theoritical predictions in Al- 4.5 pct % Cu alloy as a function of time during solidification for different cooling rate.(60)

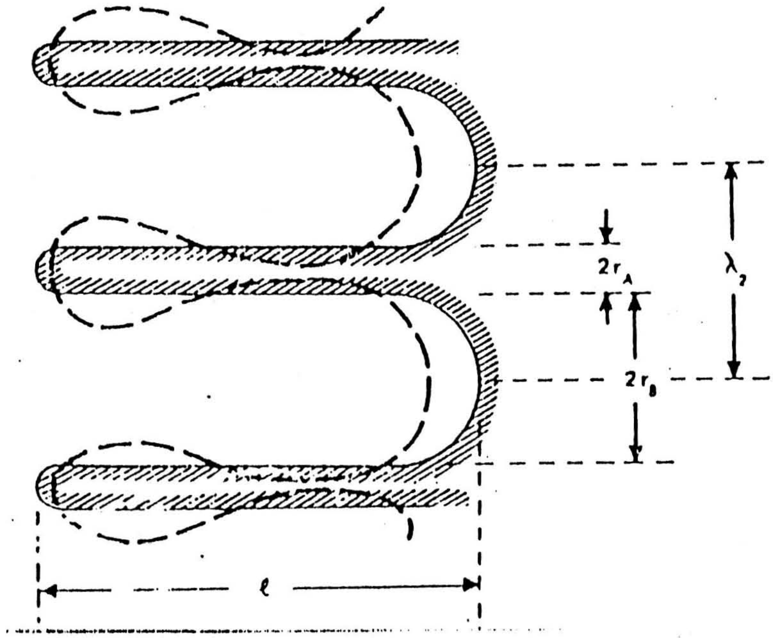

$2r_A$
λ_2
$2r_B$
ℓ

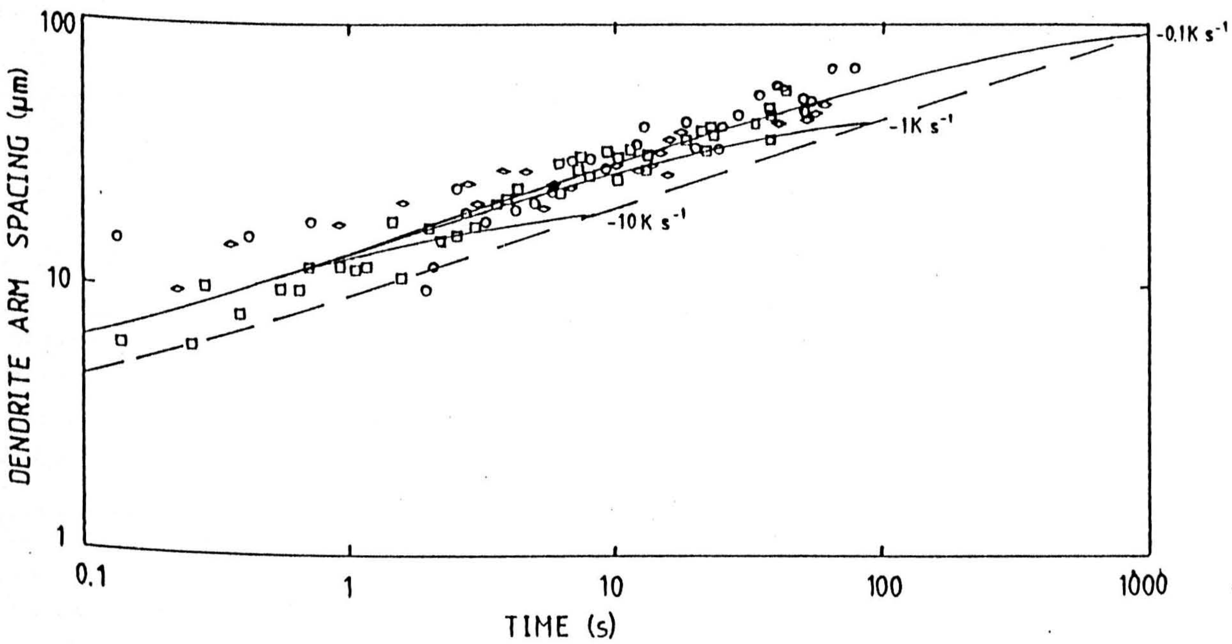

DENDRITE ARM SPACING (μm)
TIME (s)
100
10
1
0.1
1
10
100
1000
-0.1K s⁻¹
-1K s⁻¹
-10K s⁻¹

Figure 11

Mechanism of temperature gradient zone melting (TGZM) (65)

Figure 12

Model of interdendritic solidification showing solute distribution in the liquid, a , when TGZM is dominant, b , when solidification is dominant (65)

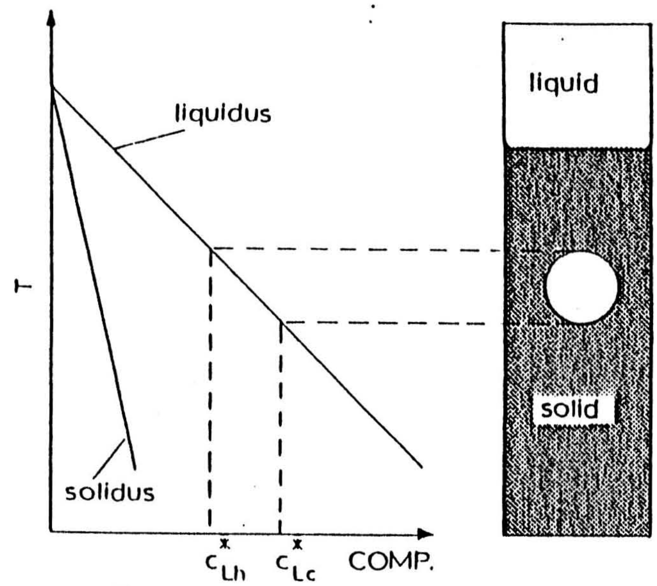

T
liquidus
solidus
c^*_{Lh}
c^*_{Lc}
COMP.
liquid
solid

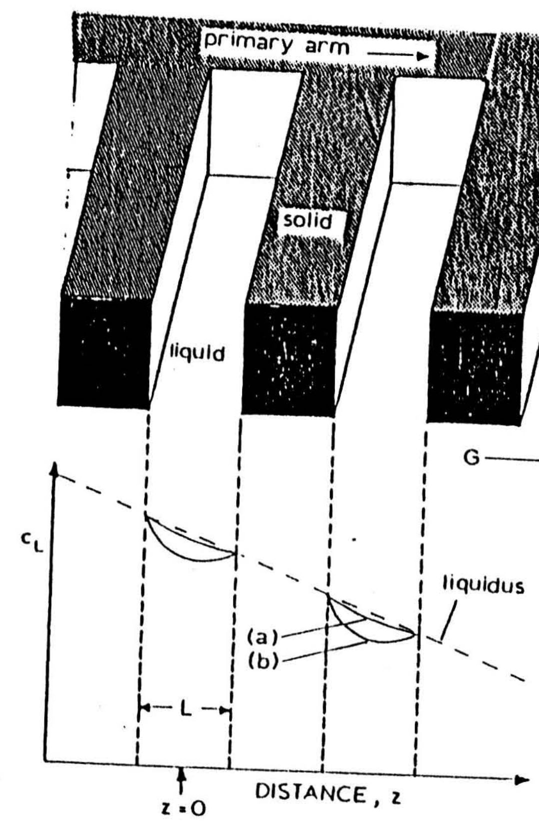

primary arm
solid
liquid
G
c_L
liquidus
(a)
(b)
L
z = 0
DISTANCE, z

Figure 13

Coefficients of equilibrium partition of solute elements between austenite and liquid iron in Fe-C-Si and Fe-C-Mn ternary alloys(a) and in Fe-C-Si-Mn quarternary alloys(b); C concentration of liquid is for Fe-C binary system (81)

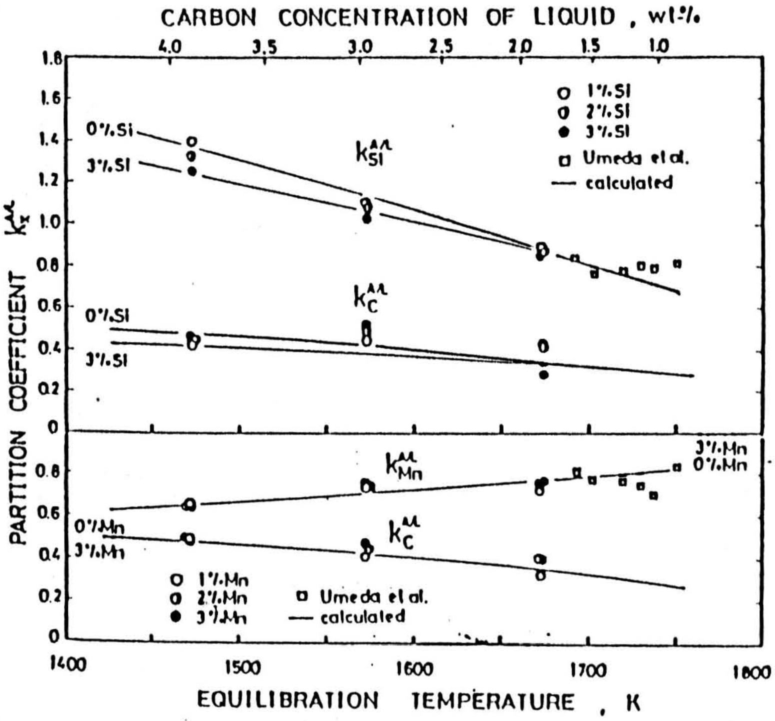

CARBON CONCENTRATION OF LIQUID , wt%
PARTITION COEFFICIENT
EQUILIBRATION TEMPERATURE , K
1% Si
2% Si
3% Si
Umeda et al.
calculated
1% Mn
2% Mn
3% Mn

(a)

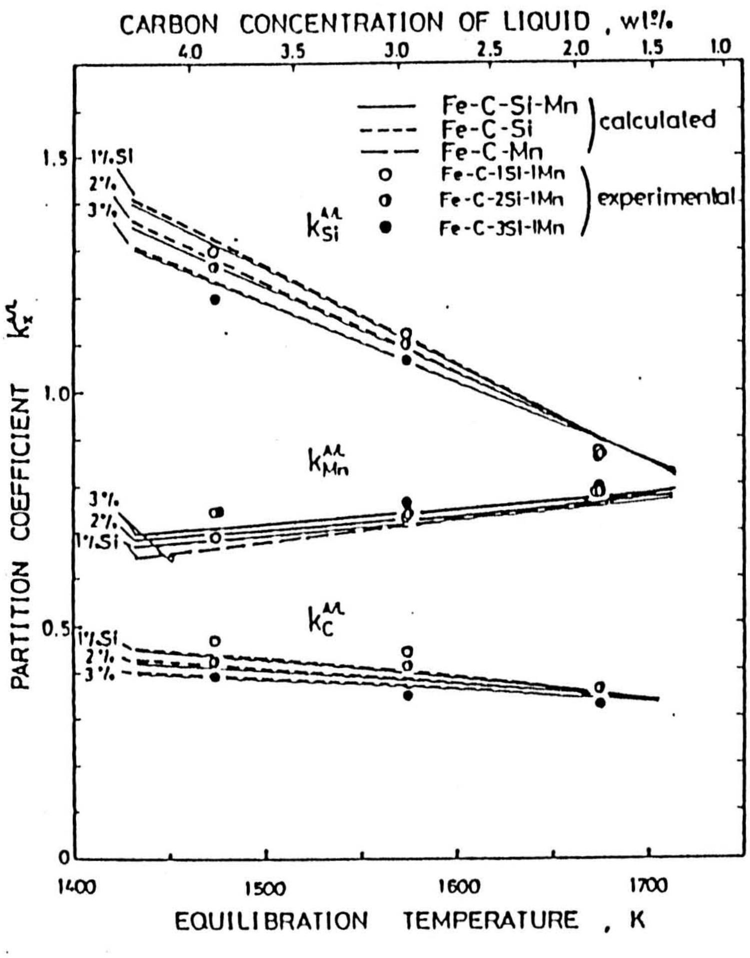

CARBON CONCENTRATION OF LIQUID , wt%
PARTITION COEFFICIENT
EQUILIBRATION TEMPERATURE , K
Fe-C-Si-Mn
Fe-C-Si
Fe-C-Mn
calculated
Fe-C-1Si-1Mn
Fe-C-2Si-1Mn
Fe-C-3Si-1Mn
experimental

(b)

Figure 14

The iron-carbon equilibrium diagram (170)

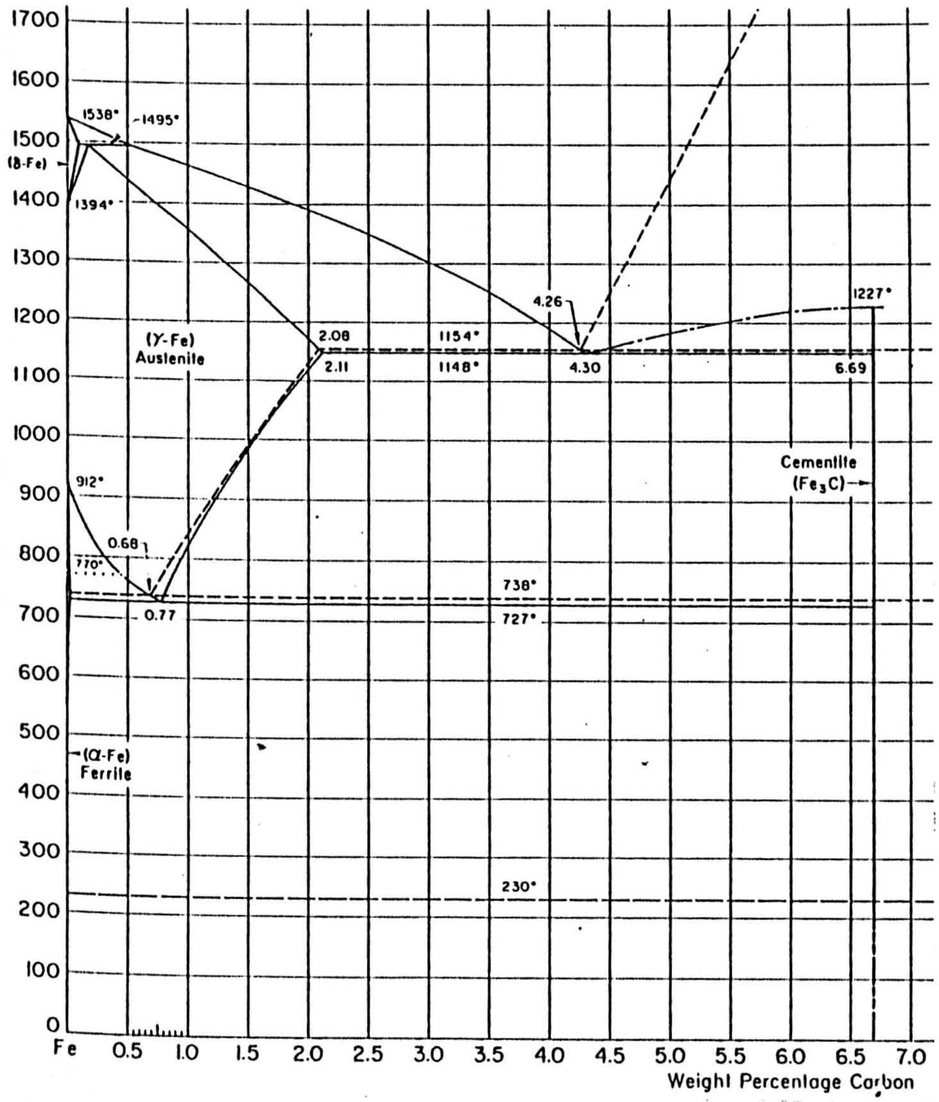
1700
1600
1500
1400
1300
1200
1100
1000
900
800
700
600
500
400
300
200
100
0
1538°
1495°
(δ-Fe)
1394°
(γ-Fe)
Austenite
4.26
1227°
2.08
1154°
2.11
1148°
4.30
6.69
Cementite
(Fe₃C)
912°
0.68
770°
738°
0.77
727°
(α-Fe)
Ferrite
230°
Fe
0.5
1.0
1.5
2.0
2.5
3.0
3.5
4.0
4.5
5.0
5.5
6.0
6.5
7.0
Weight Percentage Carbon

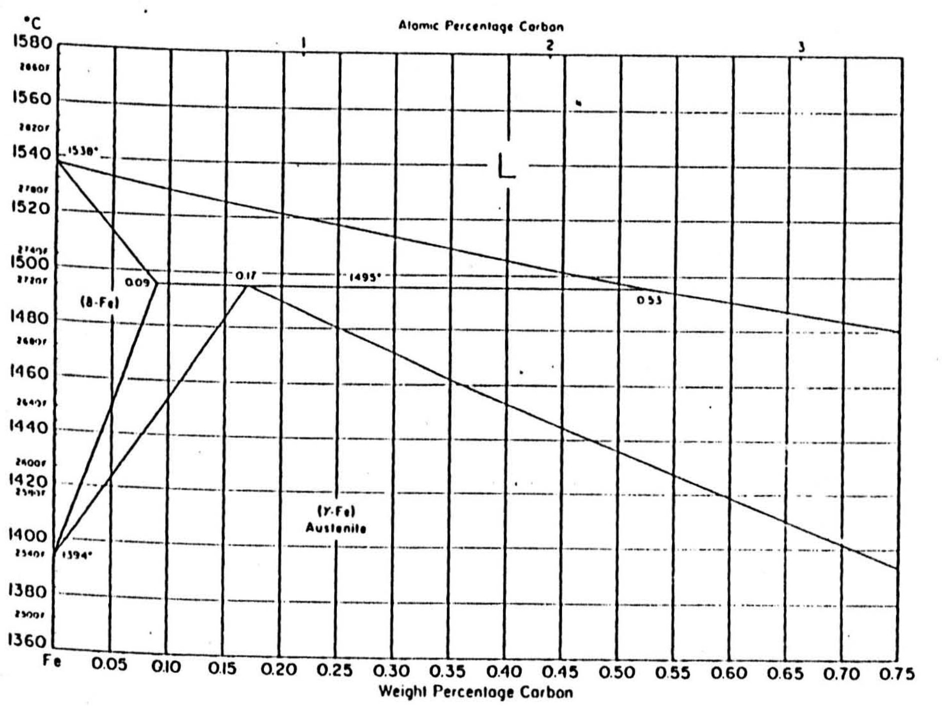
°C
Atomic Percentage Carbon
1
2
3
1580
1560
1540
1520
1500
1480
1460
1440
1420
1400
1380
1360
1538°
L
0.09
0.17
1495°
0.53
(δ-Fe)
(γ-Fe)
Austenite
1394°
Fe
0.05
0.10
0.15
0.20
0.25
0.30
0.35
0.40
0.45
0.50
0.55
0.60
0.65
0.70
0.75
Weight Percentage Carbon

Figure 15

The iron-manganese equilibrium diagram (170)

Figure 16

The manganese-carbon equilibrium diagram (170)

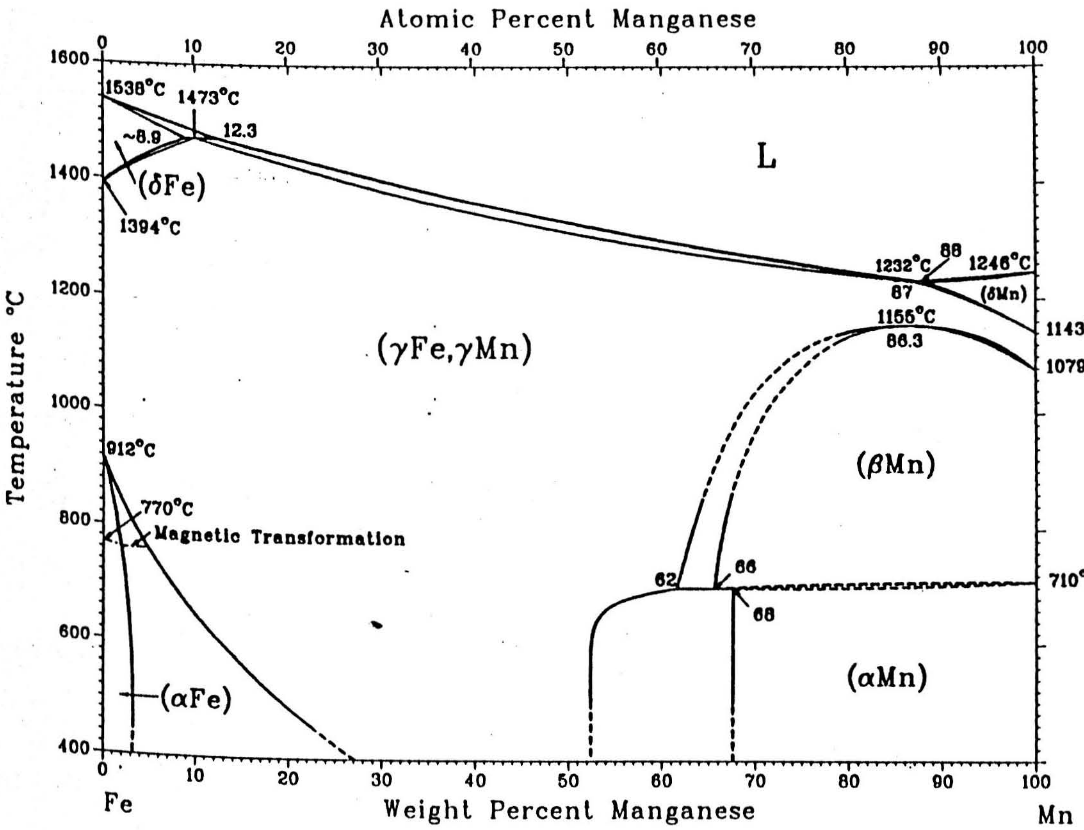

Atomic Percent Manganese
Temperature °C
Weight Percent Manganese
Fe
Mn
L
(δFe)
(γFe,γMn)
(βMn)
(αMn)
(αFe)
(δMn)
1538°C
1473°C
12.3
~8.9
1394°C
1232°C
88
1246°C
87
1155°C
86.3
1143°C
1079°C
912°C
770°C
Magnetic Transformation
62
66
68
710°C

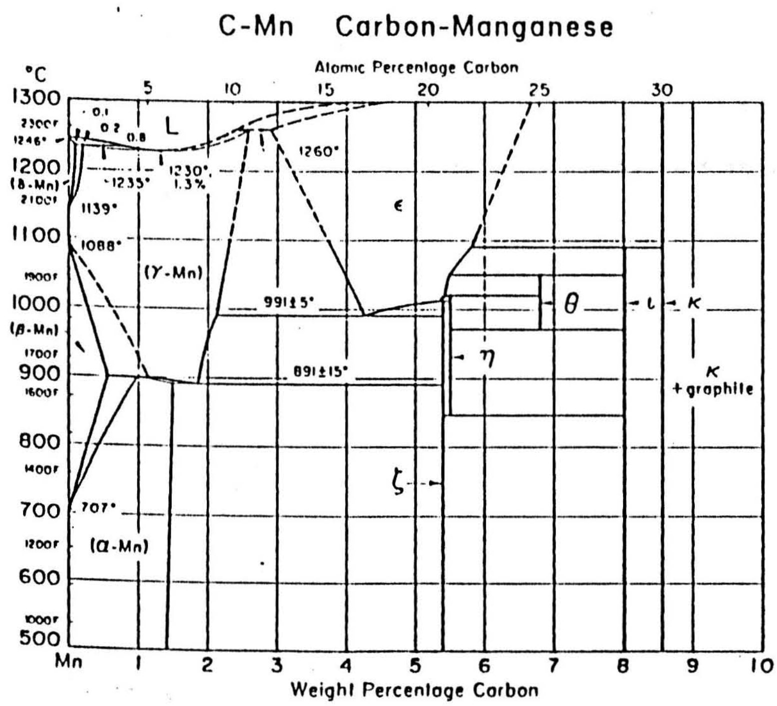

C-Mn Carbon-Manganese
Atomic Percentage Carbon
Weight Percentage Carbon
°C
Mn
L
1260°
1230°, 1.3%
~1235°
1139°
1088°
(γ-Mn)
(δ-Mn)
(β-Mn)
(α-Mn)
991±5°
891±15°
707°
ε
θ
η
ζ
ι
κ
κ + graphite

Figure 17

The peritectic corner of the Fe - C - 1.5 % Mn equilibrium diagram (132)

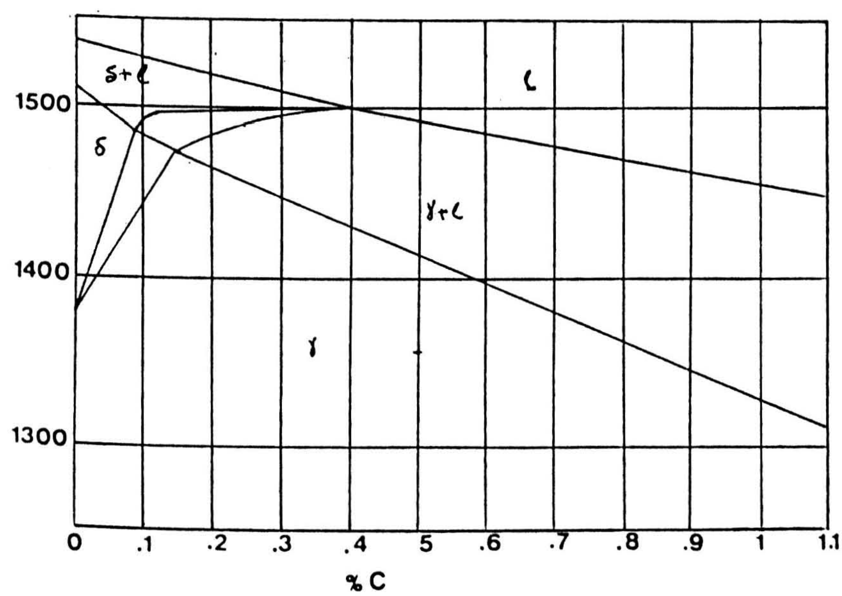

δ+L
L
1500
δ
γ+L
1400
γ
1300
0
.1
.2
.3
.4
5
.6
.7
.8
.9
1
1.1
% C

Figure 18

Photograph of directional solidification furnace

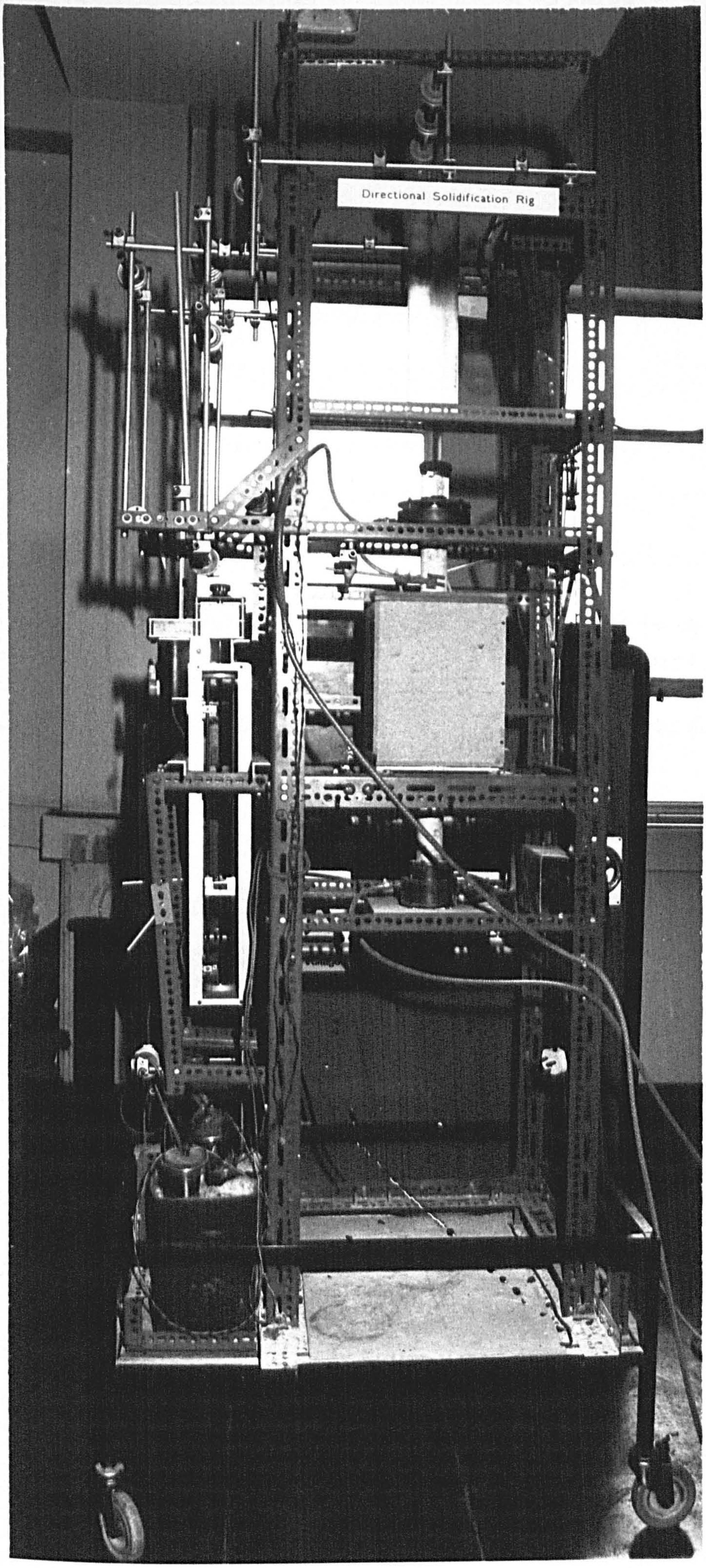
Directional Solidification Rig

Figure 19

Schematic of directional solidification furnace

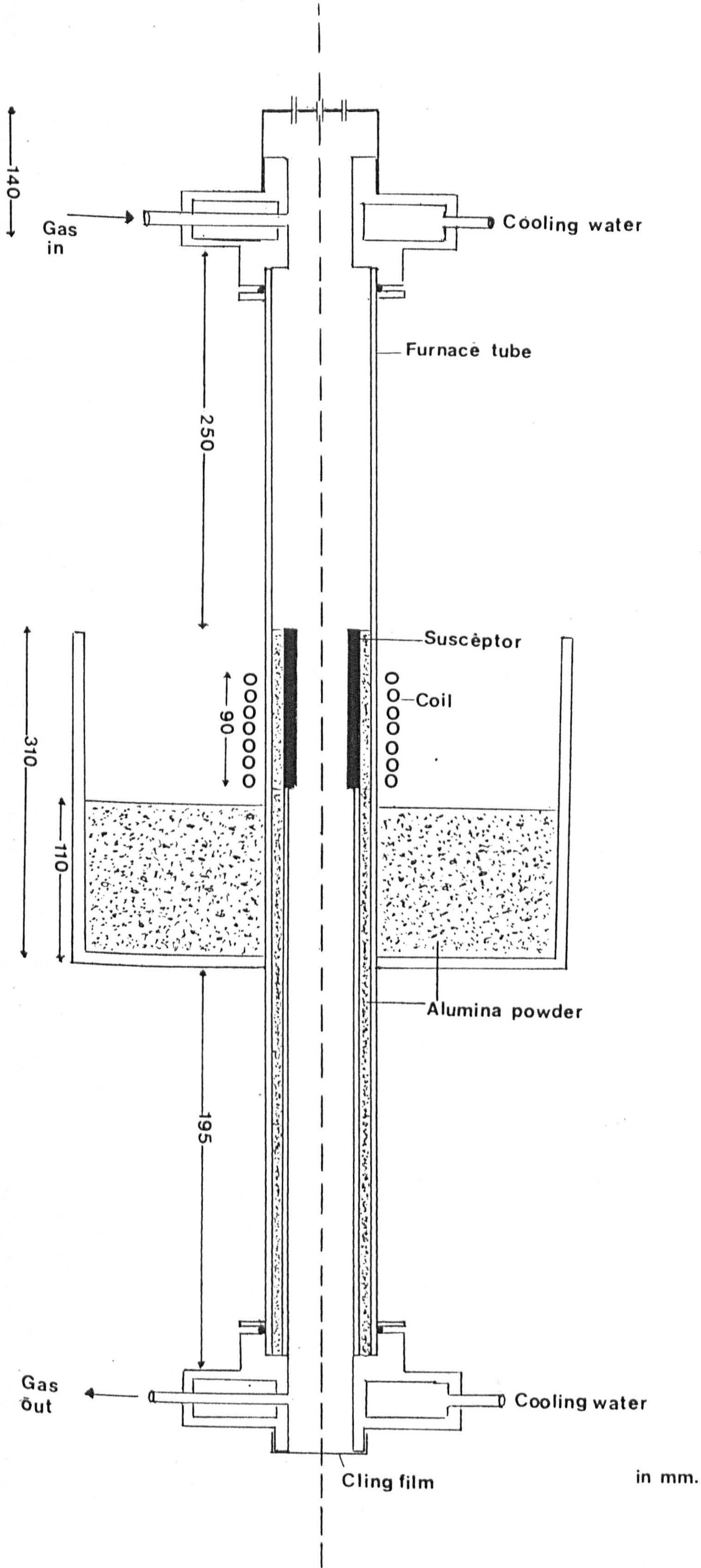
140
Gas in
Cooling water
Furnace tube
250
Susceptor
Coil
90
310
110
Alumina powder
195
Gas out
Cooling water
Cling film
in mm.

Figure 20

Construction of thermocouple and specimens

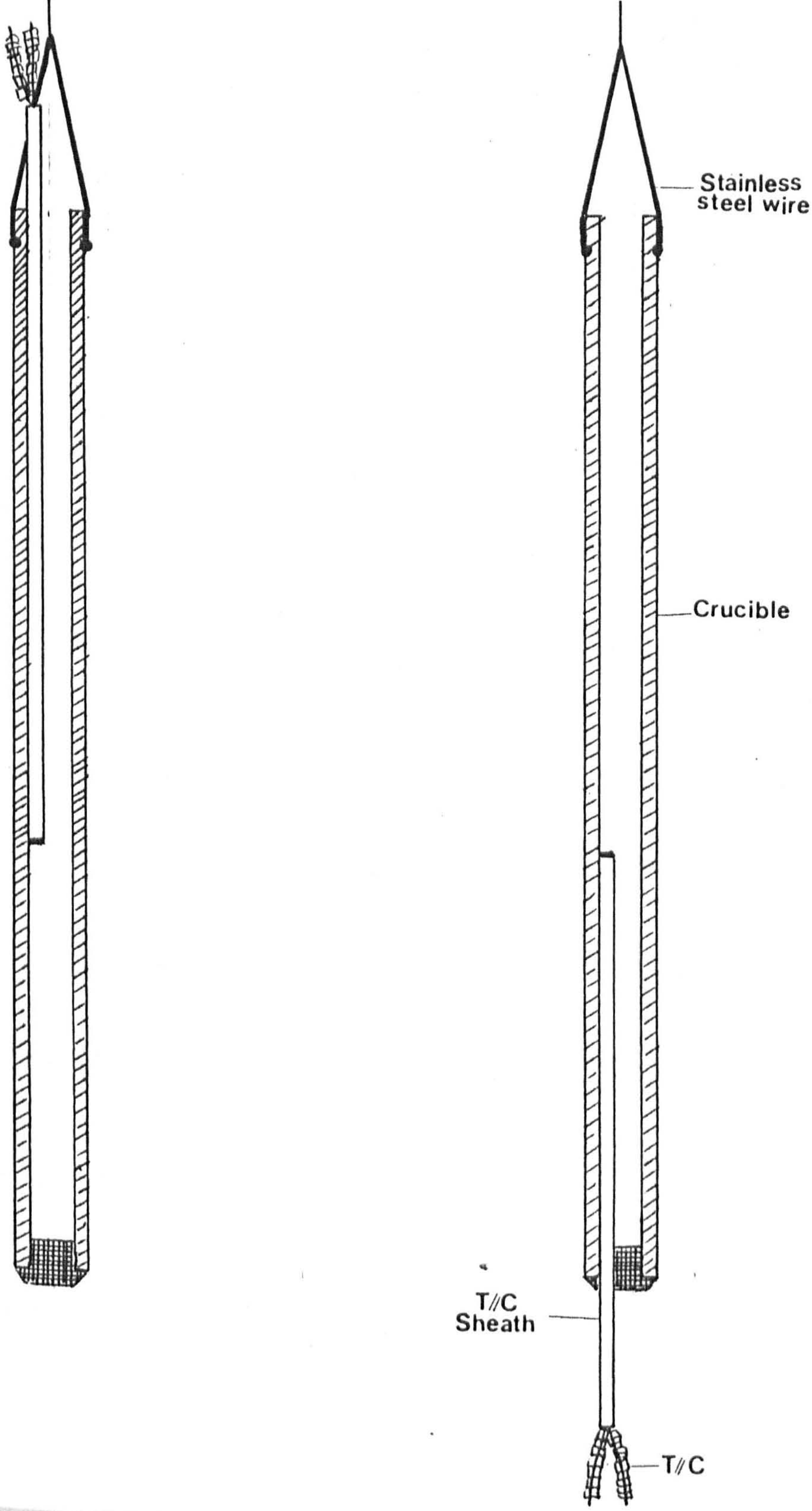
Stainless
steel wire
Crucible
T/C
Sheath
T/C

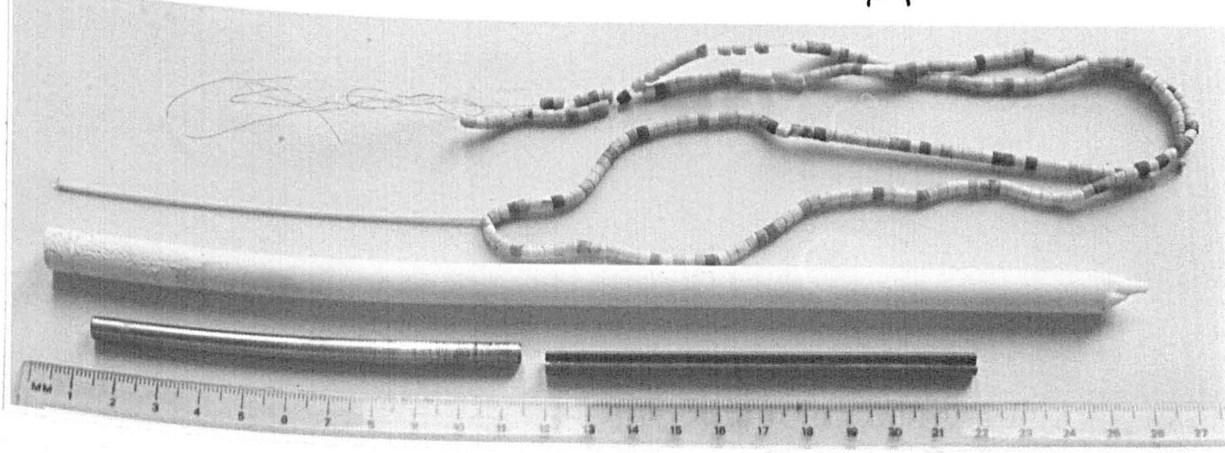

Figure 21

The cylindrical cellular primary arm model

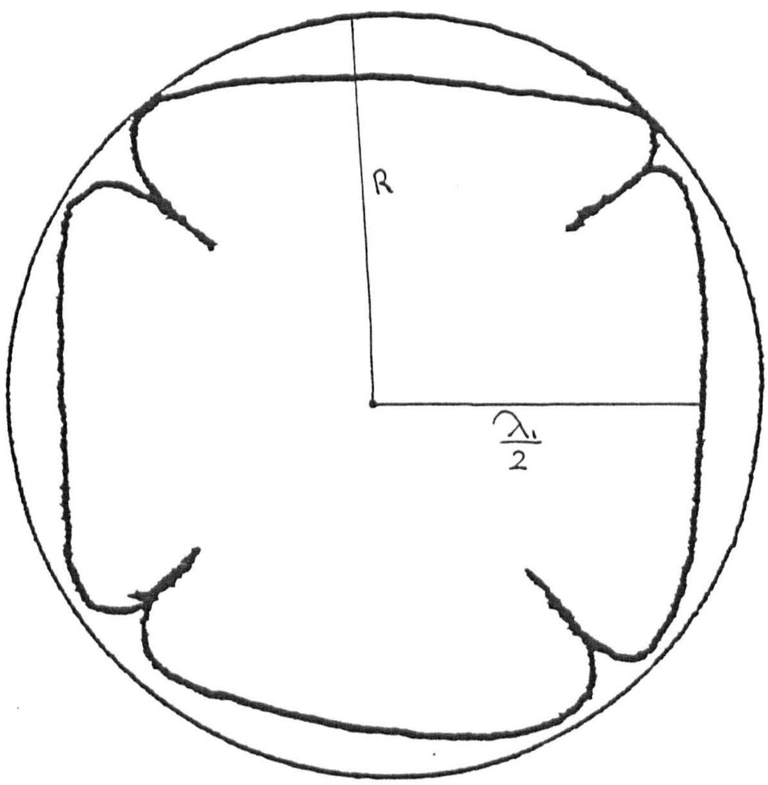
R
$\frac{\lambda_1}{2}$

Figure 22

a) the tranverse section of close packed primary arm spacing arrangement

b) the two extreme possible arrangement of secondary arms on the longidutinal section showing concave solidification model

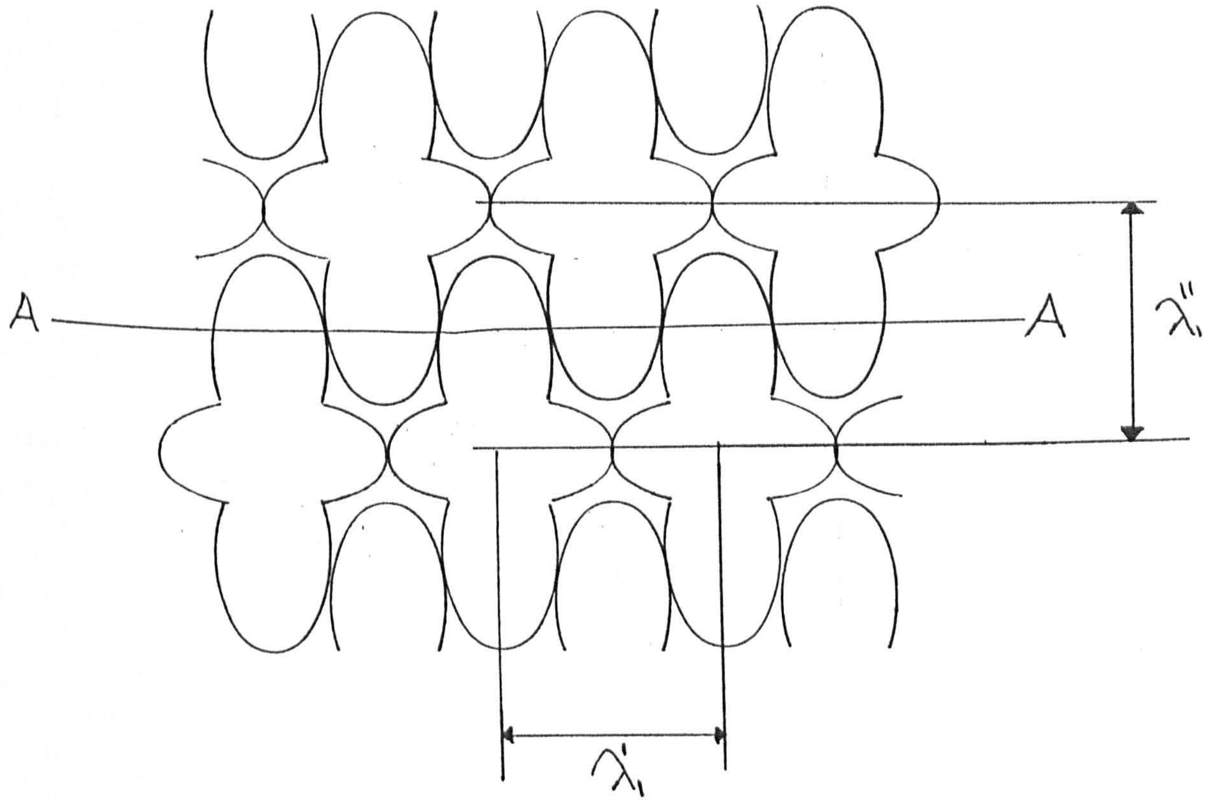
A
A
λ₁''
λ₁'

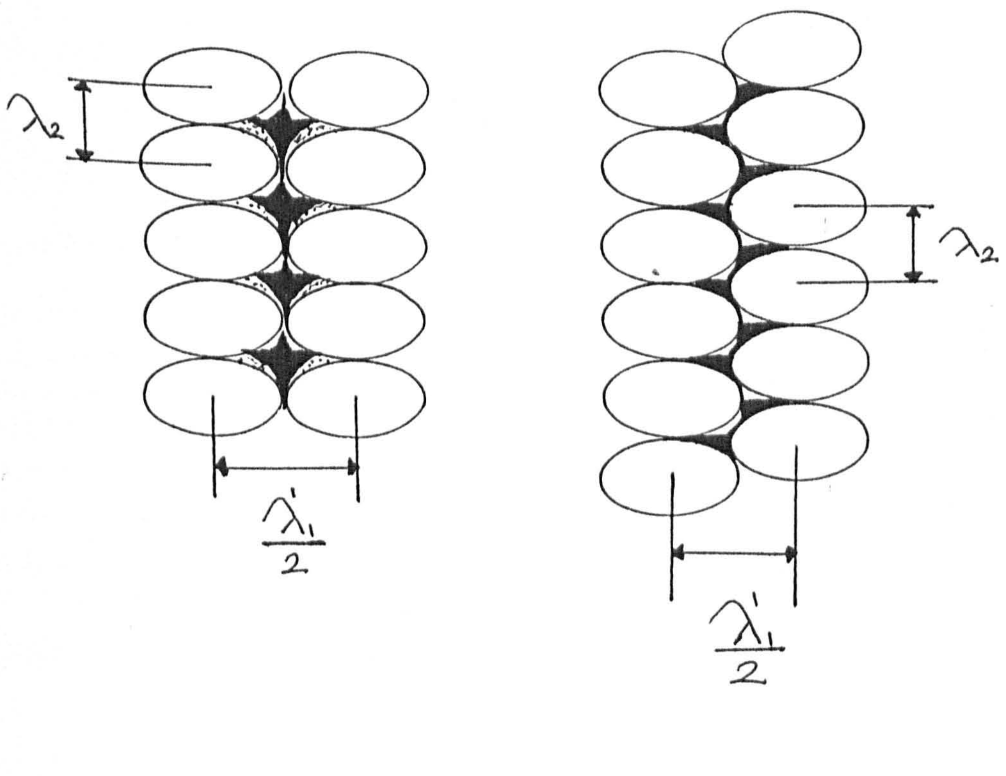
λ₂
λ₁'/2
λ₂
λ₁'/2

Figure 23

a) Volume element modelled by Brody and Flemings from ref 74 (57)

b) Dimentional form of volume element from centre of side arm to centre of the liquid pool(57)

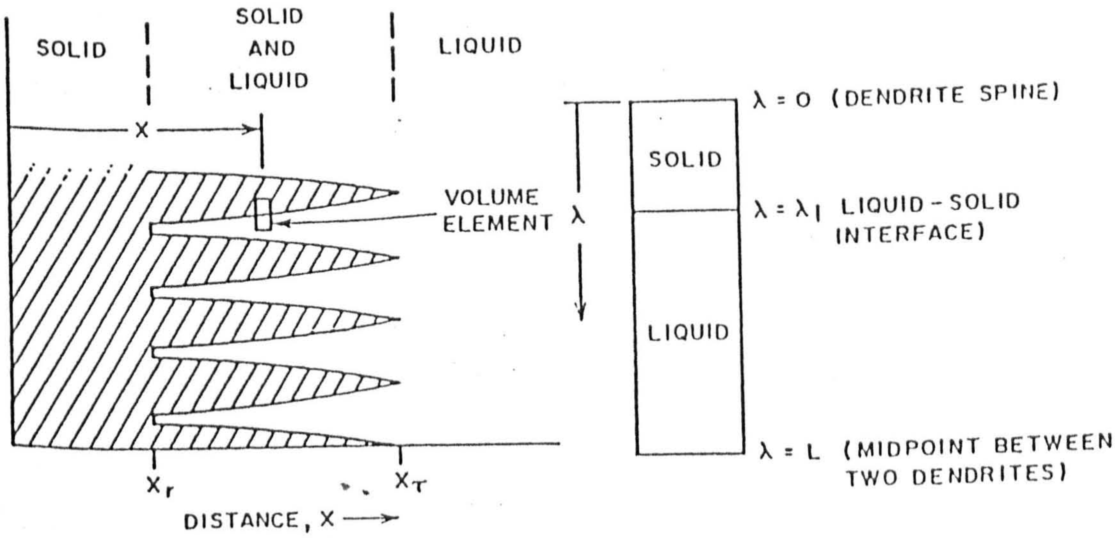
SOLID
SOLID AND LIQUID
LIQUID
X
VOLUME ELEMENT
λ
SOLID
LIQUID
λ = O (DENDRITE SPINE)
λ = λ1 LIQUID - SOLID INTERFACE)
λ = L (MIDPOINT BETWEEN TWO DENDRITES)
Xr
XT
DISTANCE, X

(a)

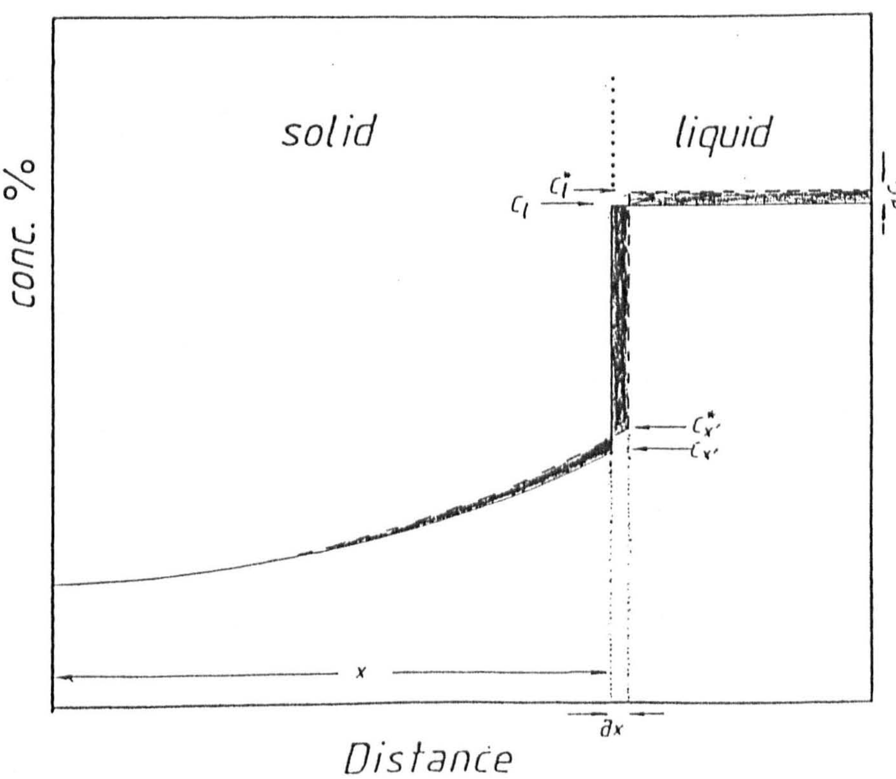
solid
liquid
conc. %
Distance
x
∂x

(b)

Figure 24

Arrangement of node points during finite difference calculations (57)

Figure 25

Volume element for side arm coarsening model (57)

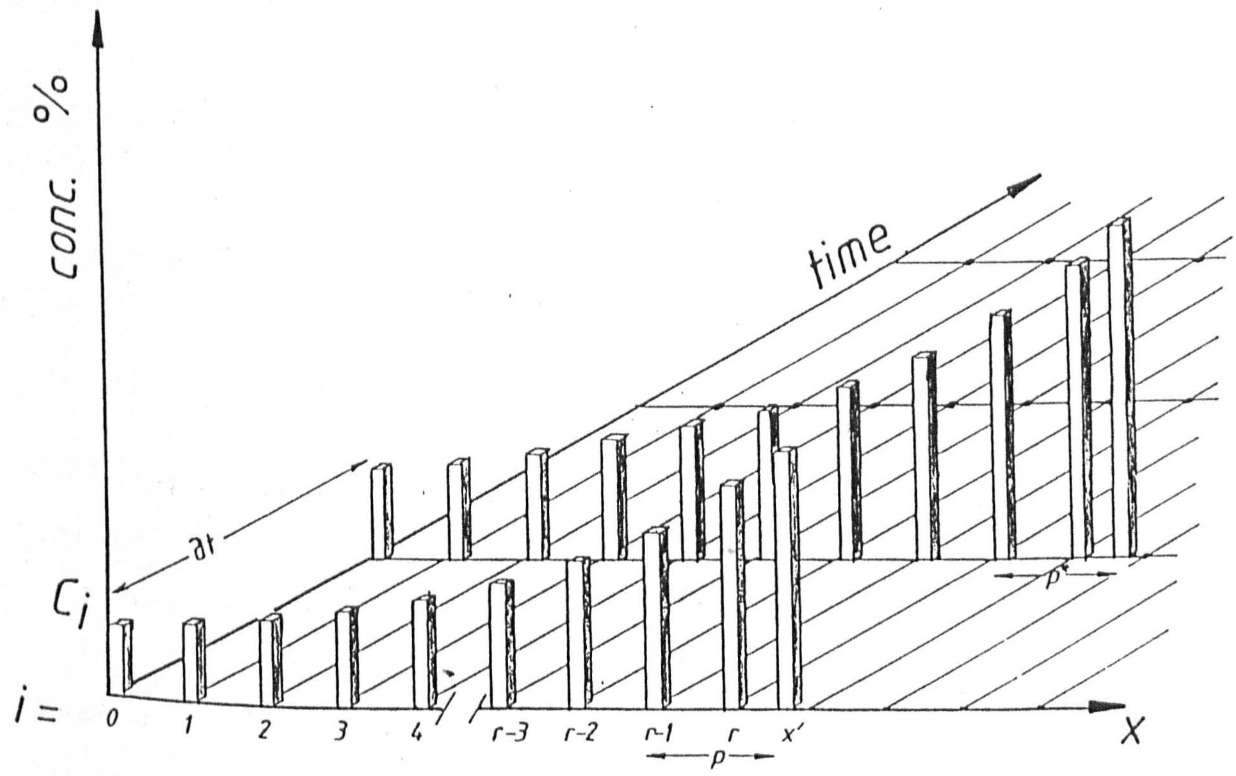

conc. %
time
Δt
C_i
i =
0
1
2
3
4
r-3
r-2
r-1
r
x'
X
p
p*

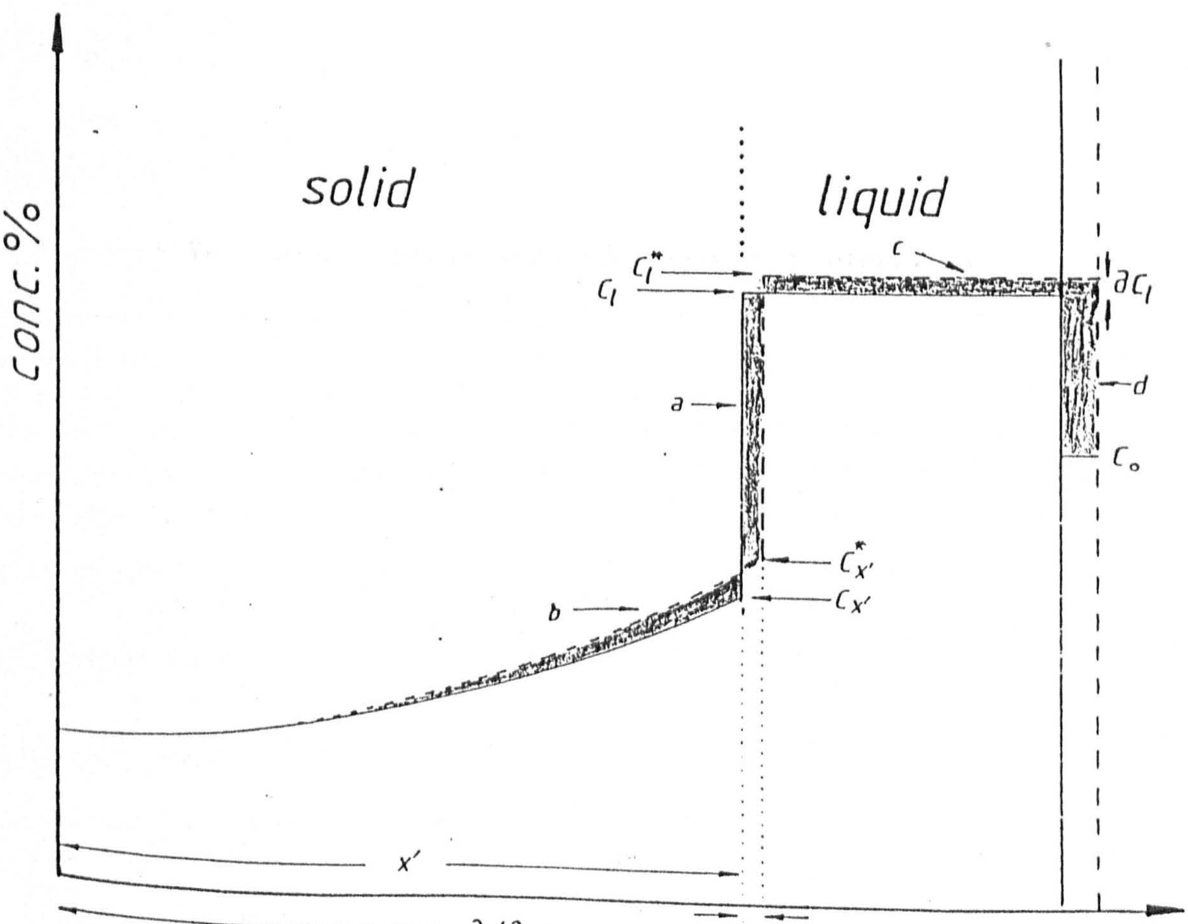

conc. %
solid
liquid
C_l^*
C_l
c
∂C_l
a
d
C_o
$C_{x'}^*$
$C_{x'}$
b
x'
λ/2
∂x
∂λ/2

Figure 26

Photomicrograph of the longitudinal section of quenched 0.8 % C showing the high segregated lines between primary arms and the morphological change of secondary arms during solidification

0.8 % C - 1.6 % Mn - Fe

Growth rate	1.5 mm/min
Temperature gradient in liquid	8.4 C/mm
Magnification	X 25.7

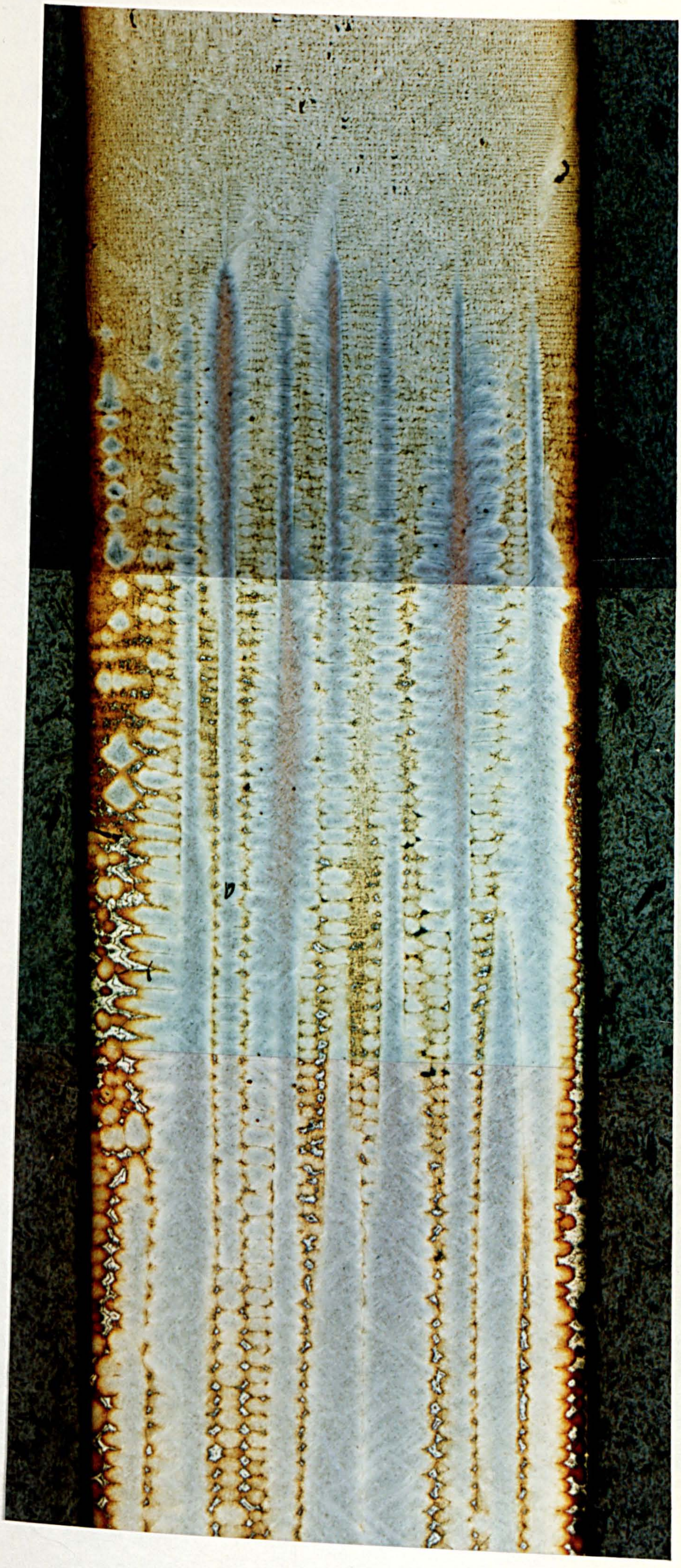

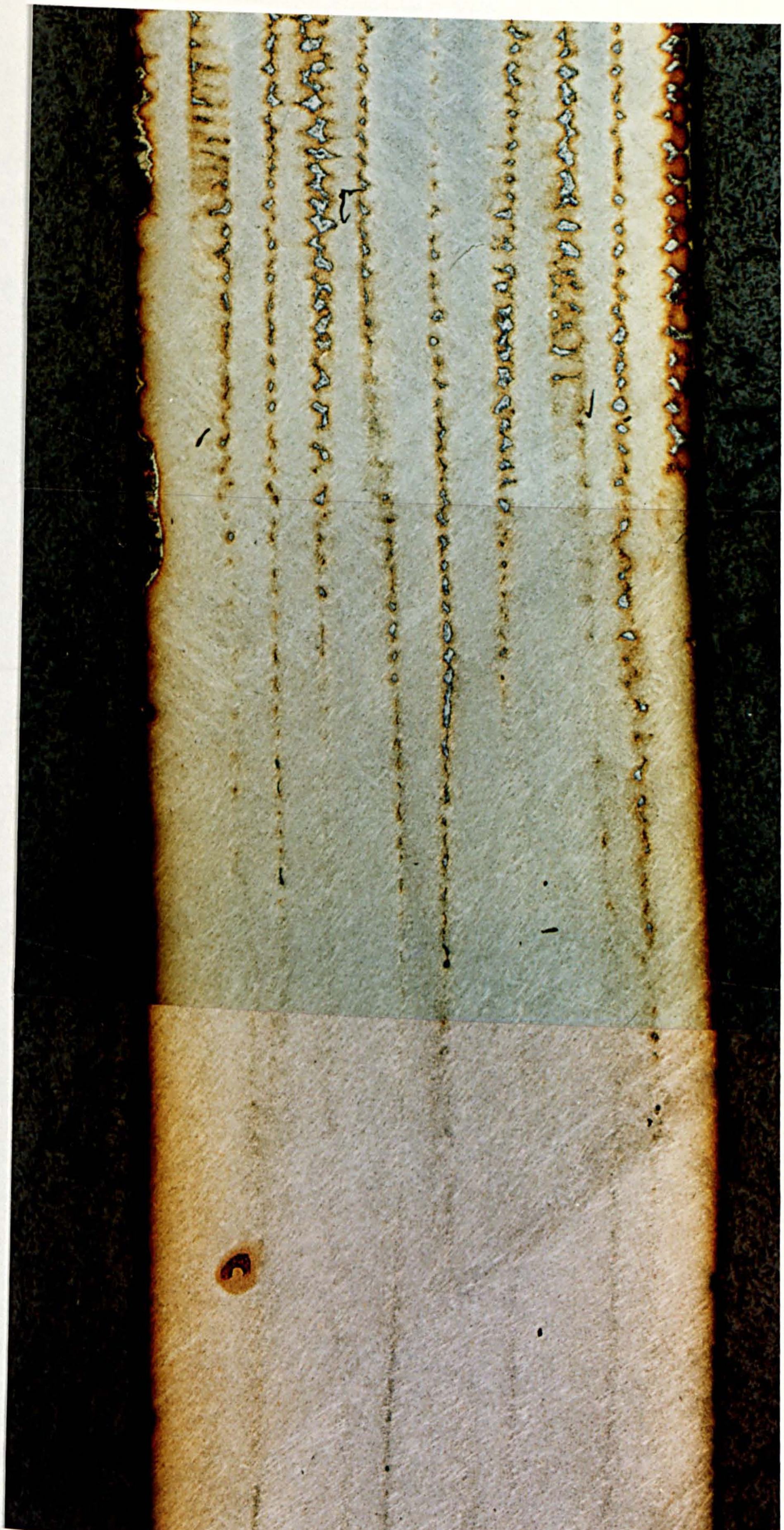

Figure 27

Photomicrograph of the morphological change in secondary arms as a result of high coalescence process leaving highly segregated points between primary arms surrounded by secondaries

0.8 % C - 1.6 % Mn - Fe

Growth rate	1.5 mm/min
Temperature gradient in liquid	8.4 C/mm
Magnification	X 137.5

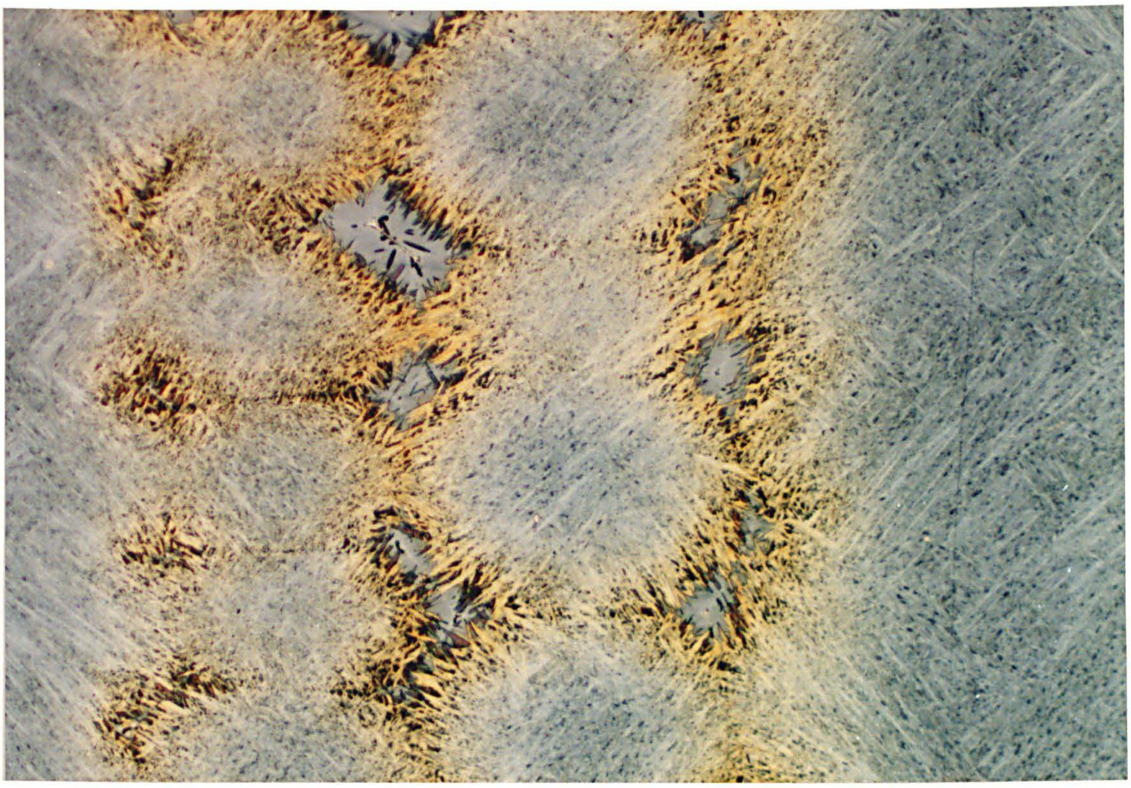

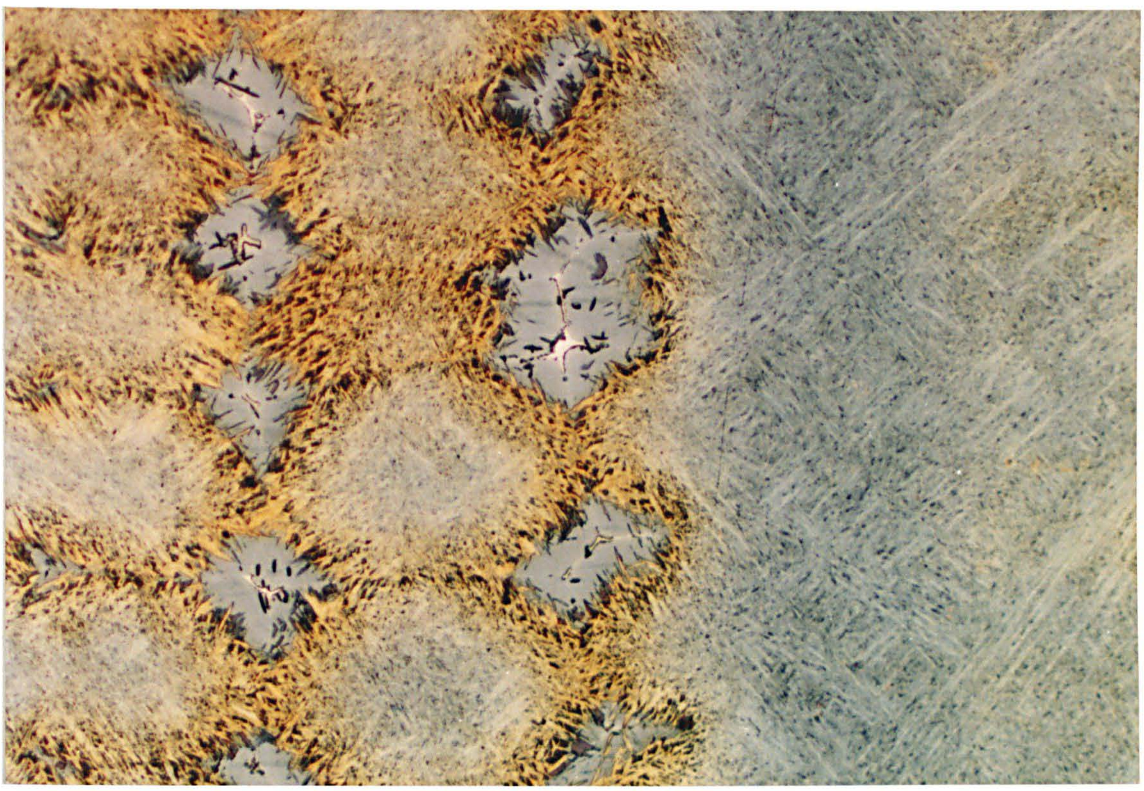

Figure 28

Photomicrograph of the longitudinal section of quenched 0.8 % C showing the highly segregated lines between primary arms and the secondary arm coarsening during solidification

0.8 % C - 1.6 % Mn - Fe

Growth rate	6 mm/min
Temperature gradient in liquid	7.2 C/mm
Magnification	X 21

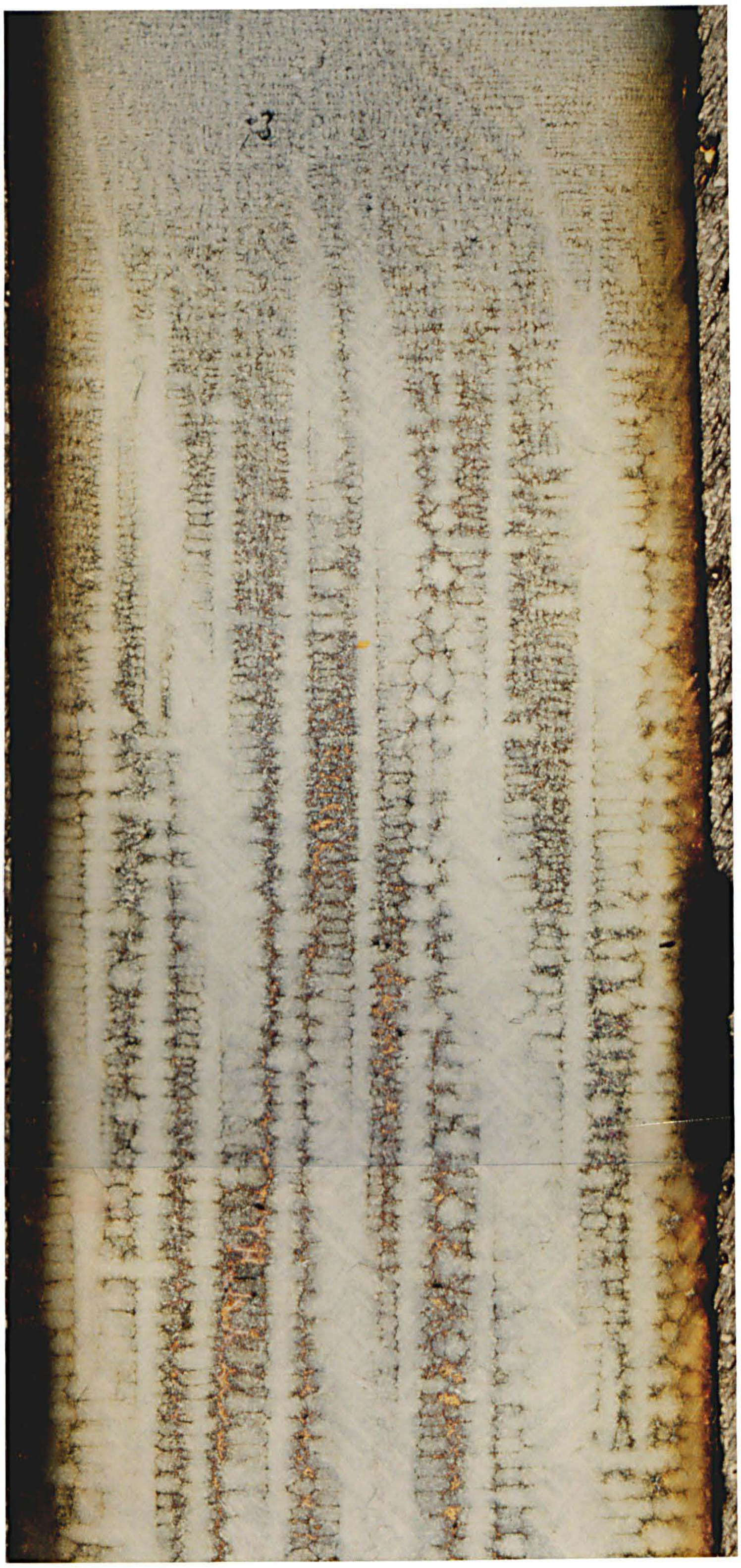

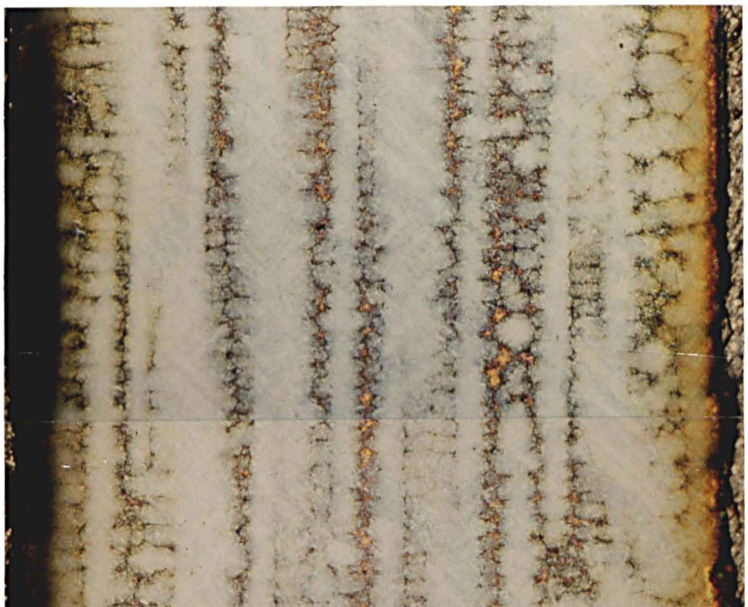

Figure 29

Photomicrograph of the longitudinal section of quenched 0.8 % C showing the highly segregated lines between primary arms and the secondary arm coarsening during solidification

0.8 % C - 1.6 % Mn - Fe

Growth rate	15 mm/min
Temperature gradient in liquid	5.9 C/mm
Magnification	X 21

Figure 30

Photomicrograph of the longitudinal section of quenched low carbon alloy showing the highly segregated lines between primary arms and the poor developed secondary arms in the short solidification range

0.1 % C - 1.6 % Mn - Fe

Growth rate	6 mm/min
Temperature gradient in liquid	7.2 C/mm
Magnification	X 21

Figure 31

Photomicrograph of the morphological change in secondary arms as a result of high coalescence and back diffusion process leaving highly segregated points between primary arms surrounded by secondary arms

0.1 % C - 1.6 % Mn - Fe

Growth rate	6 mm/min
Temperature gradient in liquid	7.2 C/mm
Magnification	X 280

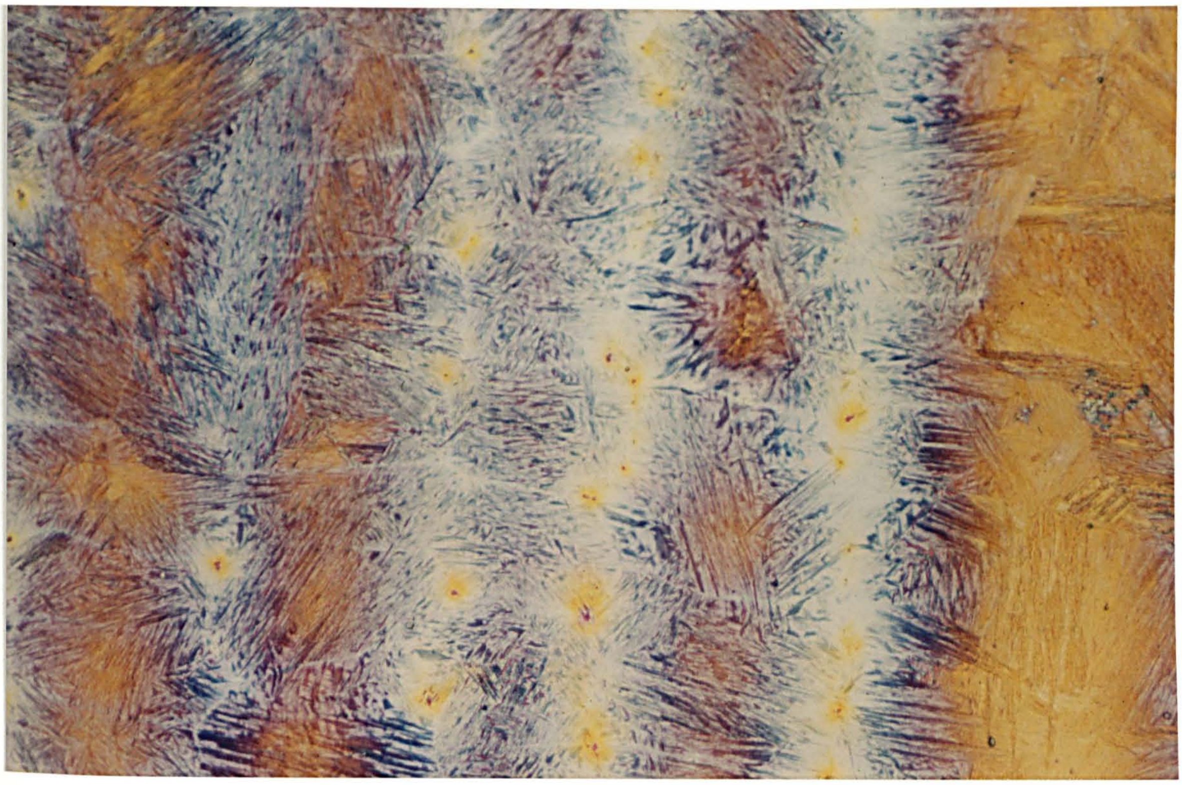

Figure 32

Photomicrograph of the transverse sections of figure 26 at the different distance behind tips showing the morphological change in the primary arms during solidification at the lowest growth rate (circular secondary arms)

0.8 % C - 1.6 % Mn - Fe

Growth rate	1.5 mm/min
Temperature gradient in liquid	8.4 C/mm

a-	0.5 mm behind tips	mag. 51.4
b-	0.5 mm behind tips	mag. 25.7
c-	2.7 mm behind tips	mag. 25.7
d-	5.9 mm behind tips	mag. 25.7
e-	10 mm behind tips	mag. 25.7
f-	20 mm behind tips	mag. 25.7

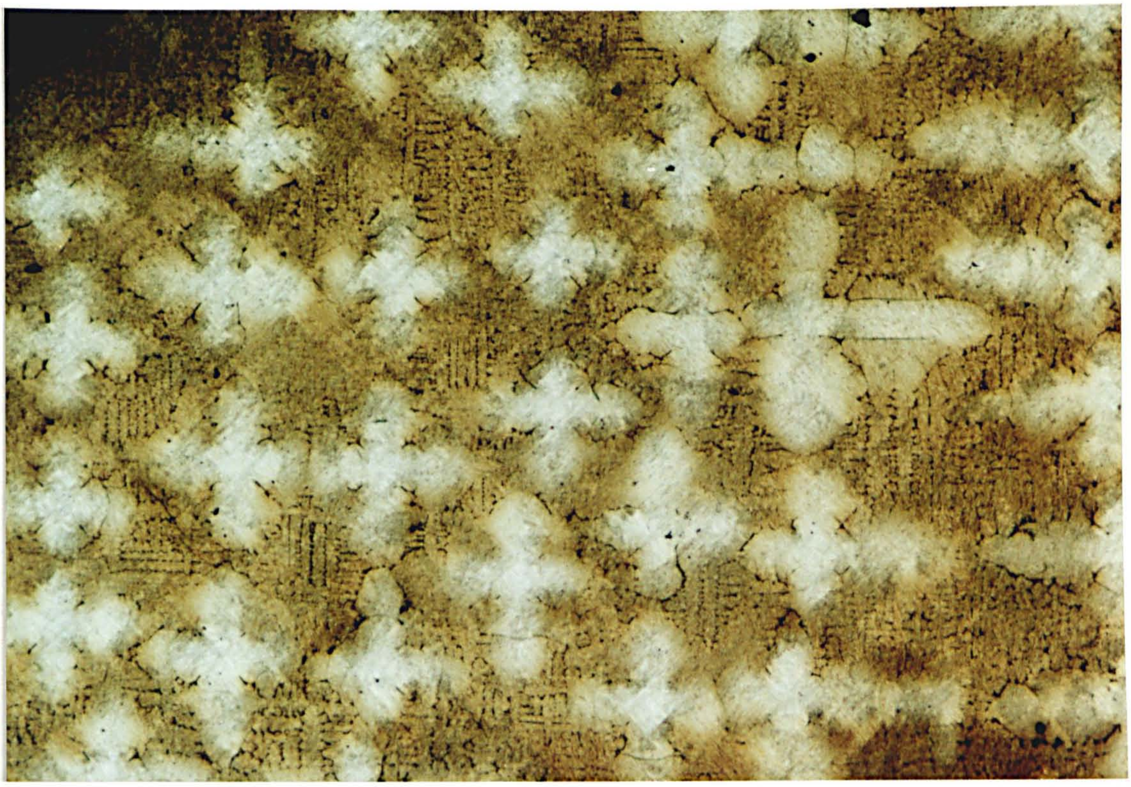

(a)

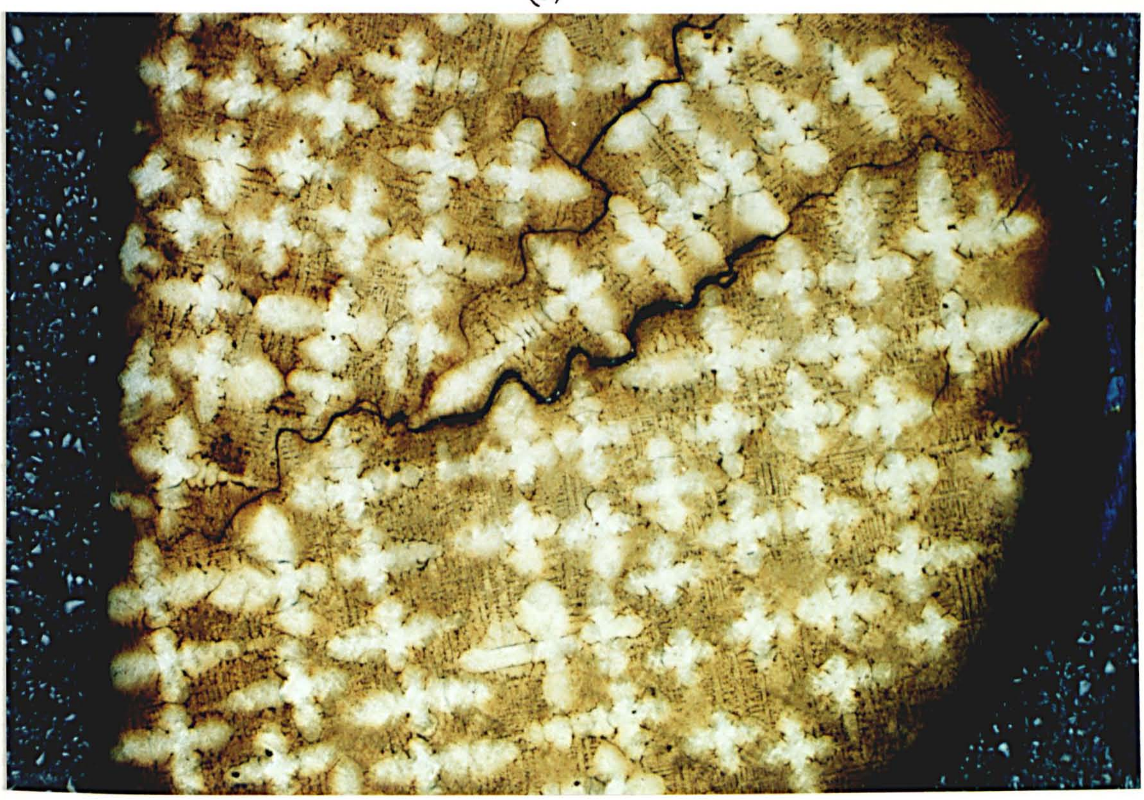

(b)

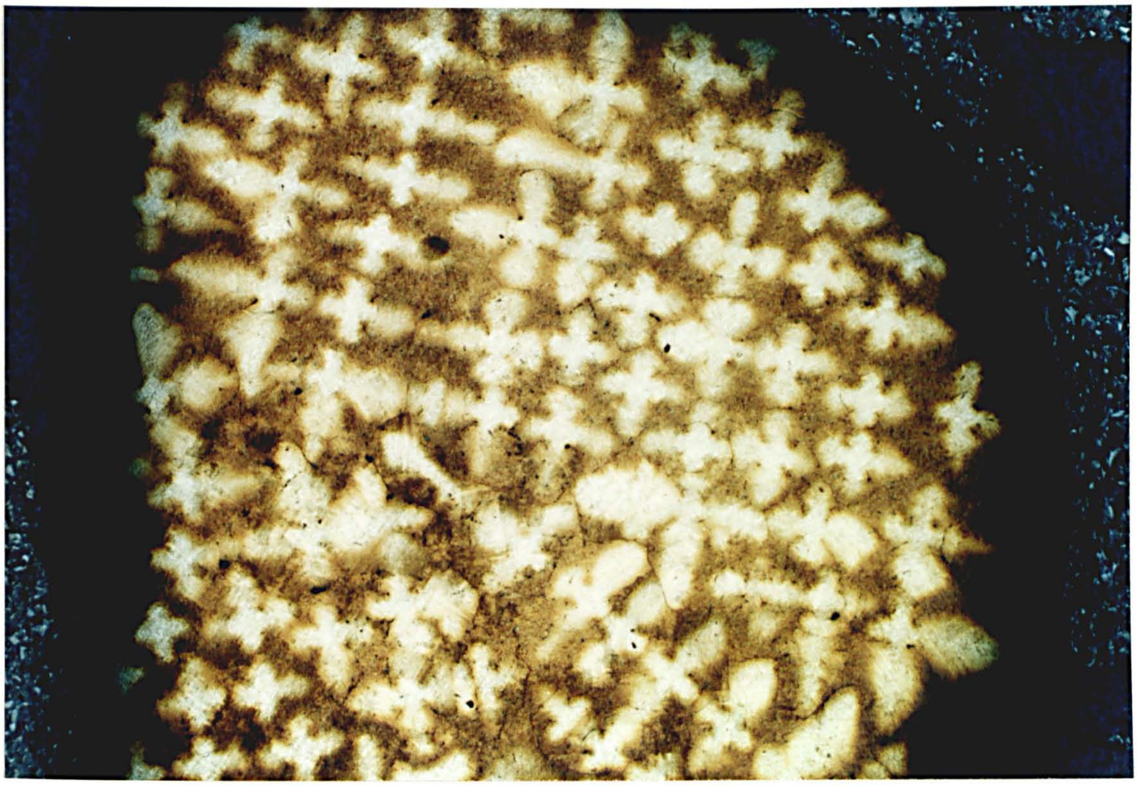

(c)

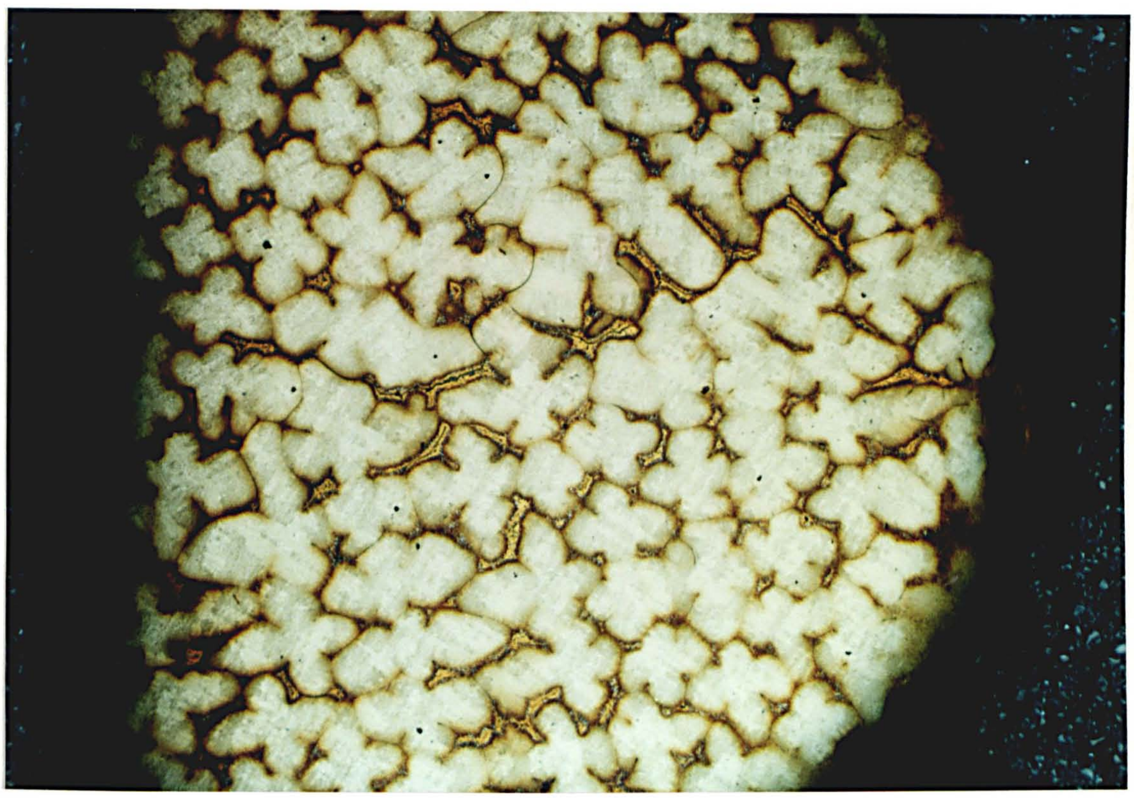

(d)

(e)

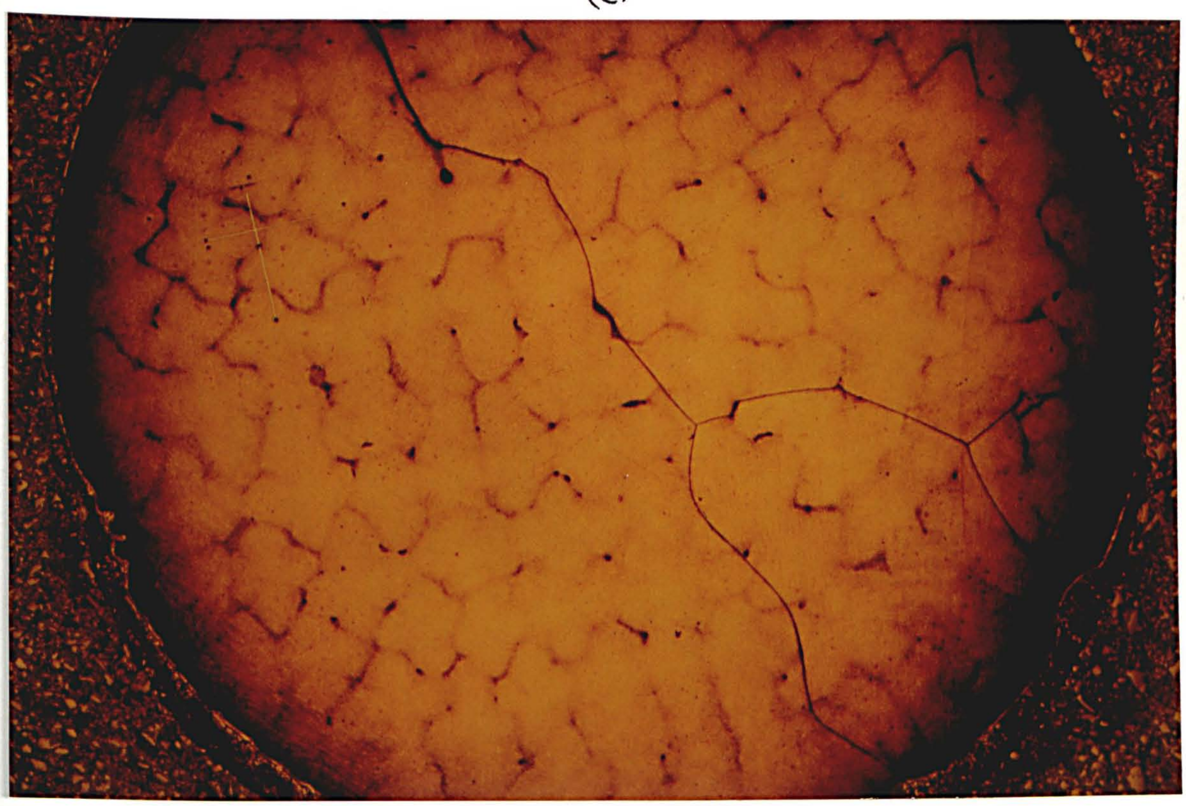

(f)

Figure 33 and 34

Photomicrographs of the transverse sections of the low carbon alloys showing the primary arm spacing with circular and poorly developed secondary arms at the lowest growth rate and indicating the delta ferrite - austenite phase transformation

(white - delta ferrite · colour - austenite)

33) 0.1 % C - 1.6 % Mn - Fe

Growth rate	1.5 mm/min
Temperature gradient in liquid	8.4 C/mm
Magnification	X 142
Temperature	1480 C
Distance	4 mm

34) 0.2 % C - 1.6 % Mn - Fe

Growth rate	1.5 mm/min
Temperature gradient in liquid	10.7 C/mm
Magnification	X 71
Temperature	1465
Distance	3.75 mm.

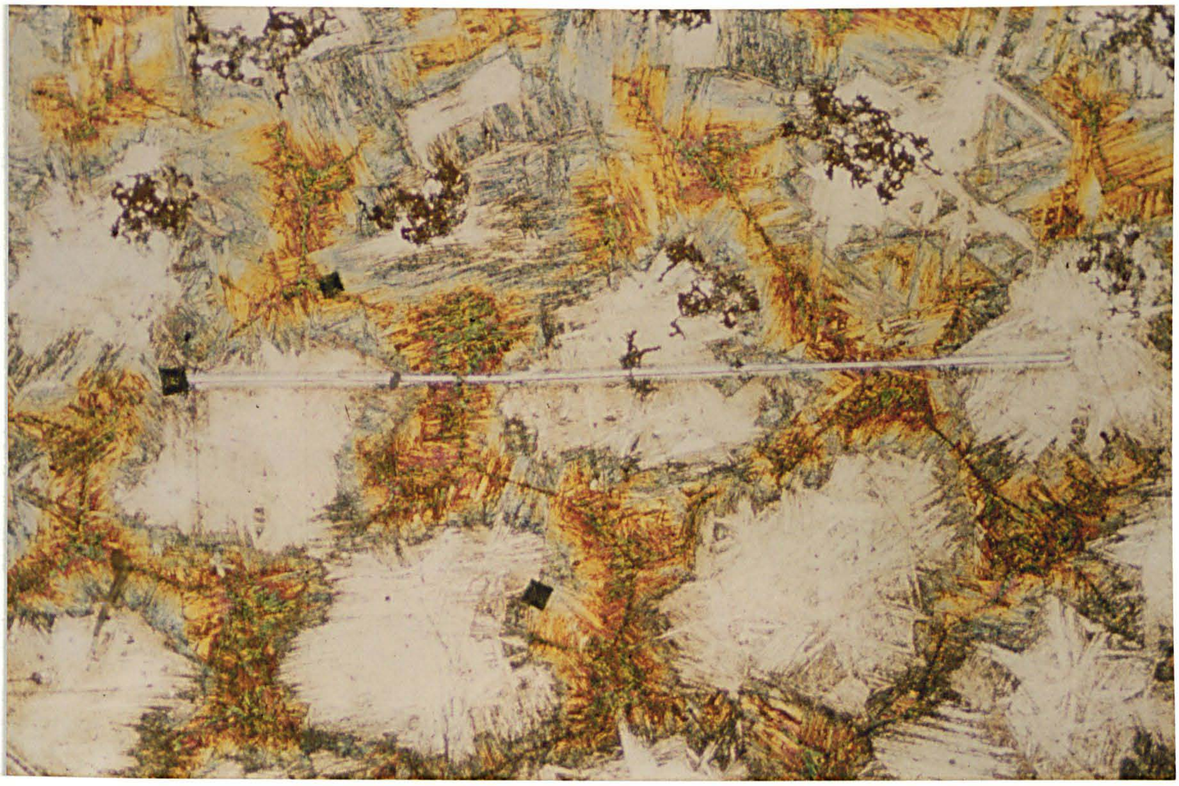

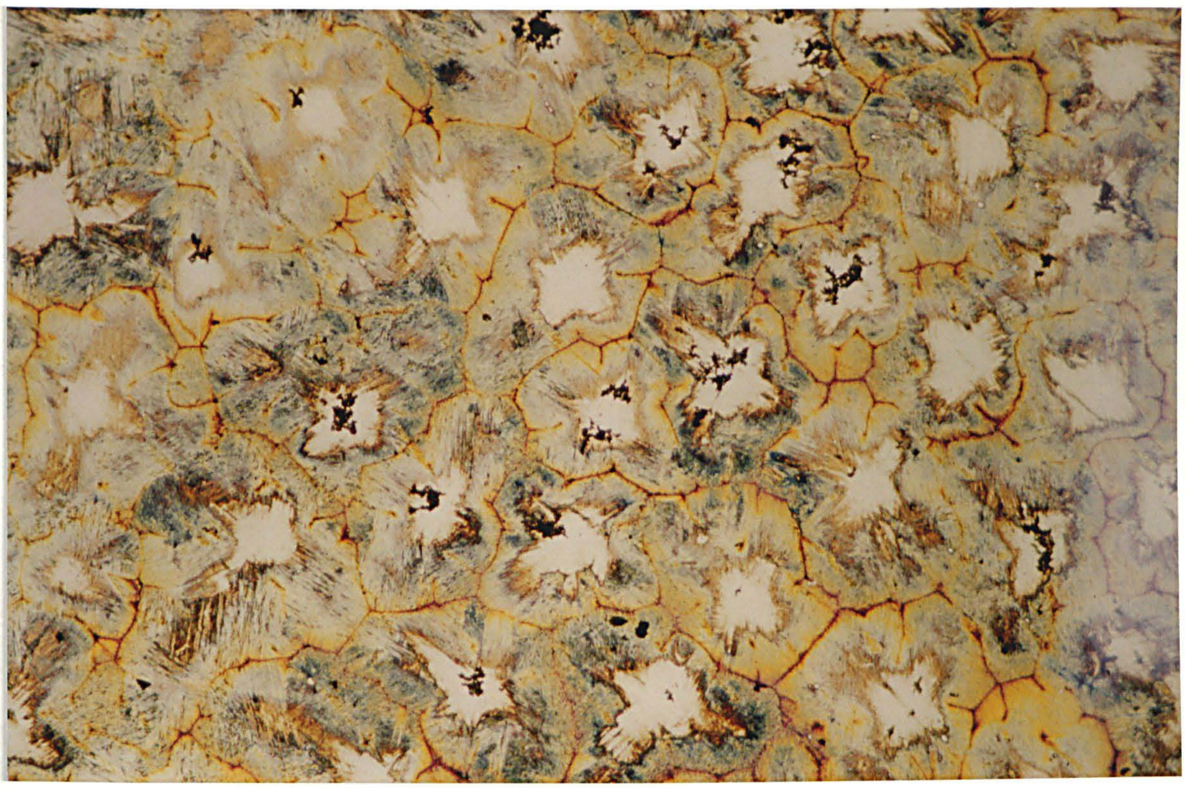

Figure 35

Photomicrograph of the transverse sections of quenched specimen showing the close packed morphological structure of primary arms (planar secondaries) at the high growth rate

0.8 % C - 1.6 % Mn - Fe

Growth rate	6 mm/min
Temperature gradient in liquid	5.5 C/mm
Magnification	X 25

a- 14 mm behind tips

b- 28 mm behind tips

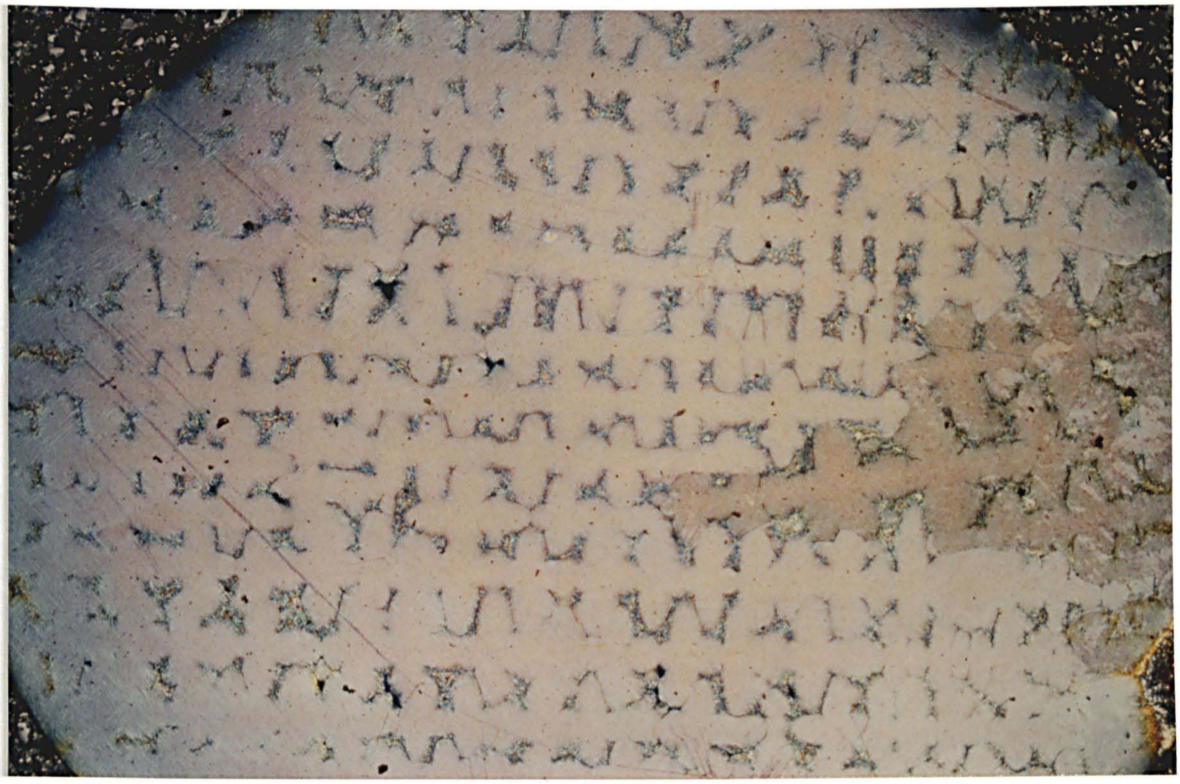
(a)

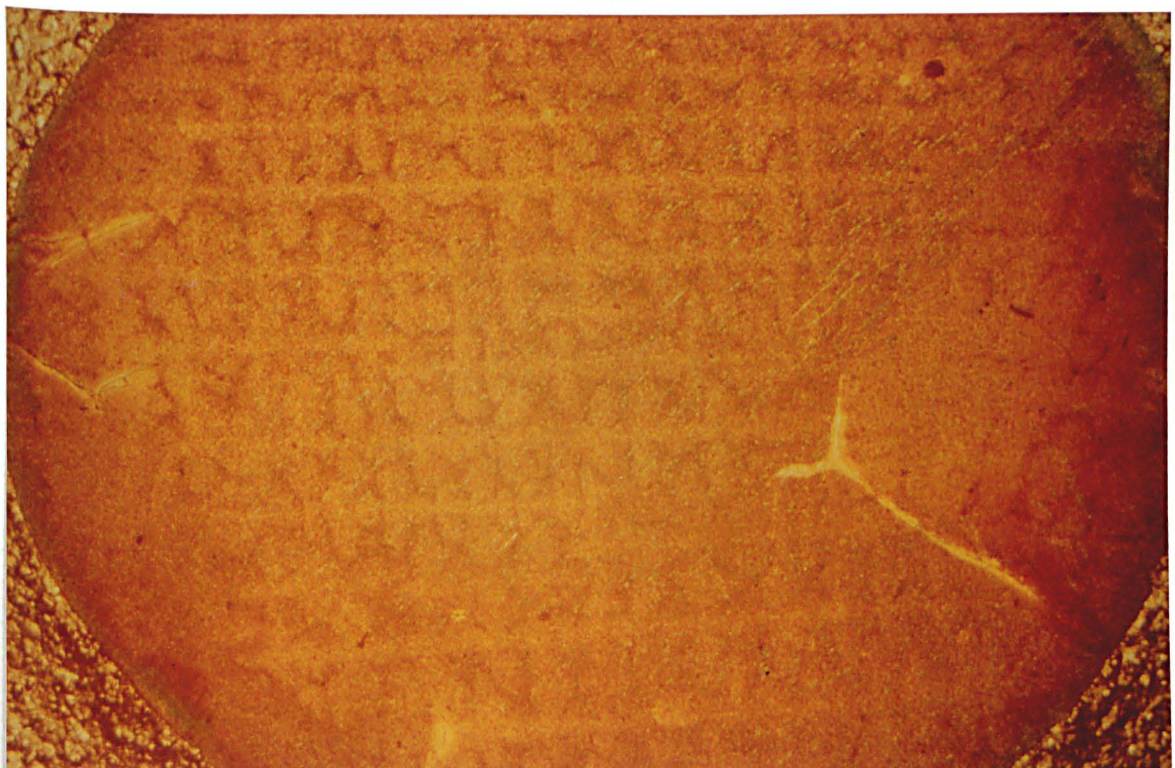
(b)

Figure 36

Photomicrograph of the close packed primary arm spacing morphology showing the effect of growth rate (comparing with figures 35 and 32)

0.8 % C - 1.6 % Mn - Fe

Growth rate	15 mm/min
Temperature gradient in liquid	5.9 C/mm
Magnification	X 25

a- 1.5 mm behind tips

b- 19 mm behind tips

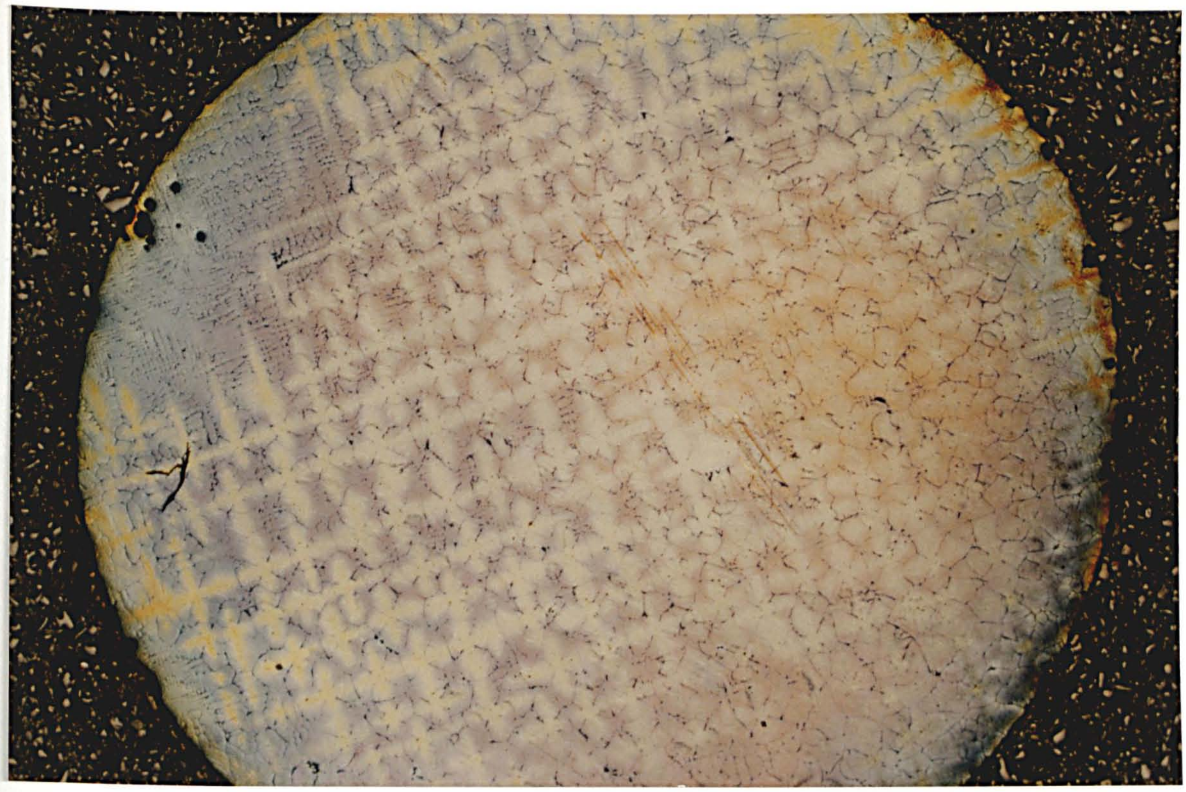
(a)

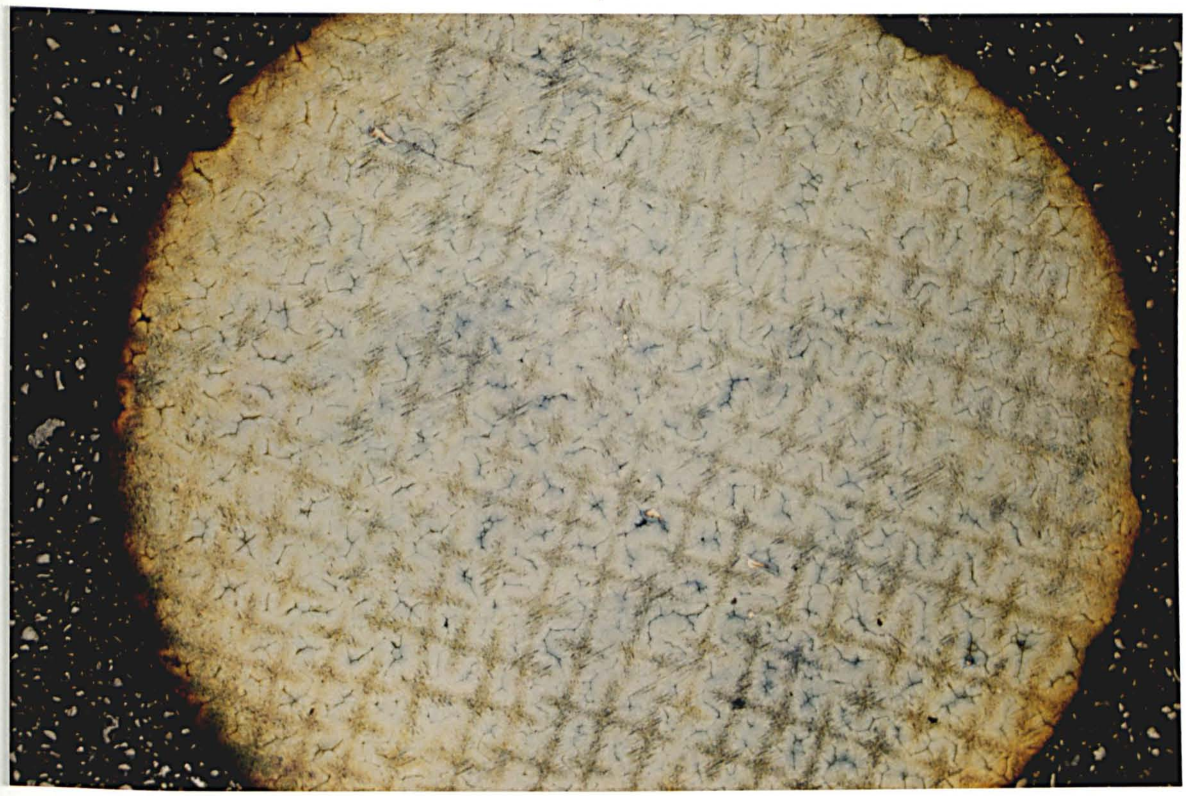
(b)

Figure 37

Photomicrograph of the planar secondary arms at the high magnification

0.4 % C - 1.6 % Mn - Fe

Magnification X 284

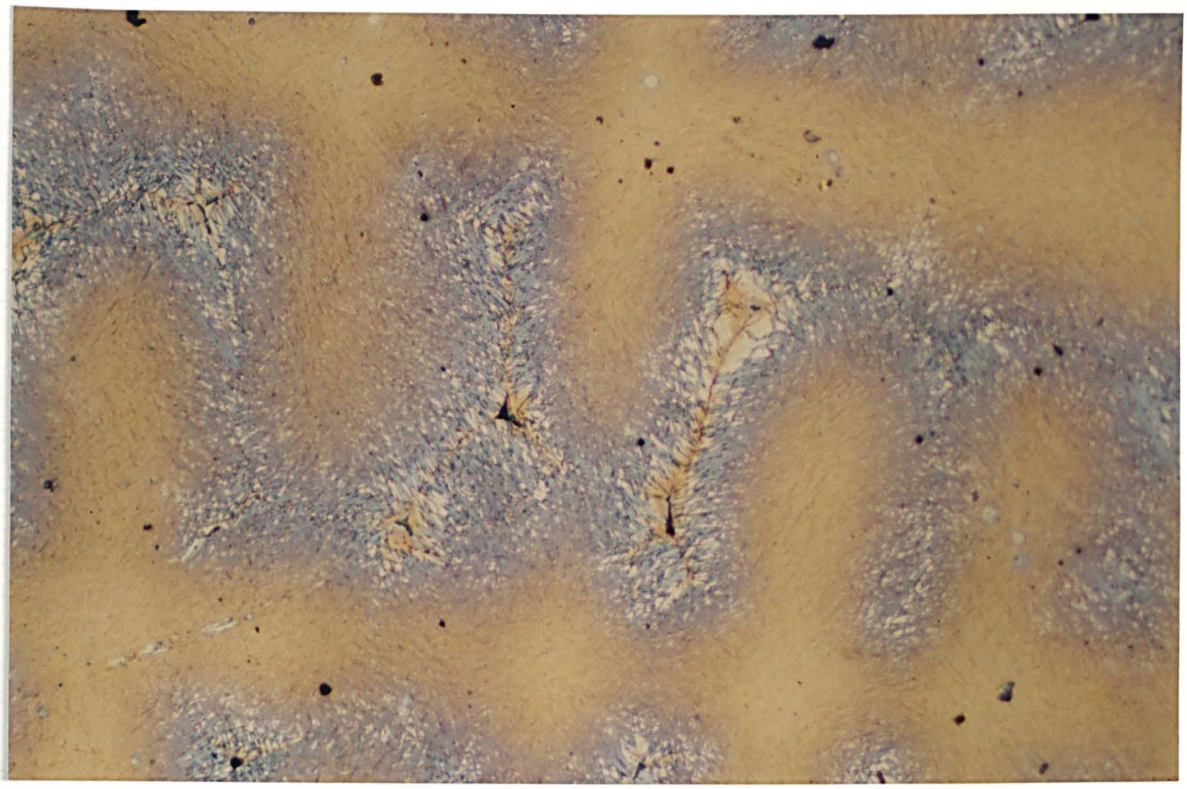

Figure 38

Photomicrographs of the transverse sections of primary arms spacing for low carbon steel showing the delta ferrite - austenite phase transformation during solidification at the different distance behind tips

0.1 % C - 1.6 % Mn - Fe

Growth rate	6 mm/min
Temperature gradient in liquid	7.2 C/mm
Magnification	X 142

a- 3 mm behind tips at 1495 C

b- 8 mm behind tips at 1440 C

c- 14 mm behind tips at 1330 C

(a)

(b)

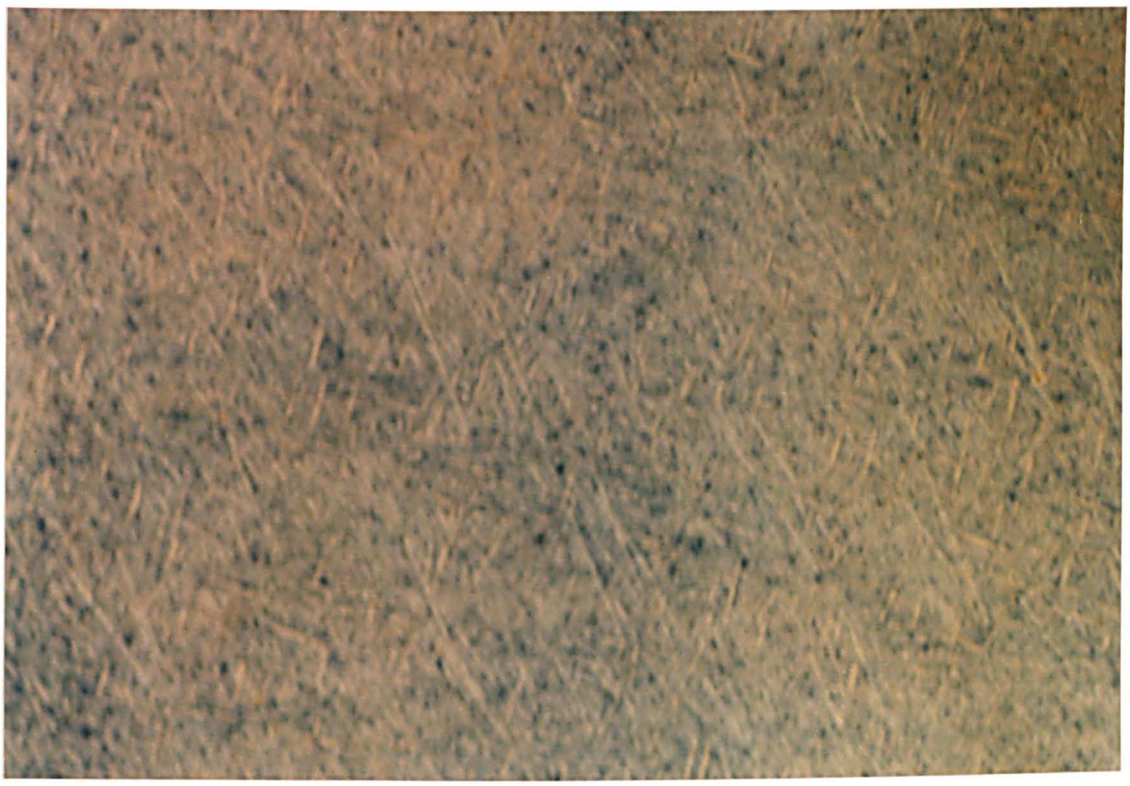

(c)

Figure 39

The change in the primary arm spacing as a function of temperature gradient in liquid and growth rate for different carbon content

a- 0.1 % C

b- 0.2 % C

c- 0.4 % C

d- 0.8 % C

- - - - - 0.5 slope

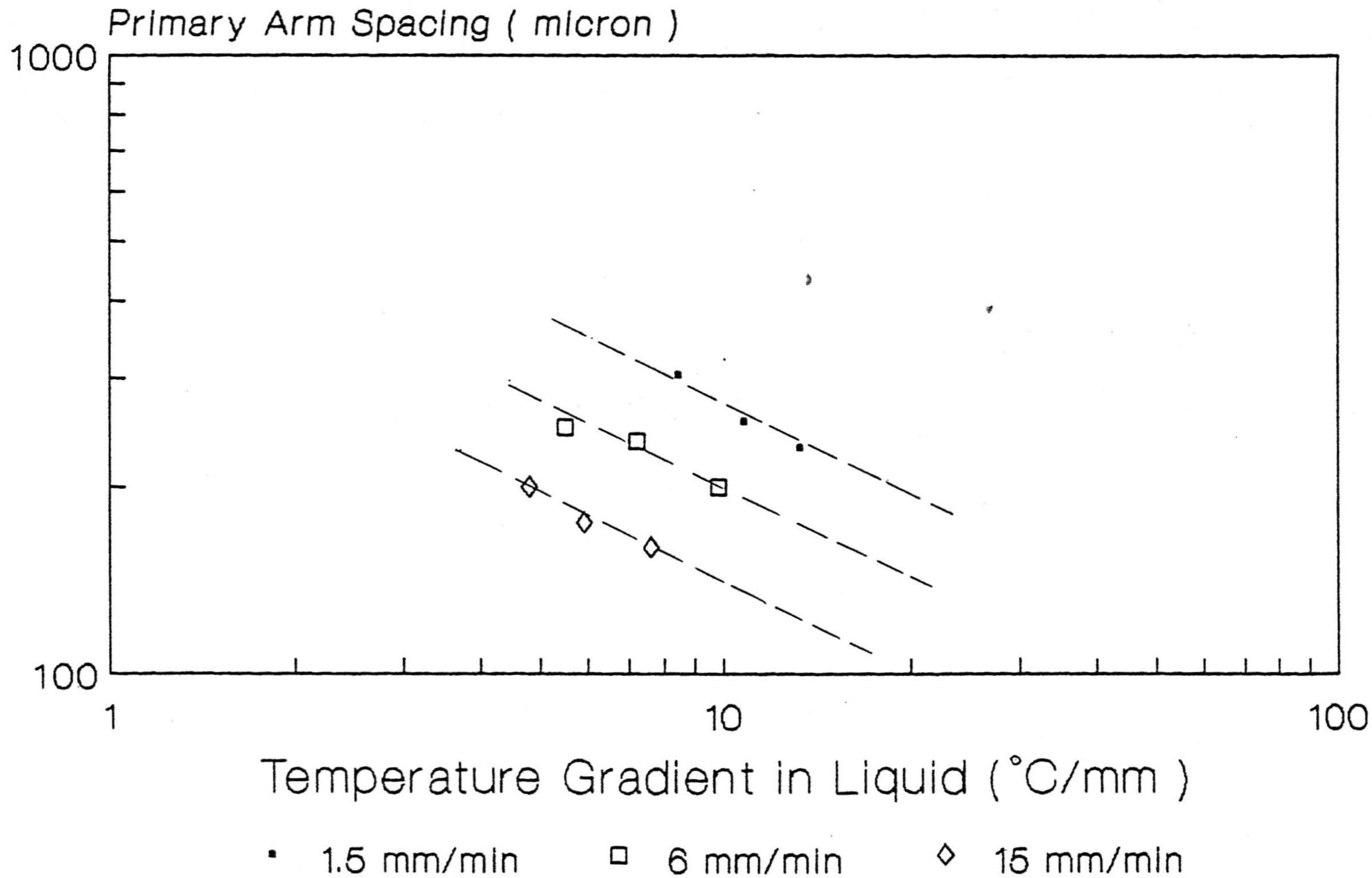
Primary Arm Spacing (micron)
1000
100
1
10
100
Temperature Gradient in Liquid (°C/mm)
1.5 mm/min
6 mm/min
15 mm/min

0.1 % C

(a)

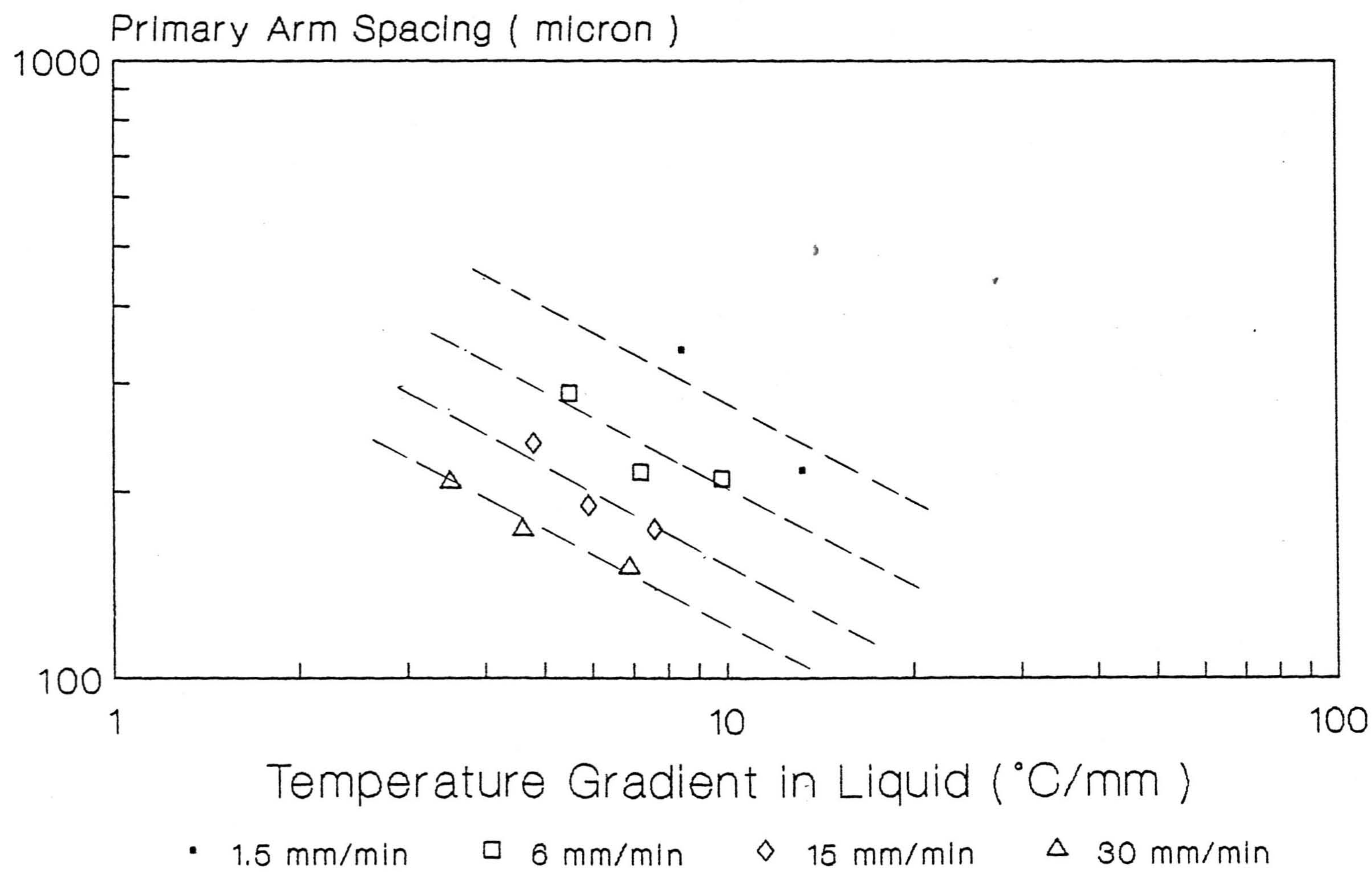
Primary Arm Spacing (micron)
1000
100
1
10
100
Temperature Gradient in Liquid (°C/mm)
1.5 mm/min
6 mm/min
15 mm/min
30 mm/min

0.2 % C

(b)

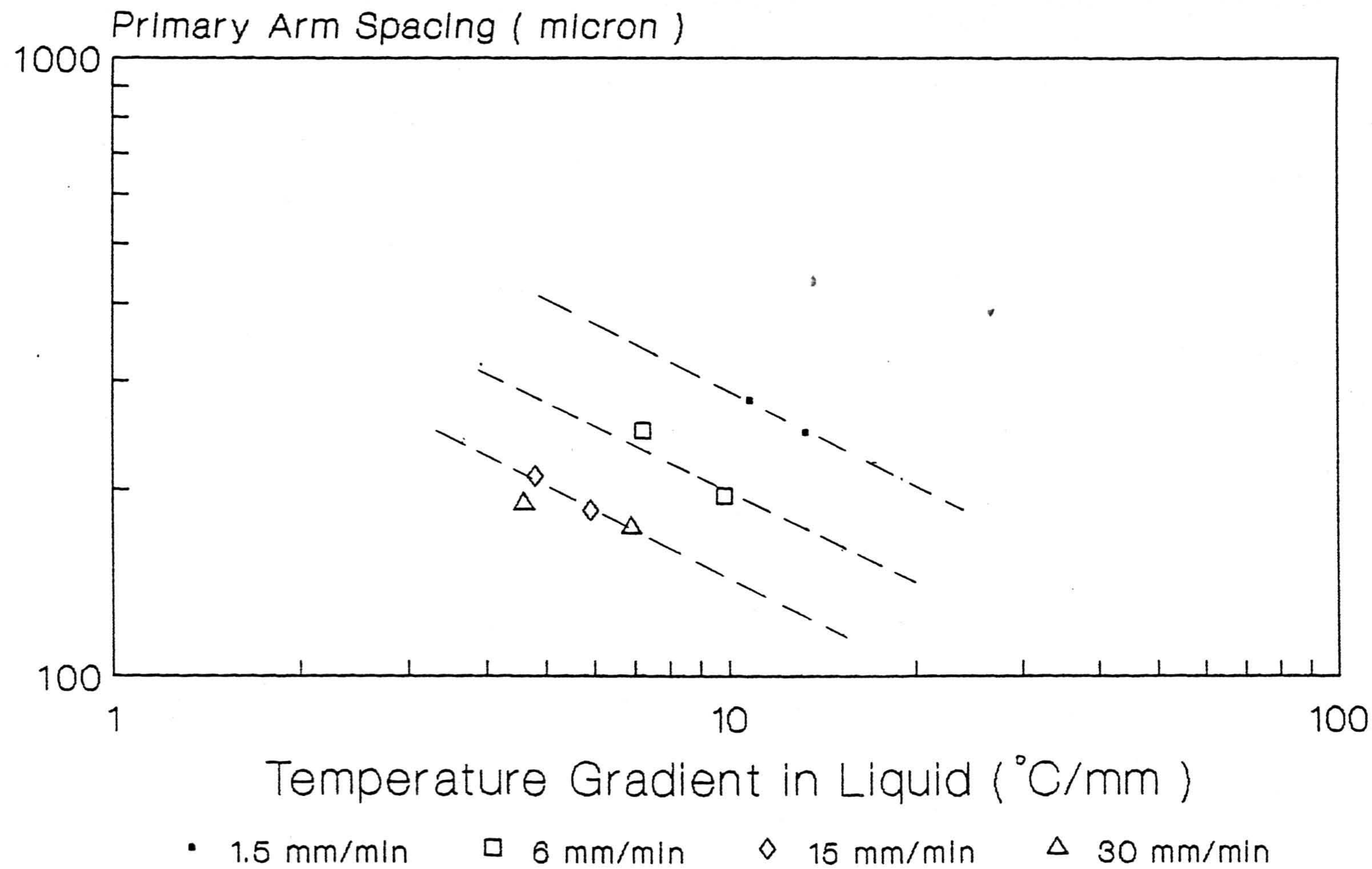
Primary Arm Spacing (micron)
1000
100
1
10
100
Temperature Gradient in Liquid (°C/mm)
1.5 mm/min
6 mm/min
15 mm/min
30 mm/min

0.4 % C

(c)

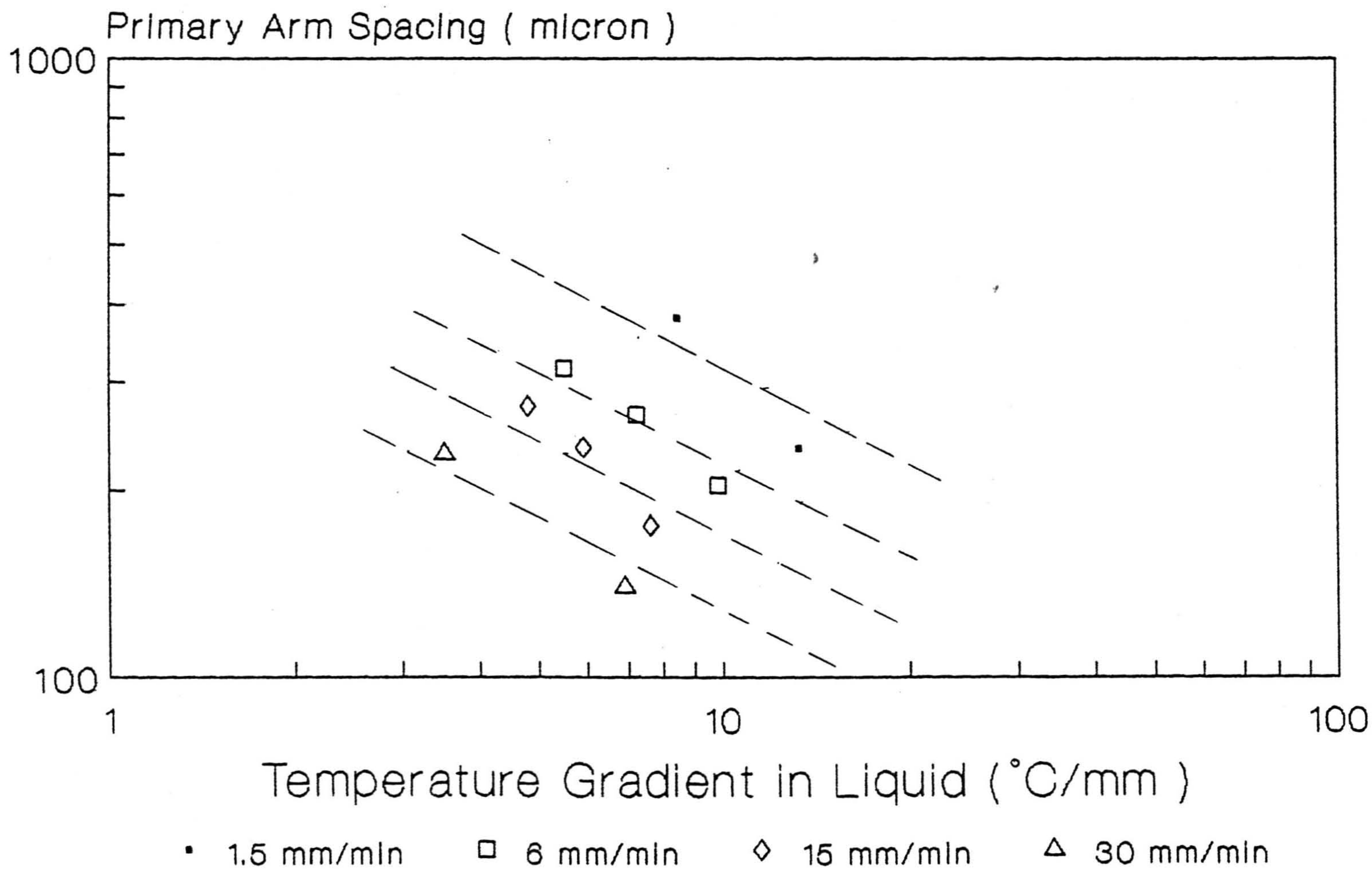
Primary Arm Spacing (micron)
1000
100
1
10
100
Temperature Gradient in Liquid (°C/mm)
1.5 mm/min
6 mm/min
15 mm/min
30 mm/min

0.8 % C

(d)

Figure 40

The change in primary arm spacing as a function of growth rate at the temperature gradient of 5.5 C/mm and 8 C/mm. Data are taken from the straight lines in figure 15-d. Experimental measurements near these gradients are also included on the figure. (0.8 % C - 1.6 % Mn - Fe)

- - - - - - - 0.4 slope

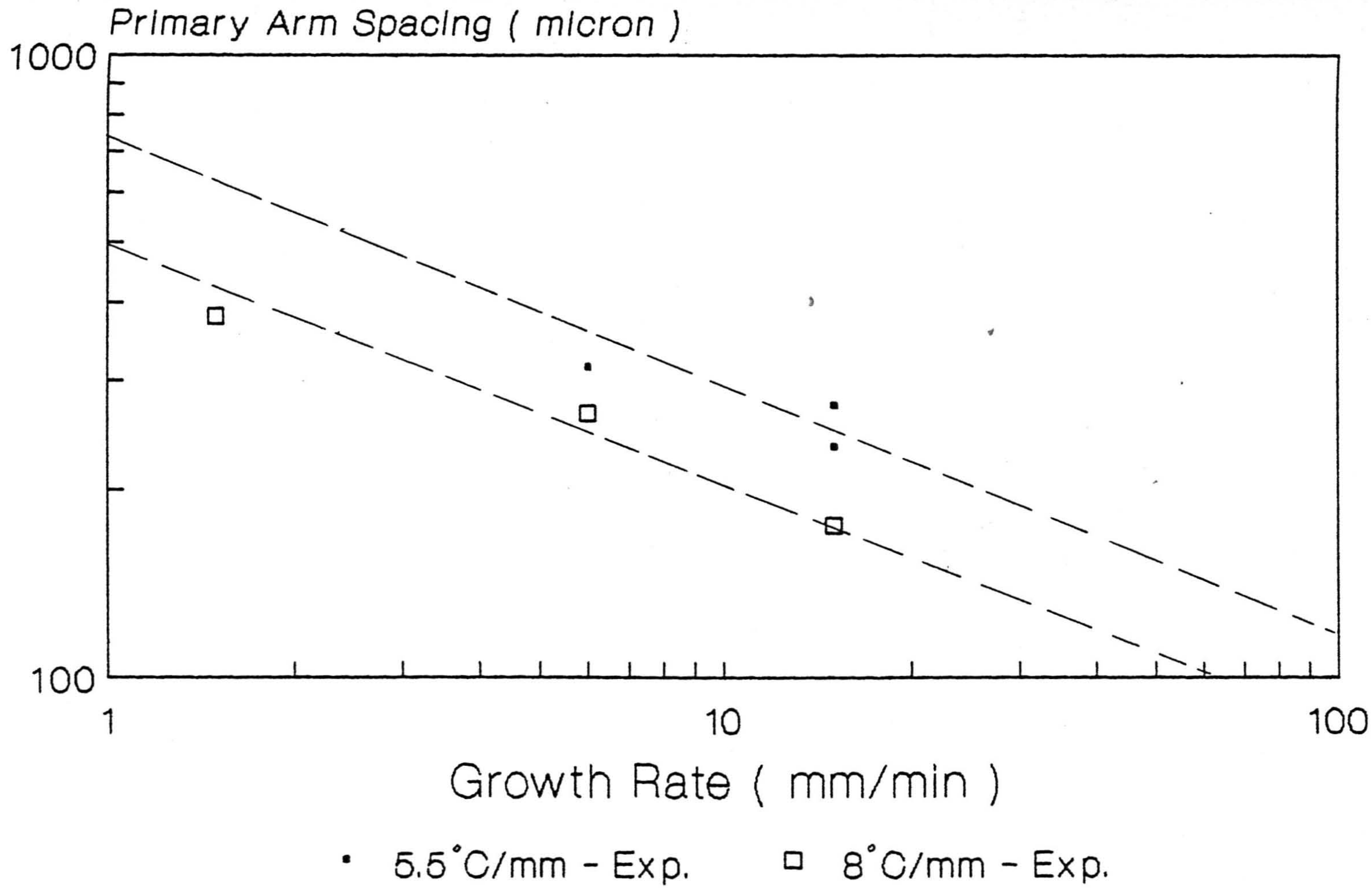
Primary Arm Spacing (micron)
1000
100
1
10
100
Growth Rate (mm/min)
5.5°C/mm - Exp.
8°C/mm - Exp.

0.8 % C

Figure 41

Comparison between theoretical prediction and experimental data for same kind of alloy groups

S-A Jacobi and Schwerdtfeger (46) 0.6 % C - 1.1 % Mn - Fe

S-B Jacobi and Schwerdtfeger (46) 1.5 % C - 1.15 % Mn - Fe

Rickinson (44) 1 % C - 1.4 % Cr - Fe

Turkeli (present work) 0.8 % C - 1.6 % Mn - Fe

Suziki and Nagoaka (43) 0.4 % C - 1 % Cr - 0.25 % Mo - Fe

Edvardsson et al. (48) 0.4 % C - 1.6 % Mn - Fe

Hunt equation prediction for 0.8 % C

Kurz-Fisher equation prediction for 0.8 % C

Trivedi equation prediction for 0.8 % C

Laxmanan's minimum undercooling and stability equation prediction for 0.8 % C

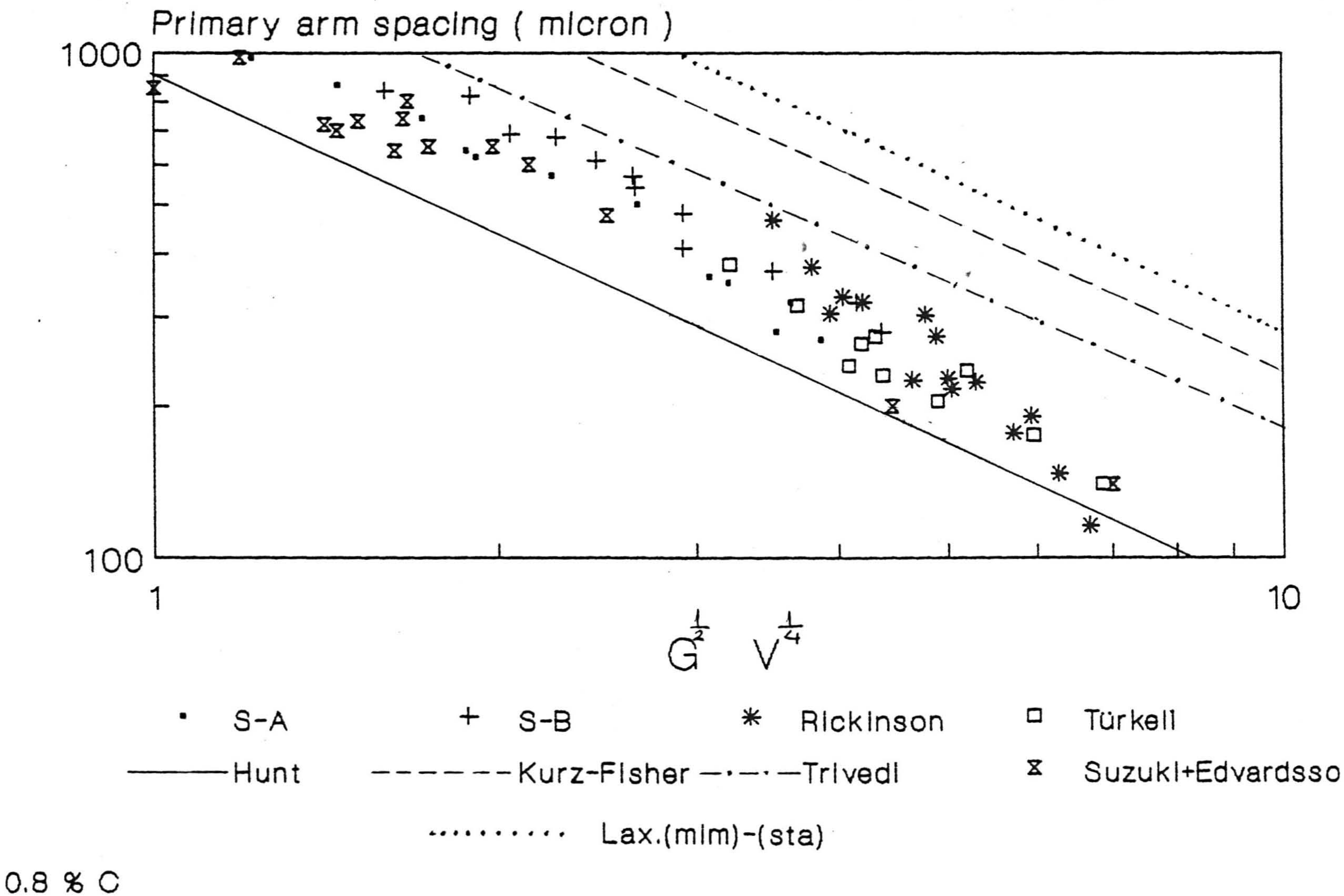
Primary arm spacing (micron)
1000
100
1
10
G^1/2 V^1/4
S-A
S-B
Rickinson
Türkell
Hunt
Kurz-Fisher
Trivedi
Suzuki+Edvardsso
Lax.(mim)-(sta)
0.8 % C

Figure 42

The effect of carbon content and temperature gradient on primary arm spacing for different growth rates

a- 1.5 mm/min

b- 6 mm/mm

c- 15 mm/min

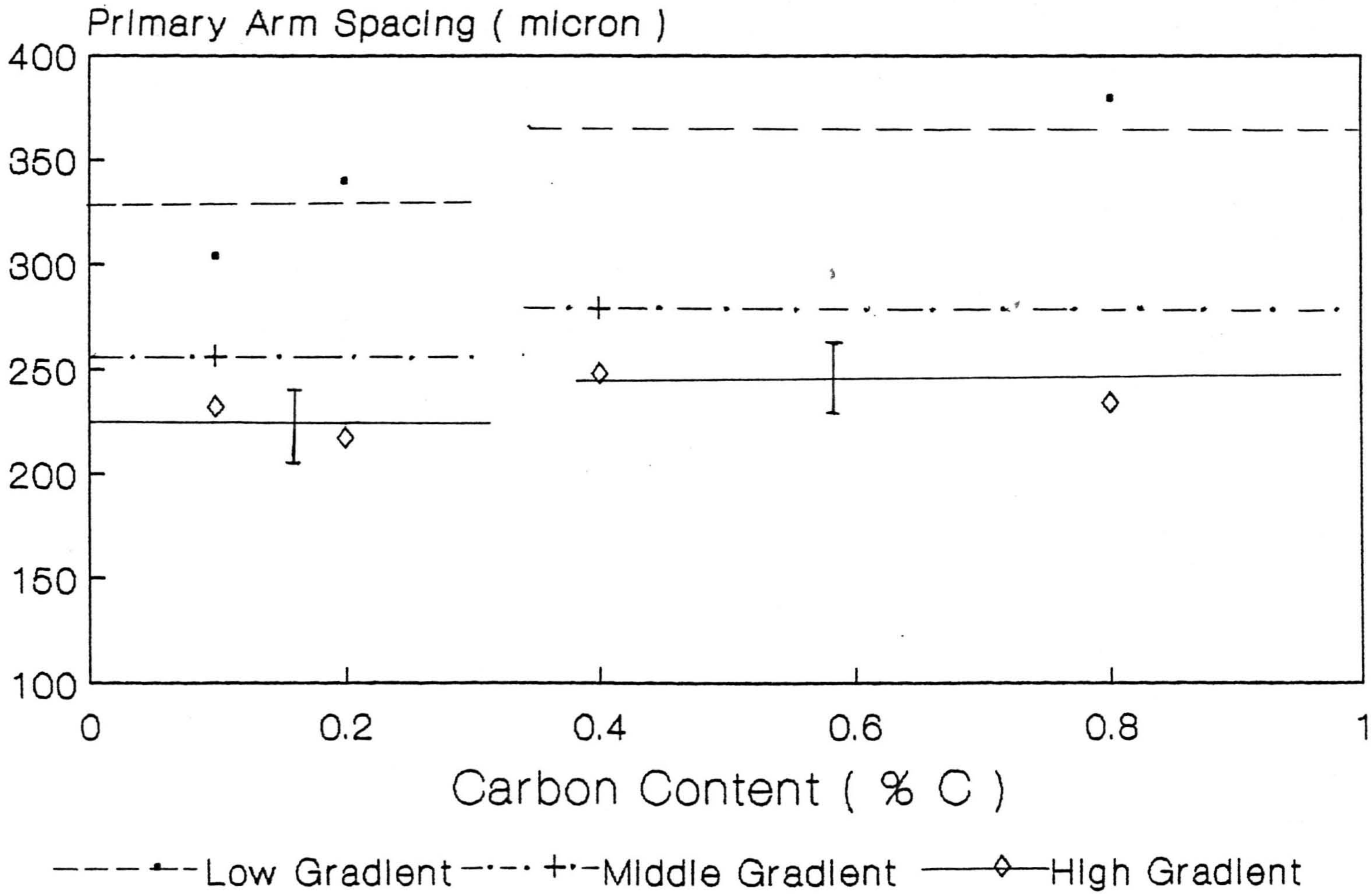
Primary Arm Spacing (micron)
400
350
300
250
200
150
100
0
0.2
0.4
0.6
0.8
1
Carbon Content (% C)
Low Gradient
Middle Gradient
High Gradient

(a)

1.5 mm/min

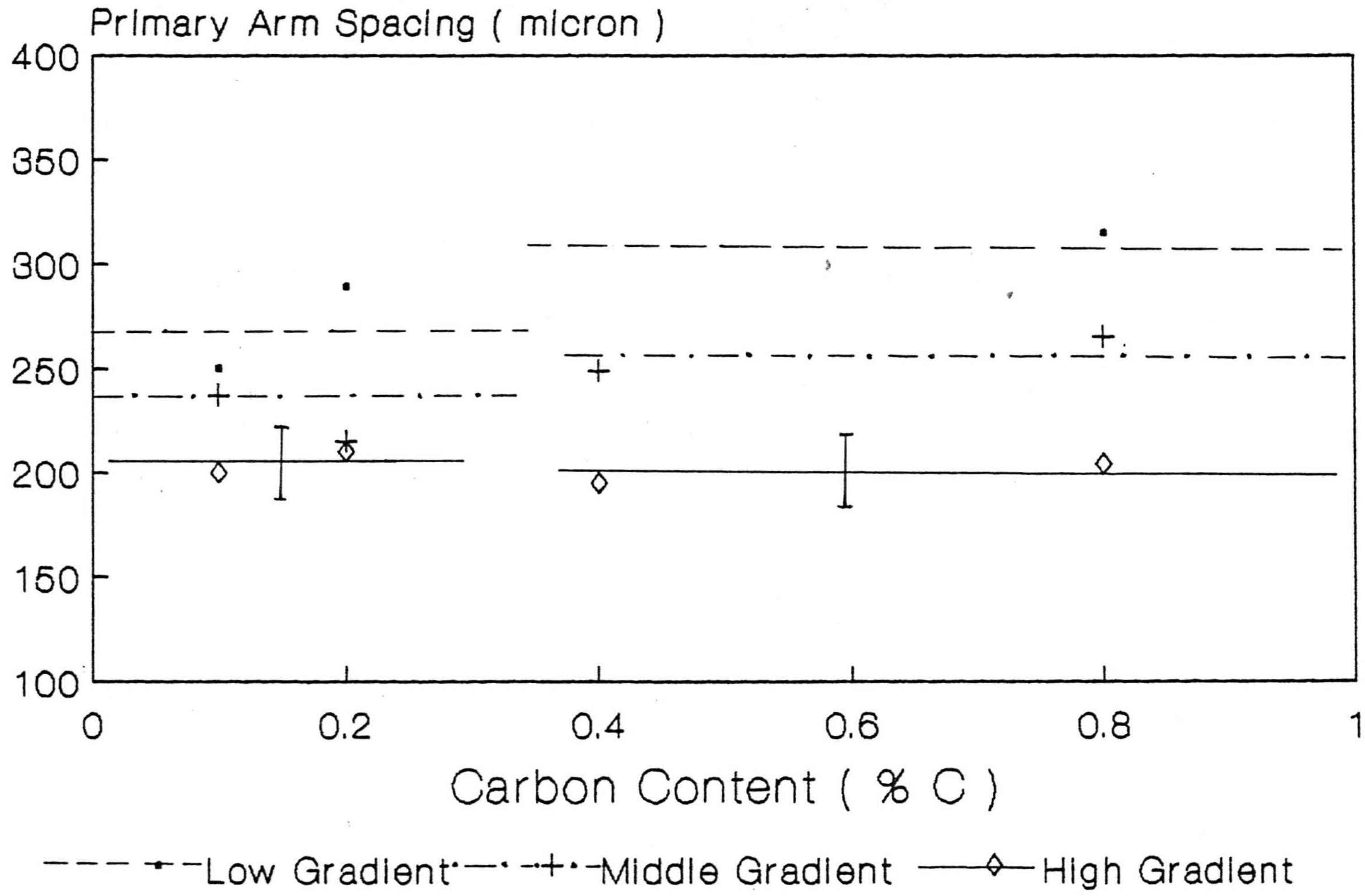

Primary Arm Spacing (micron)
400
350
300
250
200
150
100
0
0.2
0.4
0.6
0.8
1
Carbon Content (% C)
Low Gradient
Middle Gradient
High Gradient

6 mm/min

(b)

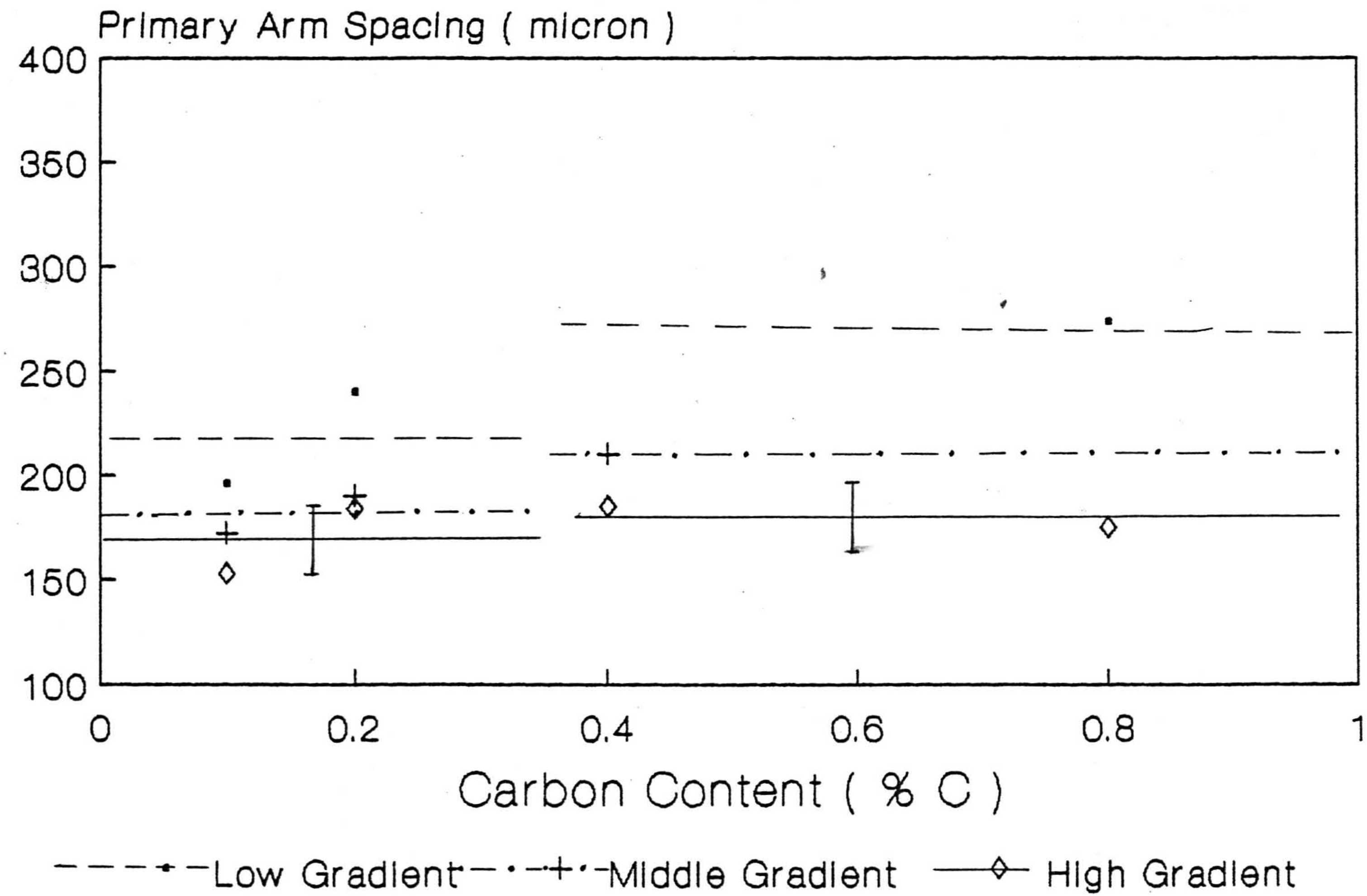

Primary Arm Spacing (micron)
400
350
300
250
200
150
100
0
0.2
0.4
0.6
0.8
1
Carbon Content (% C)
Low Gradient
Middle Gradient
High Gradient

15 mm/min

(c)

Figure 43

Comparison between Hunt equation prediction for 0.8 % C and 0.1 % C and present work data

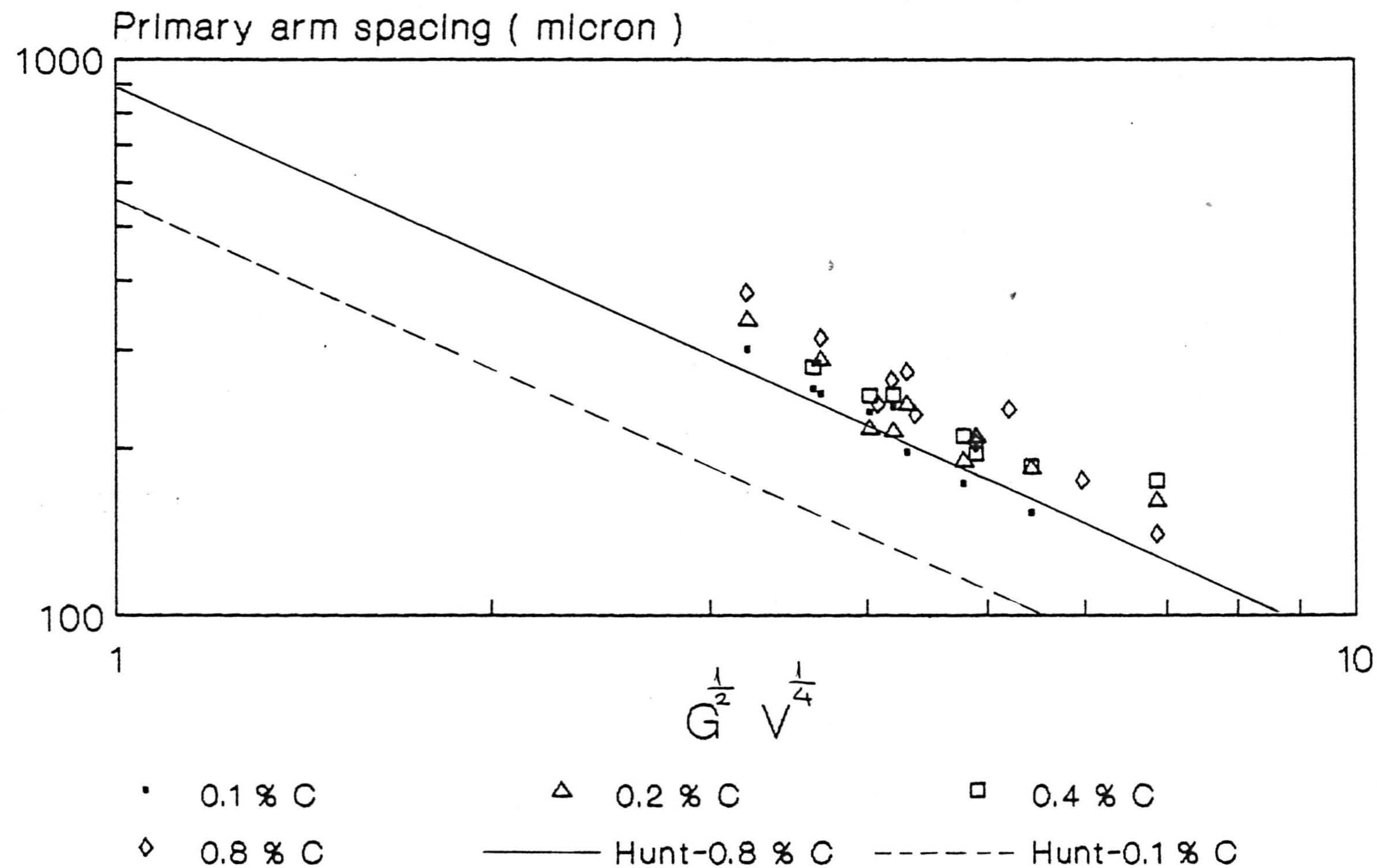

Primary arm spacing (micron)
1000
100
1
10
G^1/2 V^1/4
0.1 % C
0.2 % C
0.4 % C
0.8 % C
Hunt-0.8 % C
Hunt-0.1 % C

Figures 44 to 53

Secondary arm spacing as a function of solidification time for all carbon content and each power series

44) 0.1 % C - 1 series

45) 0.1 % C - 2 series

46) 0.2 % C - 1 series

47) 0.2 % C - 2 series

48) 0.2 % C - 3 series

49) 0.4 % C - 2 series

50) 0.4 % C - 3 series

51) 0.8 % C - 1 series

52) 0.8 % C - 2 series

53) 0.8 % C - 3 series

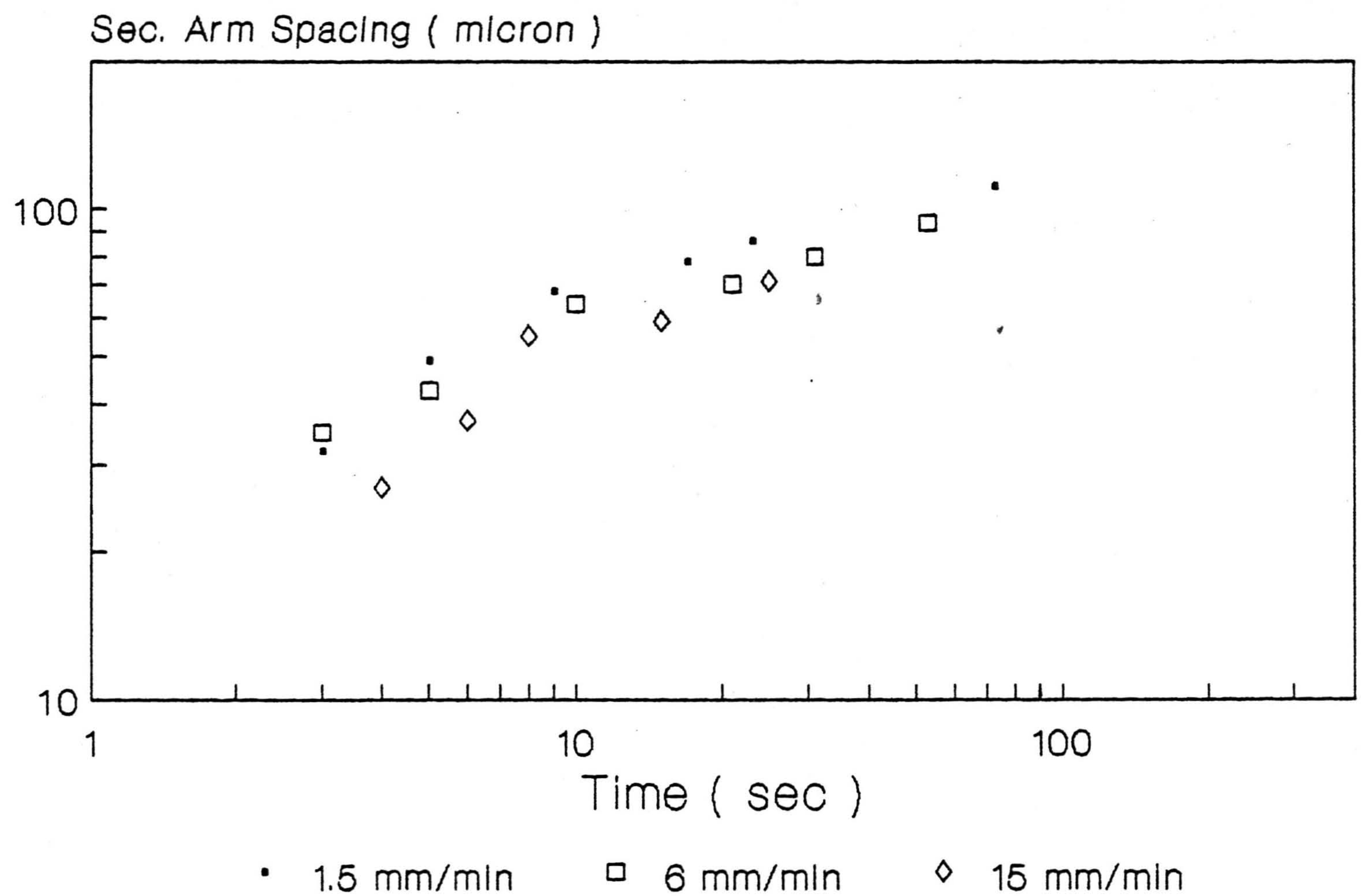

Sec. Arm Spacing (micron)
100
10
1
10
100
Time (sec)
1.5 mm/min
6 mm/min
15 mm/min

Figure 44

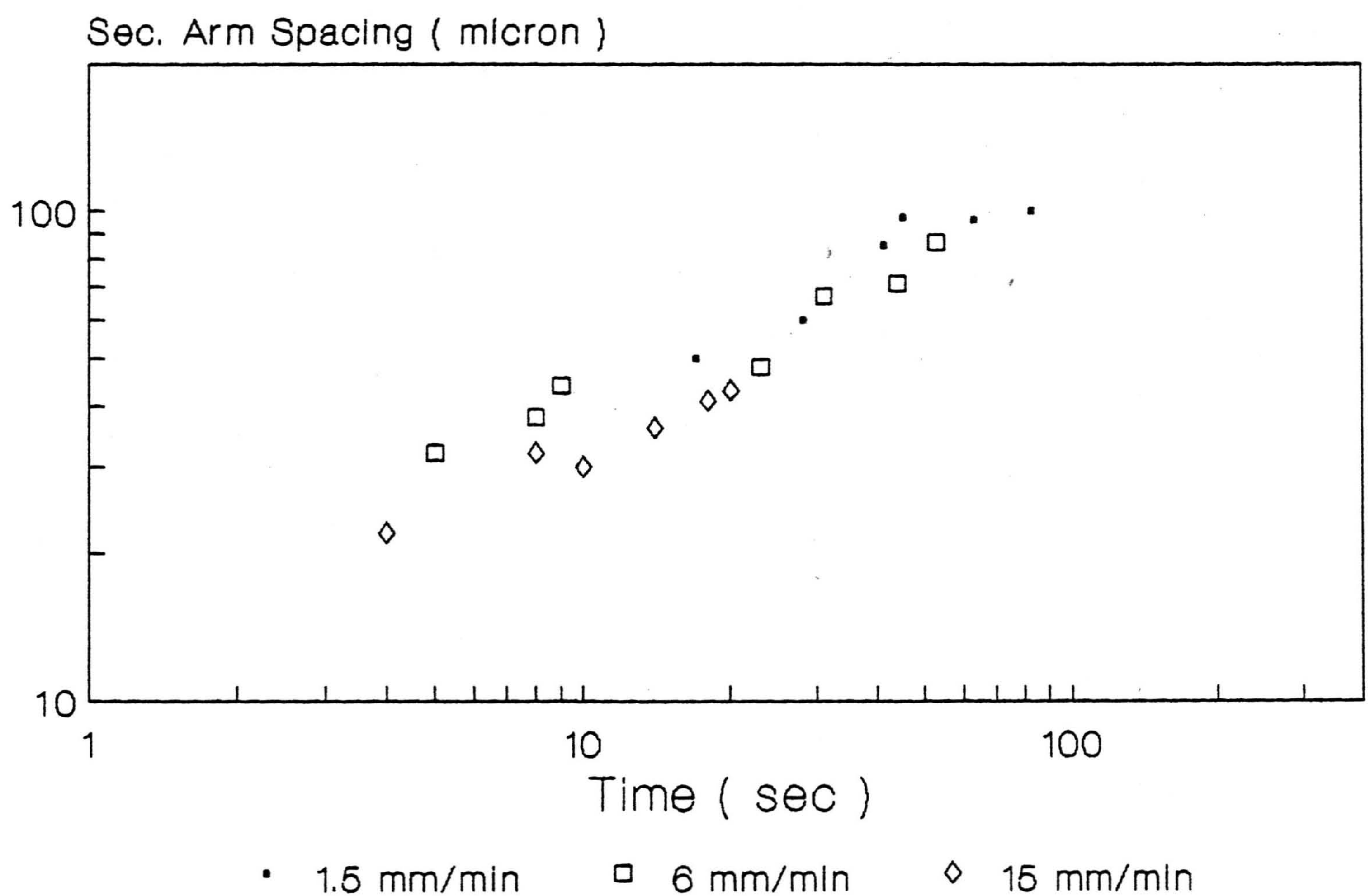
Sec. Arm Spacing (micron)
100
10
1
10
100
Time (sec)
1.5 mm/min
6 mm/min
15 mm/min

Figure 45

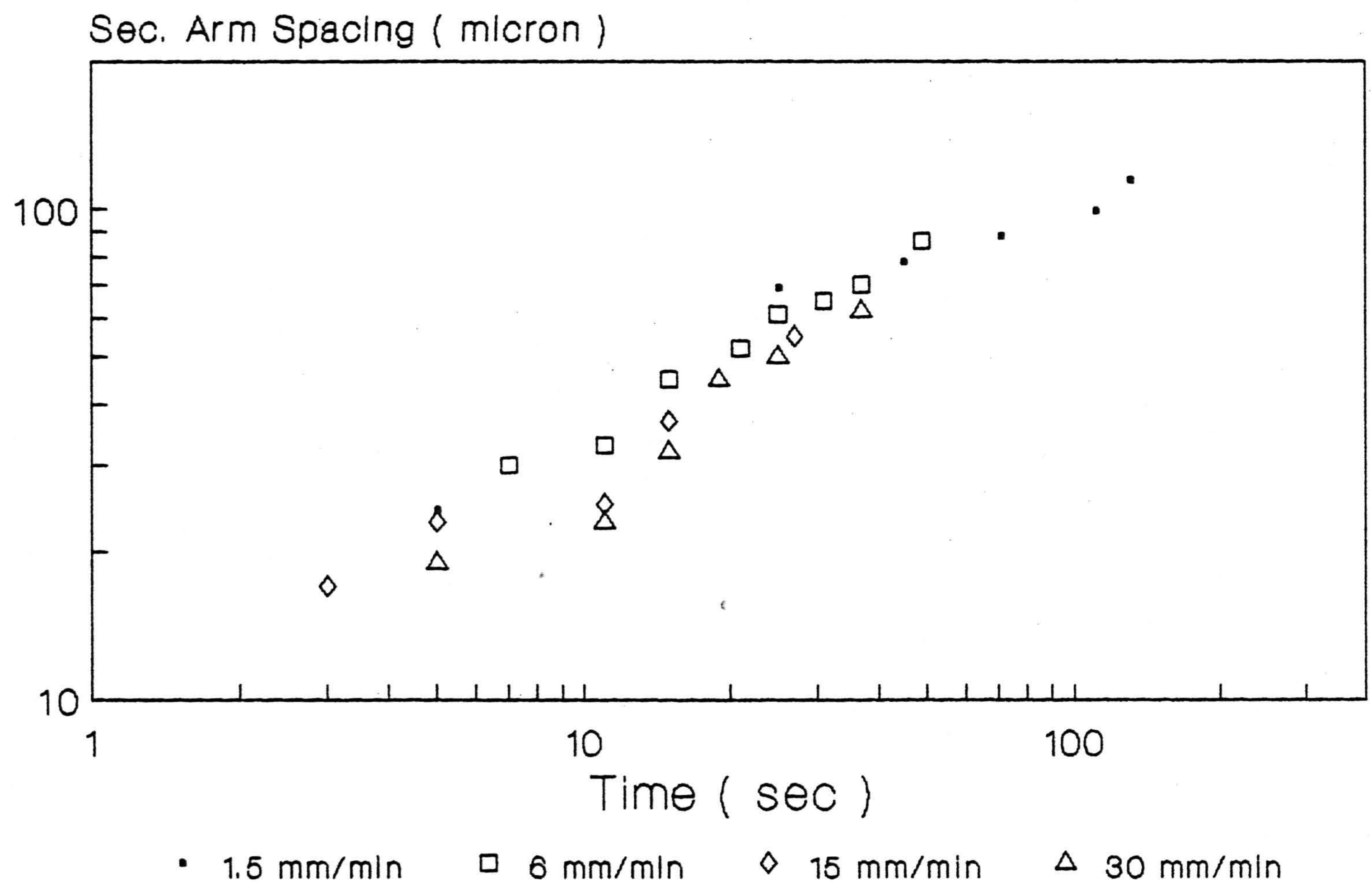

Sec. Arm Spacing (micron)
100
10
1
10
100
Time (sec)
1.5 mm/min
6 mm/min
15 mm/min
30 mm/min

Figure 46

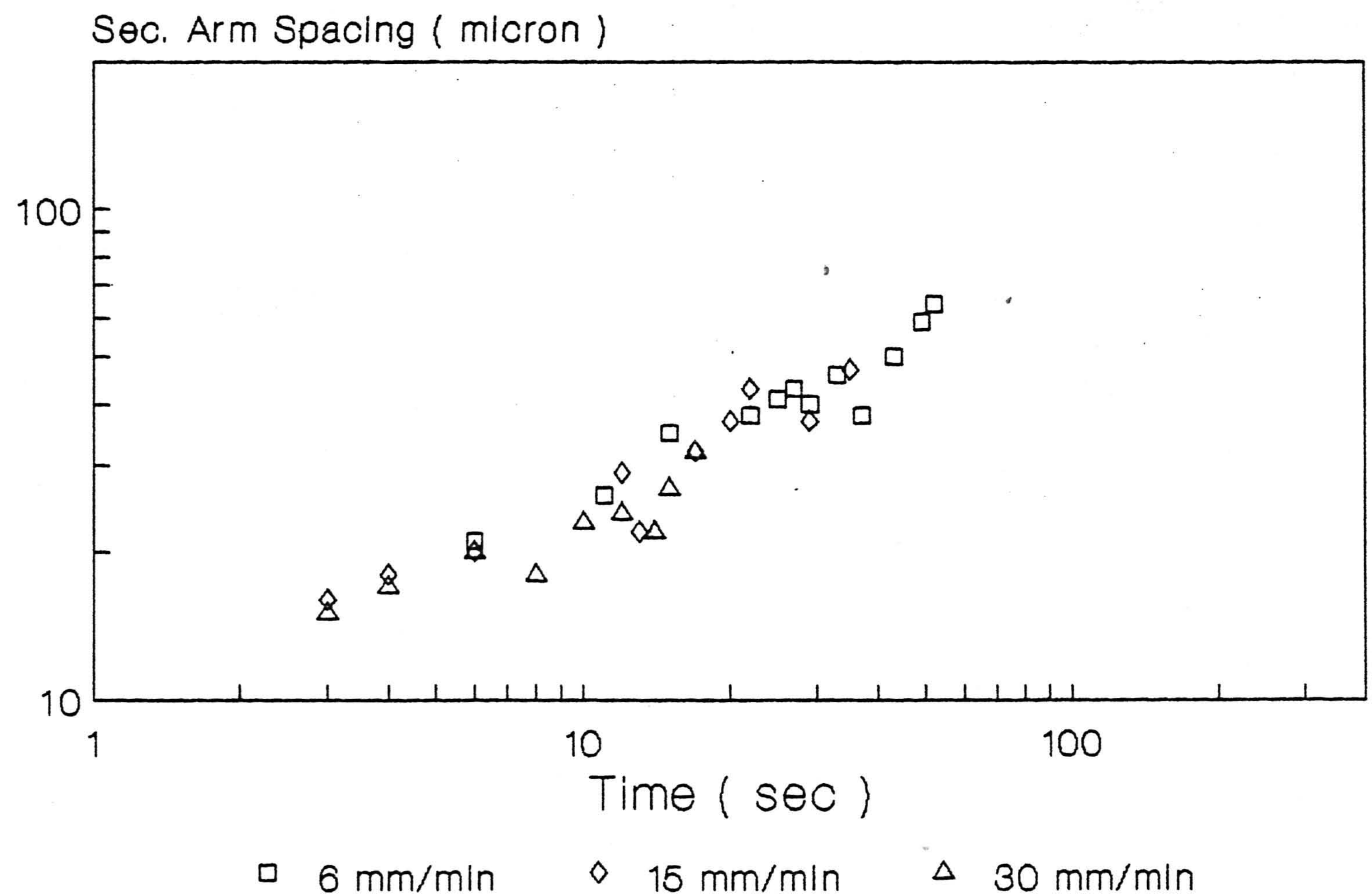
Sec. Arm Spacing (micron)
100
10
1
10
100
Time (sec)
6 mm/min
15 mm/min
30 mm/min

Figure 47

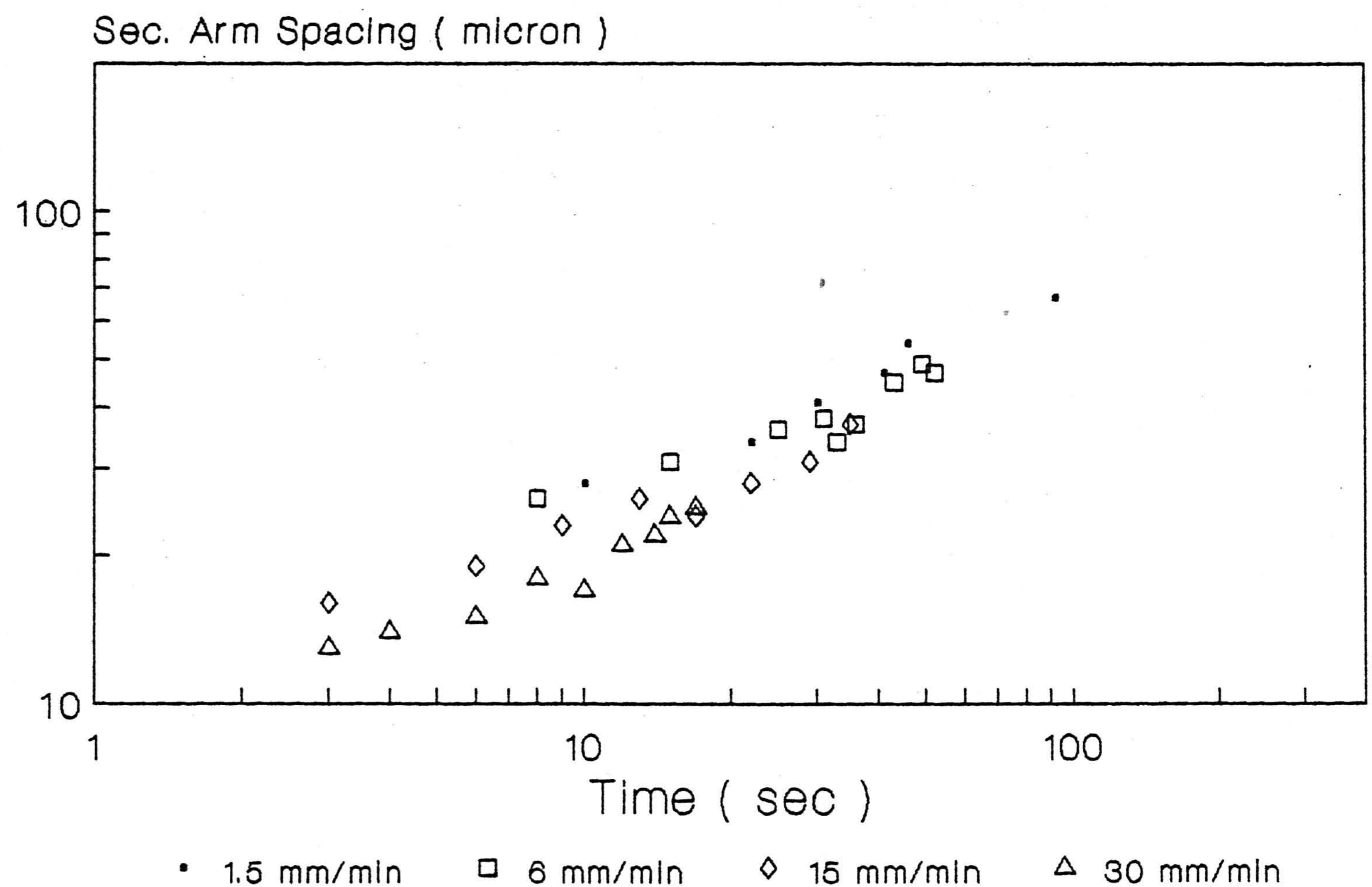

Sec. Arm Spacing (micron)
100
10
1
10
100
Time (sec)
1.5 mm/min
6 mm/min
15 mm/min
30 mm/min

Figure 48

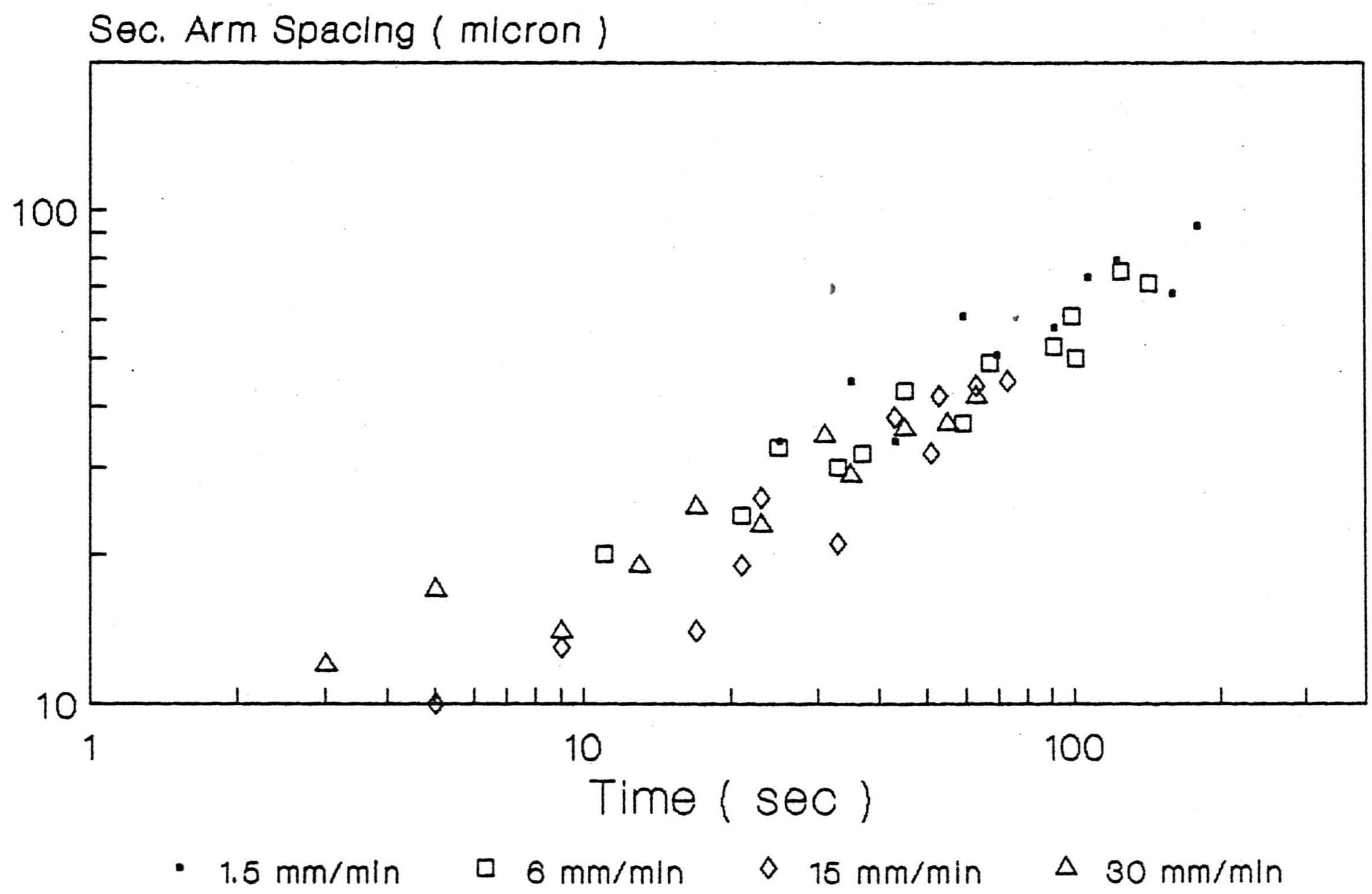

Sec. Arm Spacing (micron)
100
10
1
10
100
Time (sec)
1.5 mm/min
6 mm/min
15 mm/min
30 mm/min

Figure 49

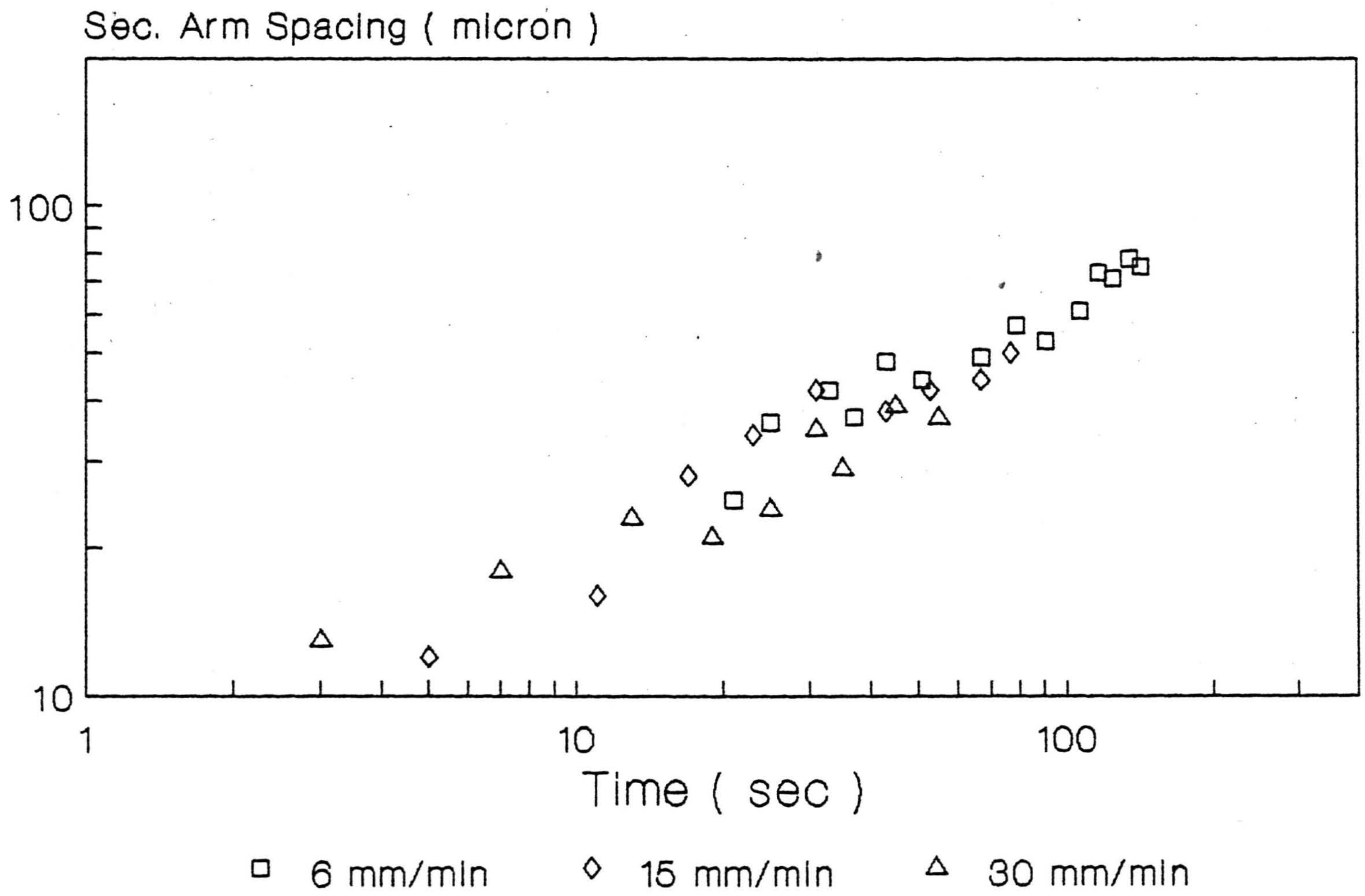
Sec. Arm Spacing (micron)
100
10
1
10
100
Time (sec)
6 mm/min
15 mm/min
30 mm/min

Figure 50

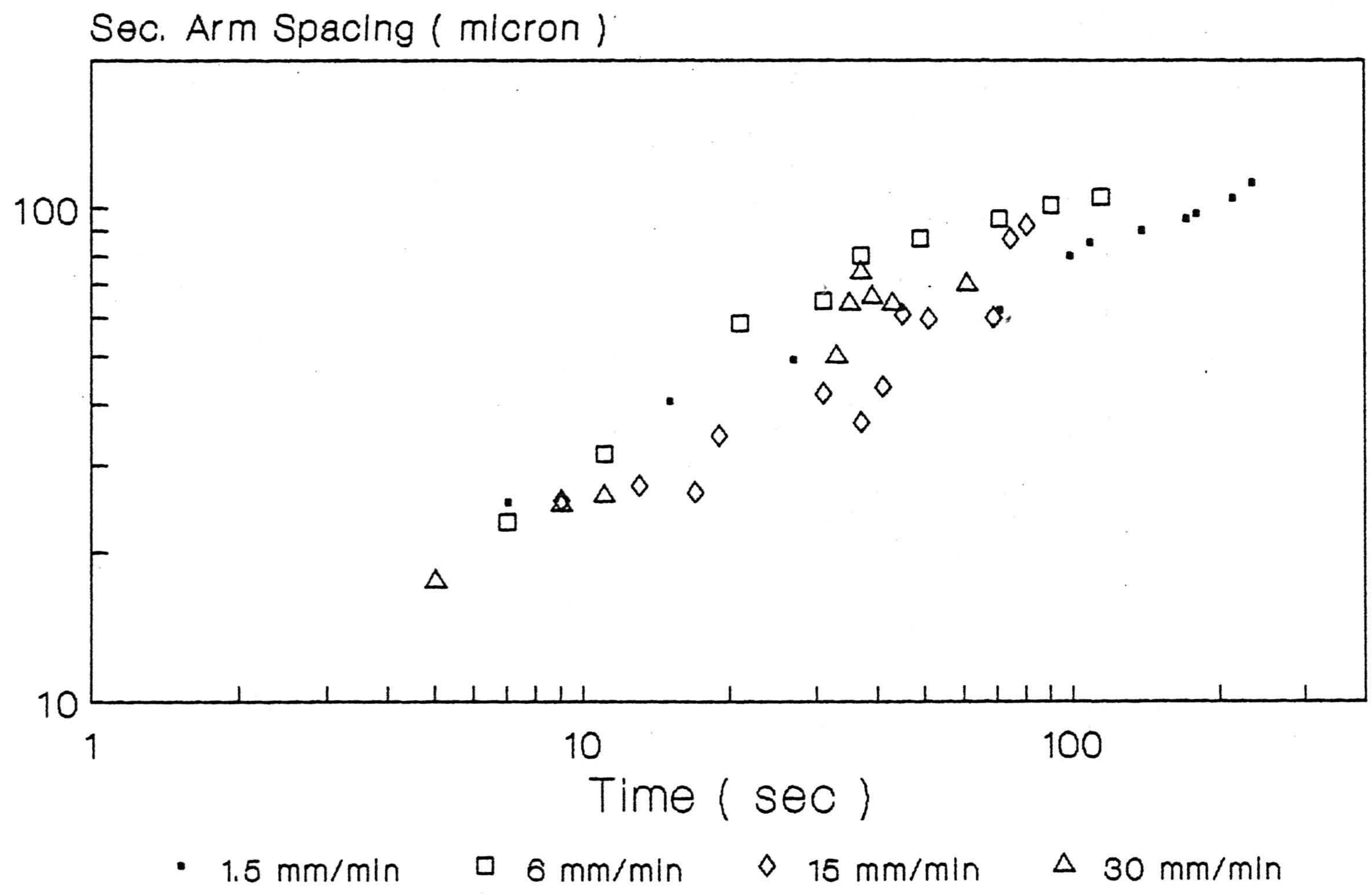
Sec. Arm Spacing (micron)
100
10
1
10
100
Time (sec)
1.5 mm/min
6 mm/min
15 mm/min
30 mm/min

Figure 51

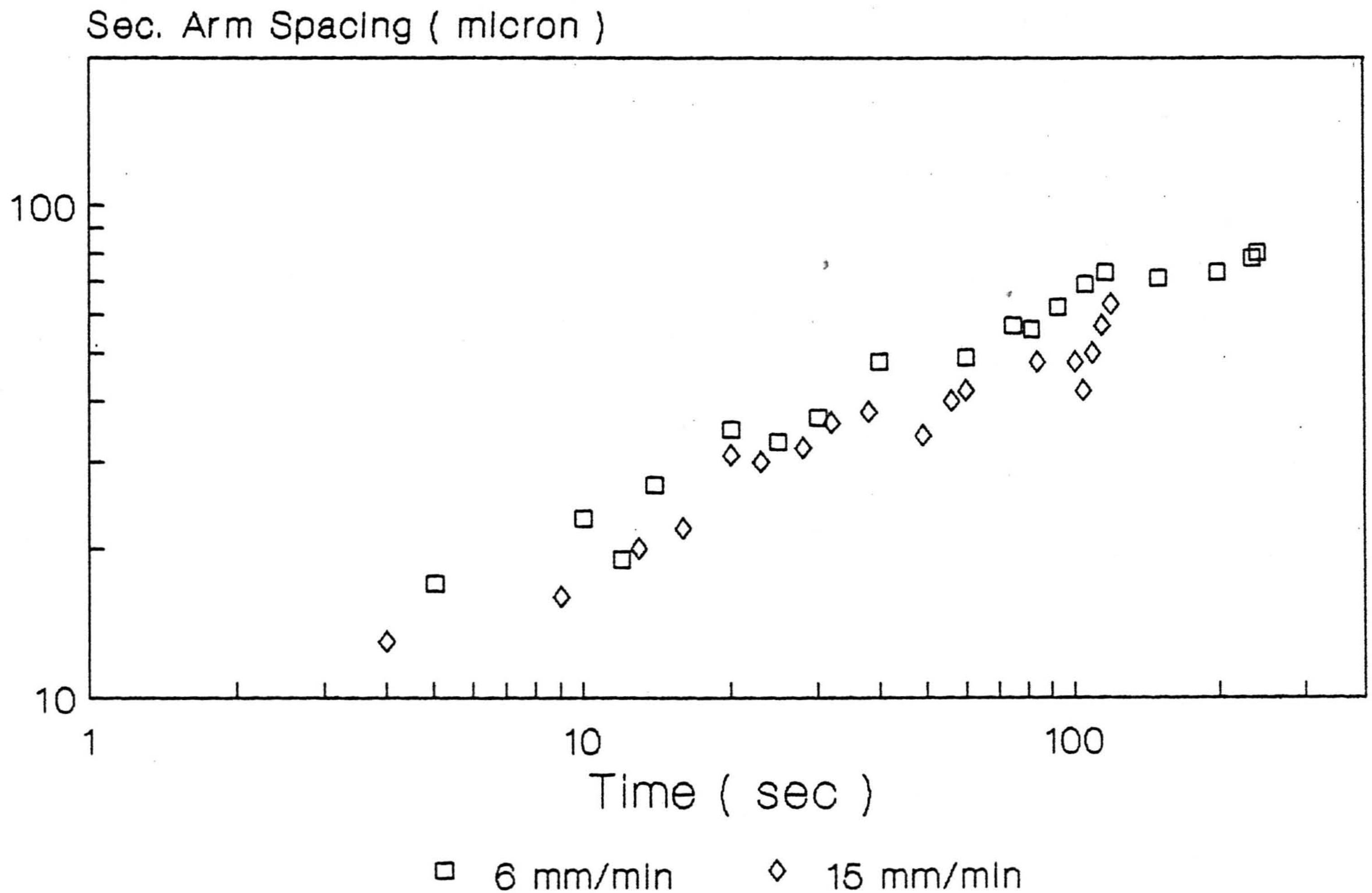
Sec. Arm Spacing (micron)
100
10
1
10
100
Time (sec)
6 mm/min
15 mm/min

Figure 52

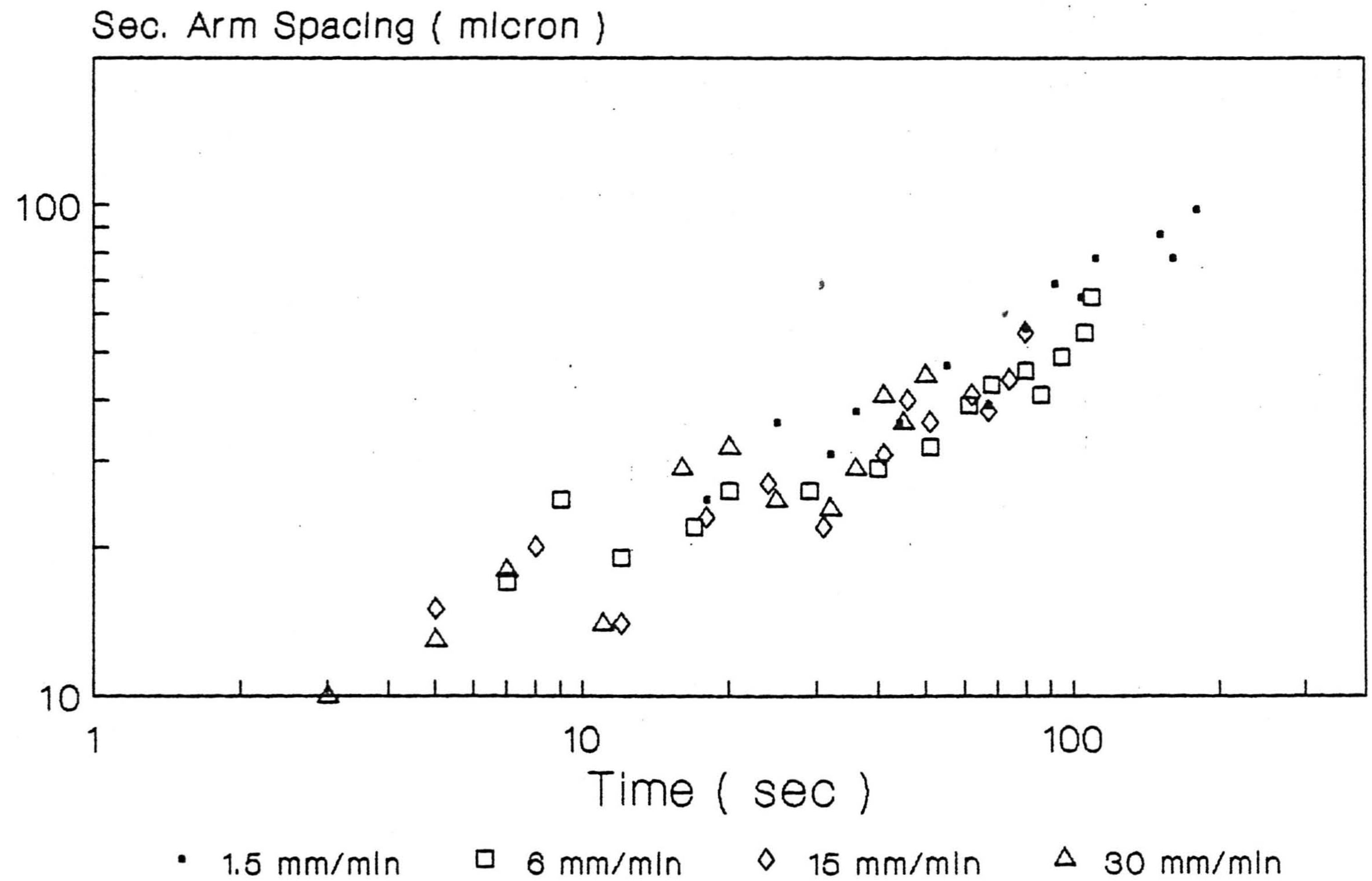
Sec. Arm Spacing (micron)
100
10
1
10
100
Time (sec)
1.5 mm/min
6 mm/min
15 mm/min
30 mm/min

Figure 53

Figure 54

Typical longitudinal sections of secondary arms. Hardness indentation show the chosen electron micro-probe analyse lines through and perpendicular to the secondary arms

0.8 % C - 1.6 % Mn - Fe

Magnification 51.3

a- 0.9 mm behind tips

b- 2 mm behind tips

c- 3.8 mm behind tips

d- 6 mm behind tips

e- 26 mm behind tips

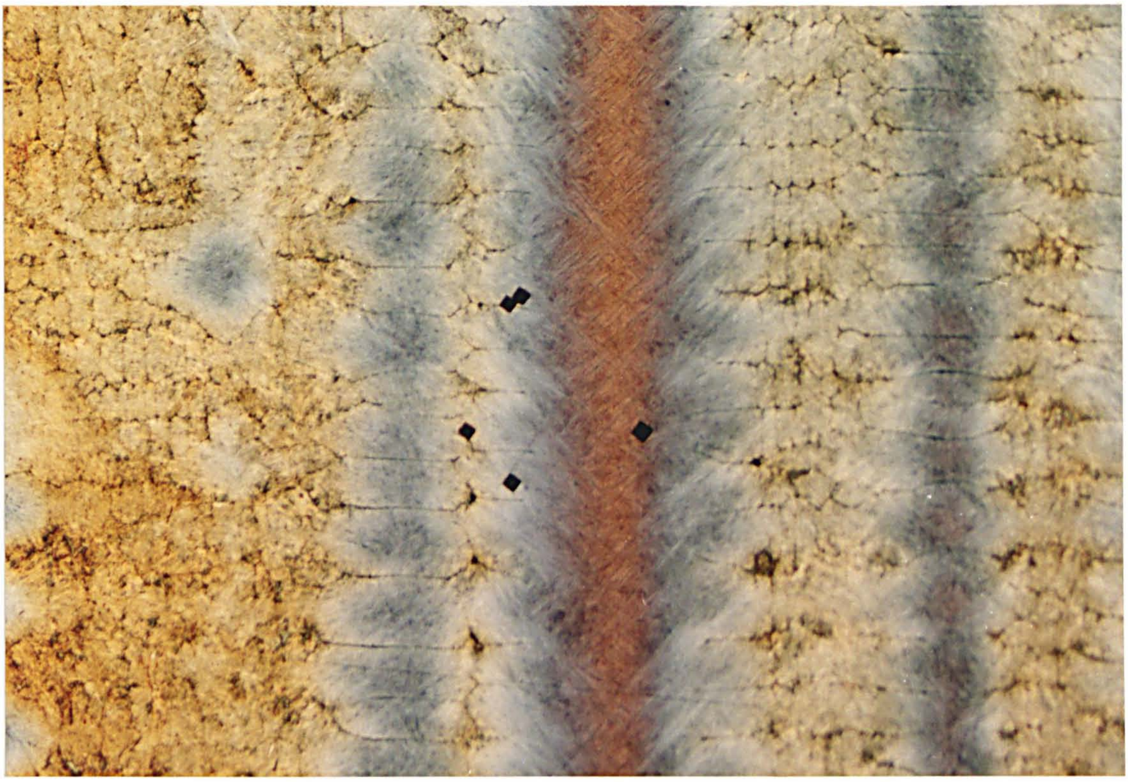

(a)

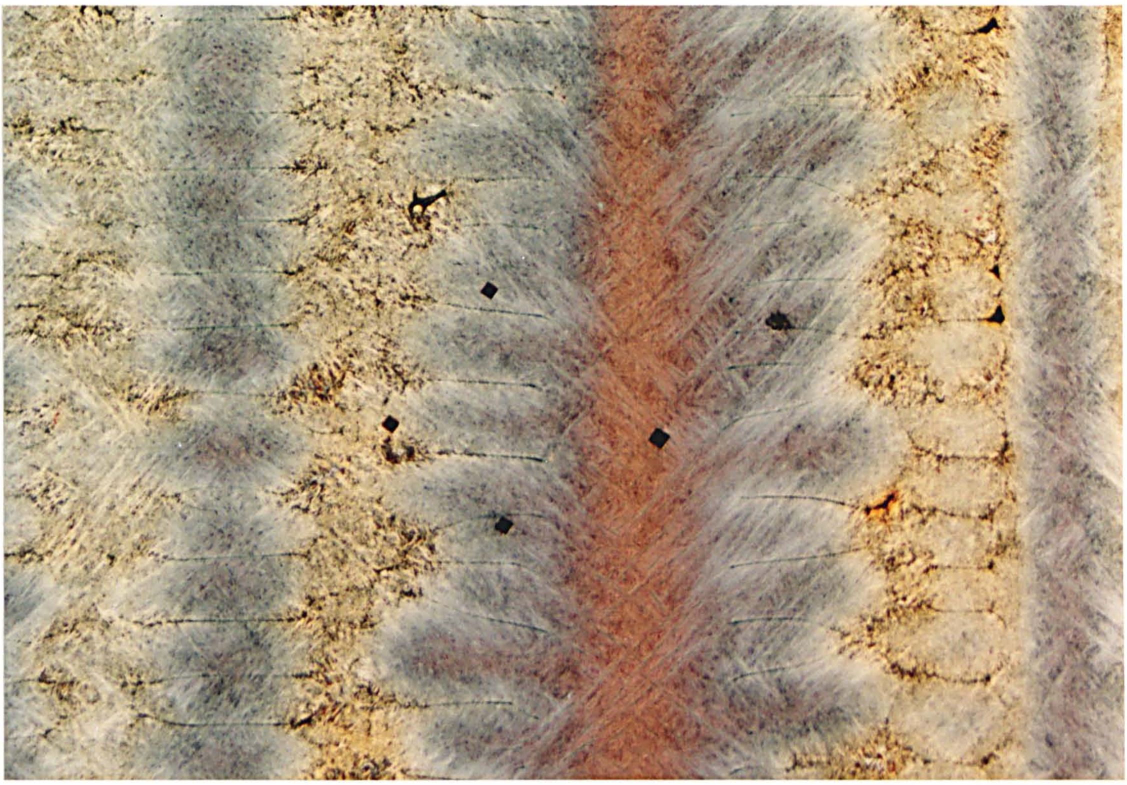

(b)

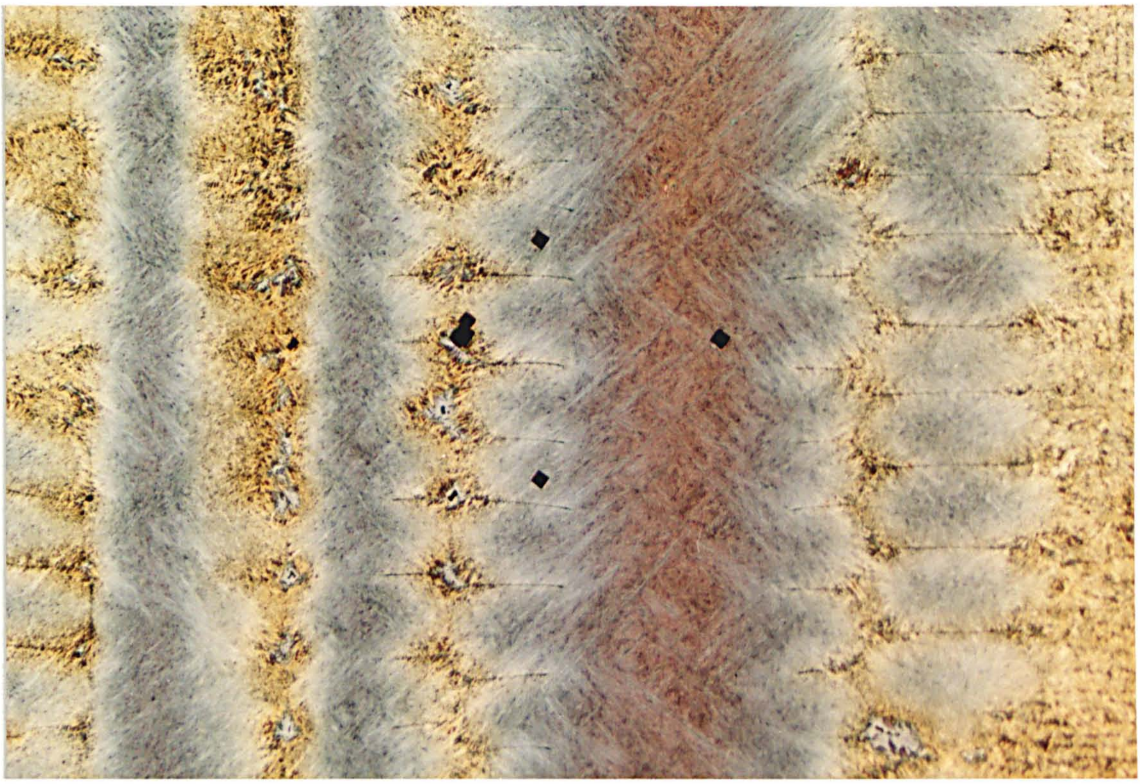

(c)

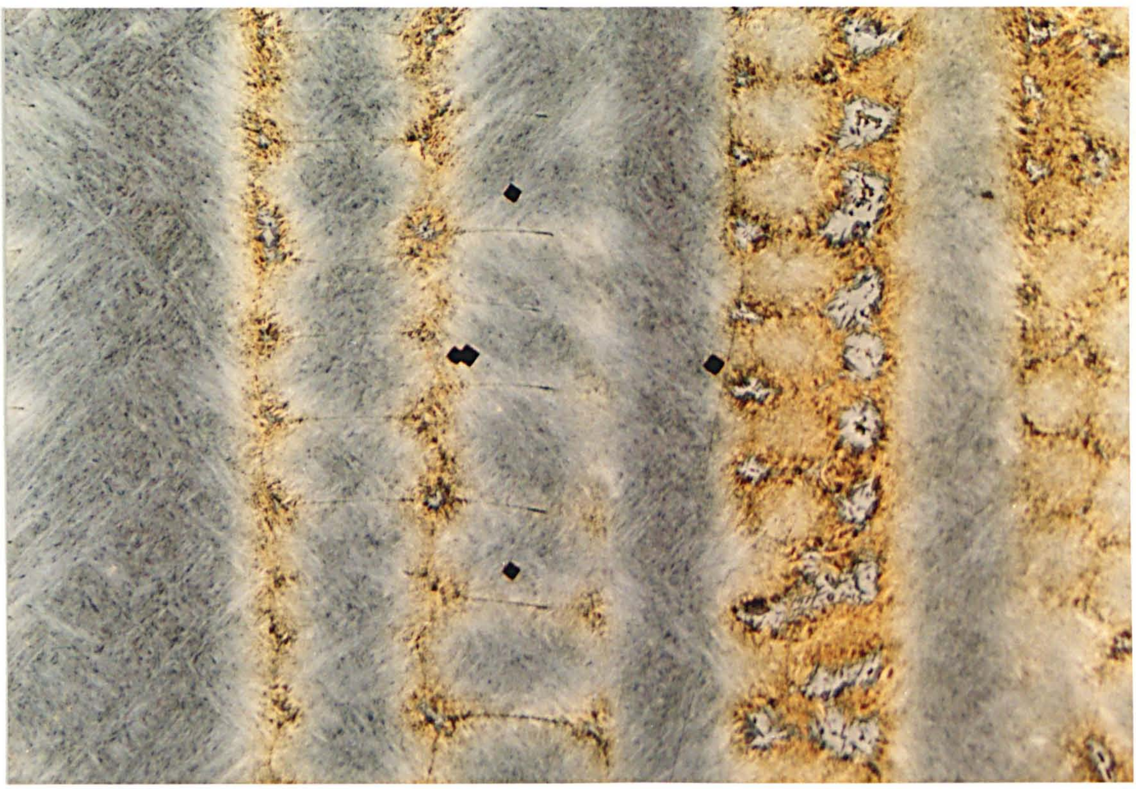

(d)

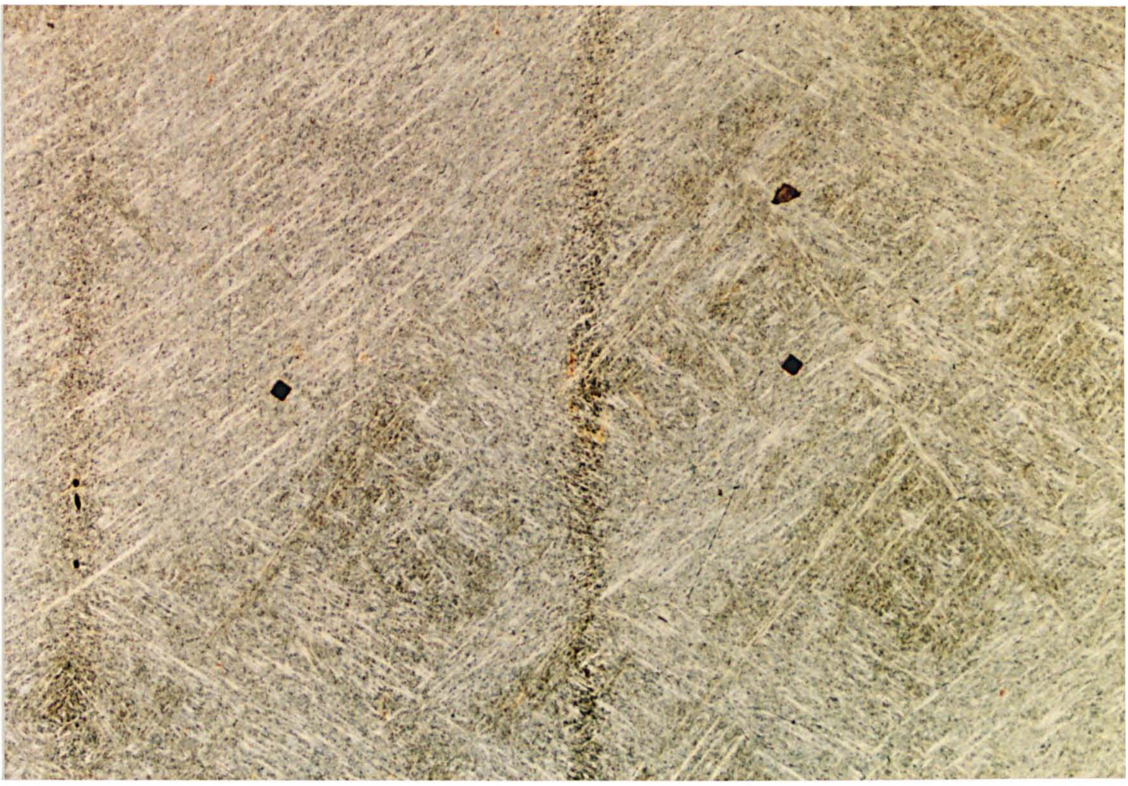

(e)

Figure 55

The change of Cmin as a function of temperature below liquidus and growth rate for 0.1 % C - 1.6 % Mn - Fe alloy

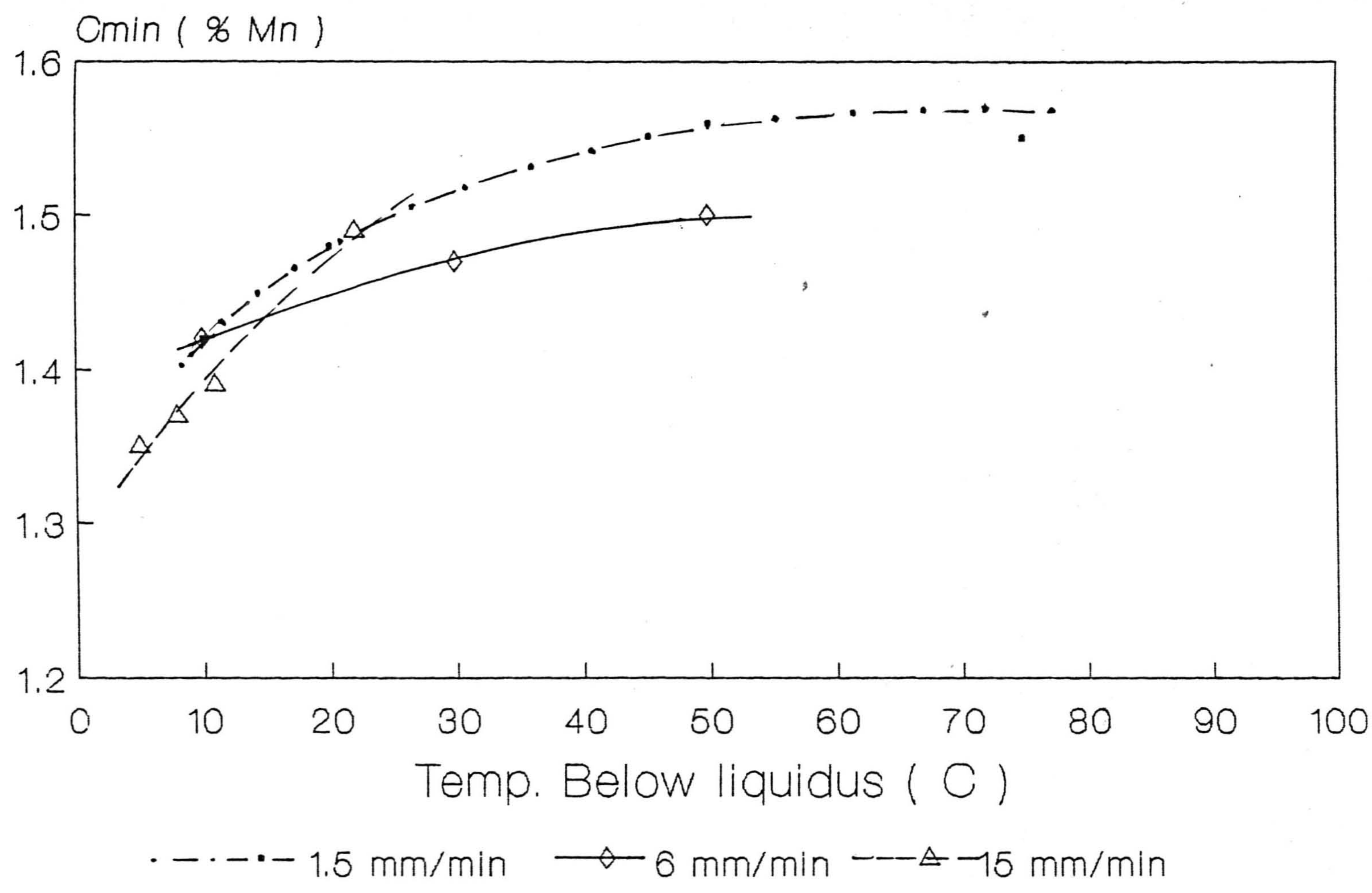

Cmin (% Mn)
1.6
1.5
1.4
1.3
1.2
0
10
20
30
40
50
60
70
80
90
100
Temp. Below liquidus (C)
1.5 mm/min
6 mm/min
15 mm/min

0.1 % C

Figure 56

The change in Cmin as a function of temperature below liquidus and growth rate for 0.2 % C - 1.6 % Mn - Fe alloy

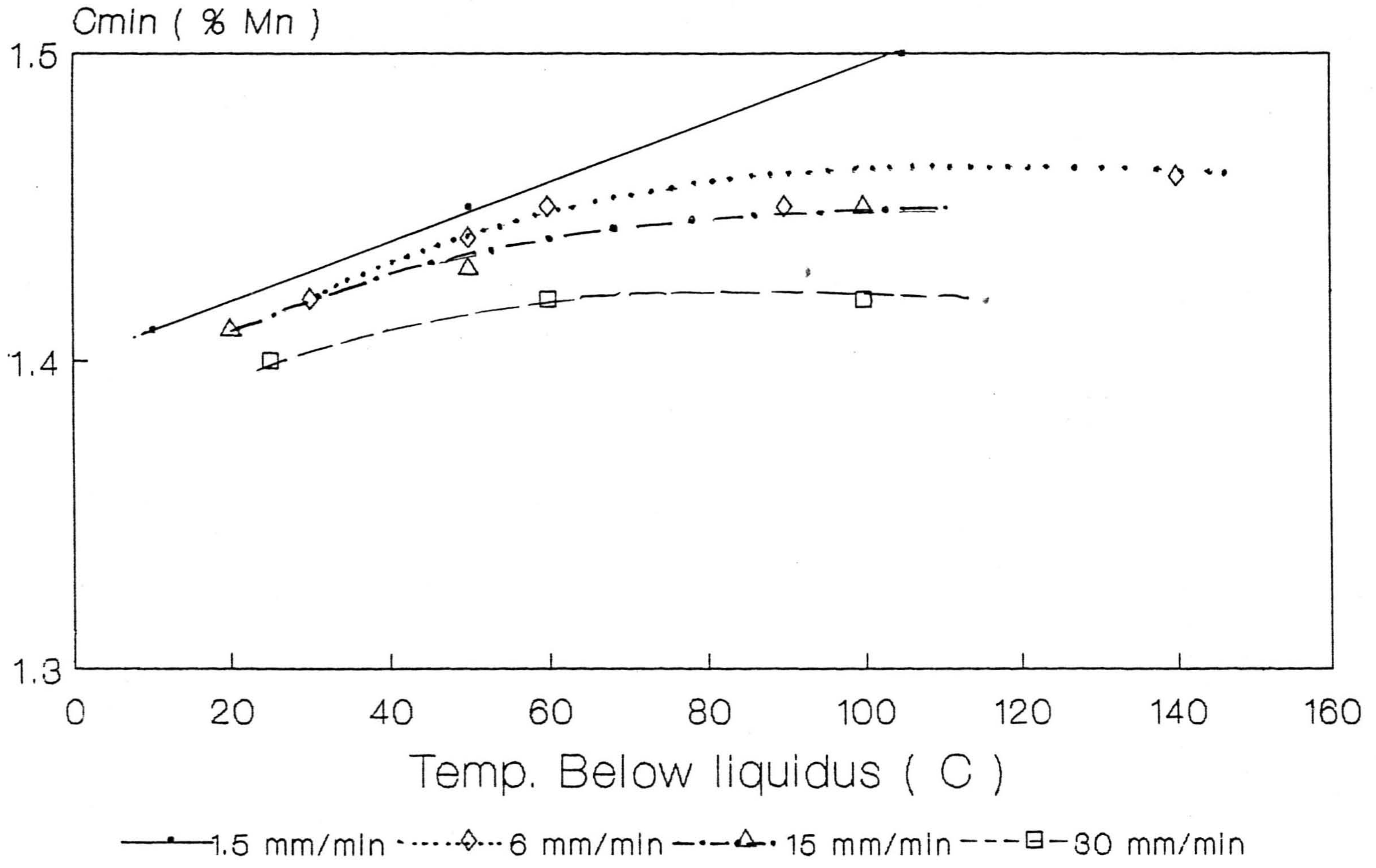
Cmin (% Mn)
1.5
1.4
1.3
0
20
40
60
80
100
120
140
160
Temp. Below liquidus (C)
1.5 mm/min
6 mm/min
15 mm/min
30 mm/min

0.2 % C

Figure 57

The change of Cmin as a function of temperature below liquidus and gradient in liquid for 0.2 % C - 1.6 % Mn - Fe alloy at 30 mm/min

Low Gradient	3.5 C/mm
Middle Gradient	4.6 C/mm
High Gradient	6.9 C/mm

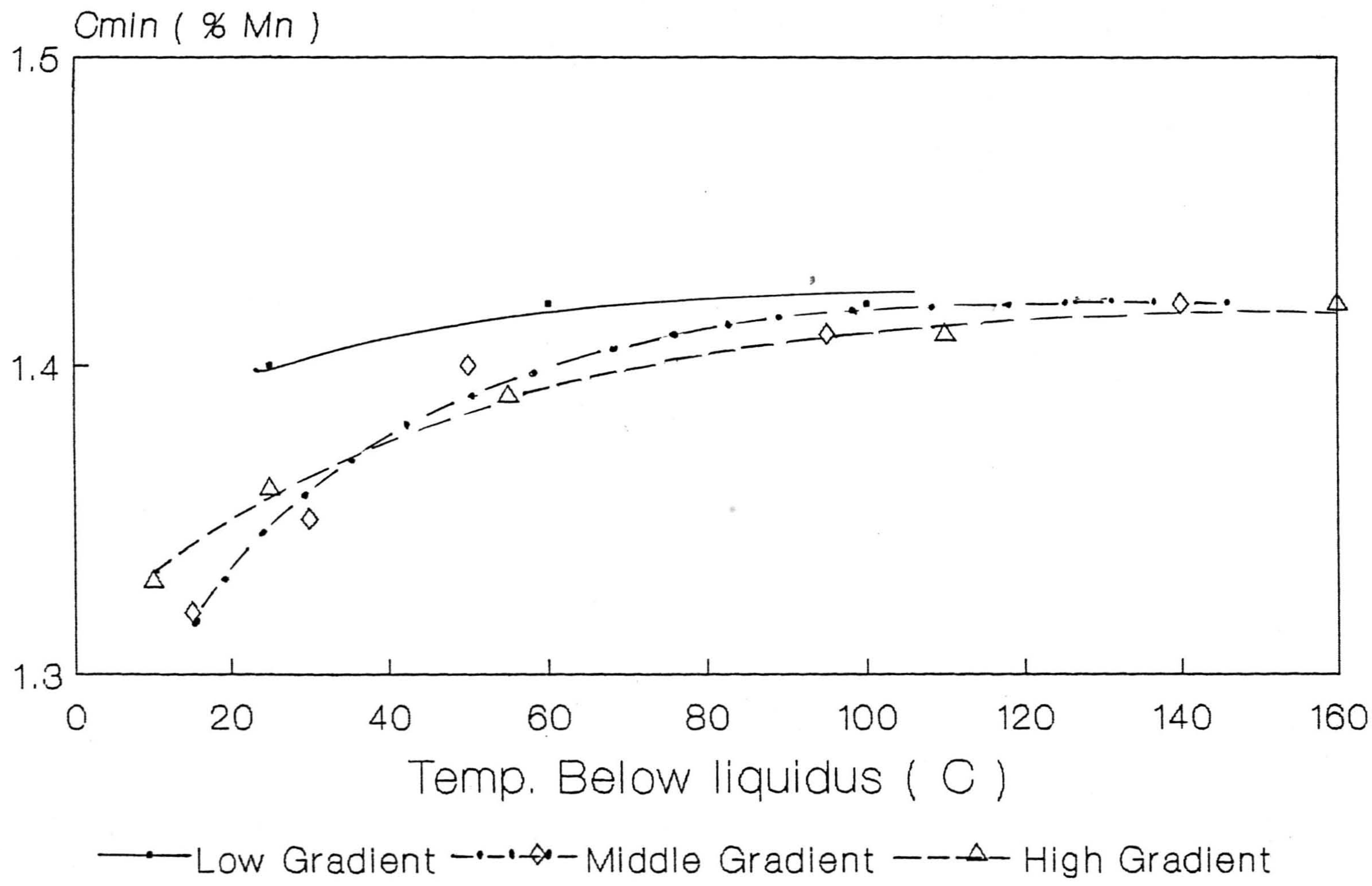
Cmin (% Mn)
1.5
1.4
1.3
0
20
40
60
80
100
120
140
160
Temp. Below liquidus (C)
Low Gradient
Middle Gradient
High Gradient

0.2 % C - 30 mm/min

Figure 58

The change of Cmin as a function of temperature below liquidus and gradient in liquid for 0.2 % C - 1.6 % Mn - Fe alloy at 6 mm/min

Low Gradient	5.5 C/mm
Middle Gradient	7.2 C/mm
High Gradient	9.8 C/mm

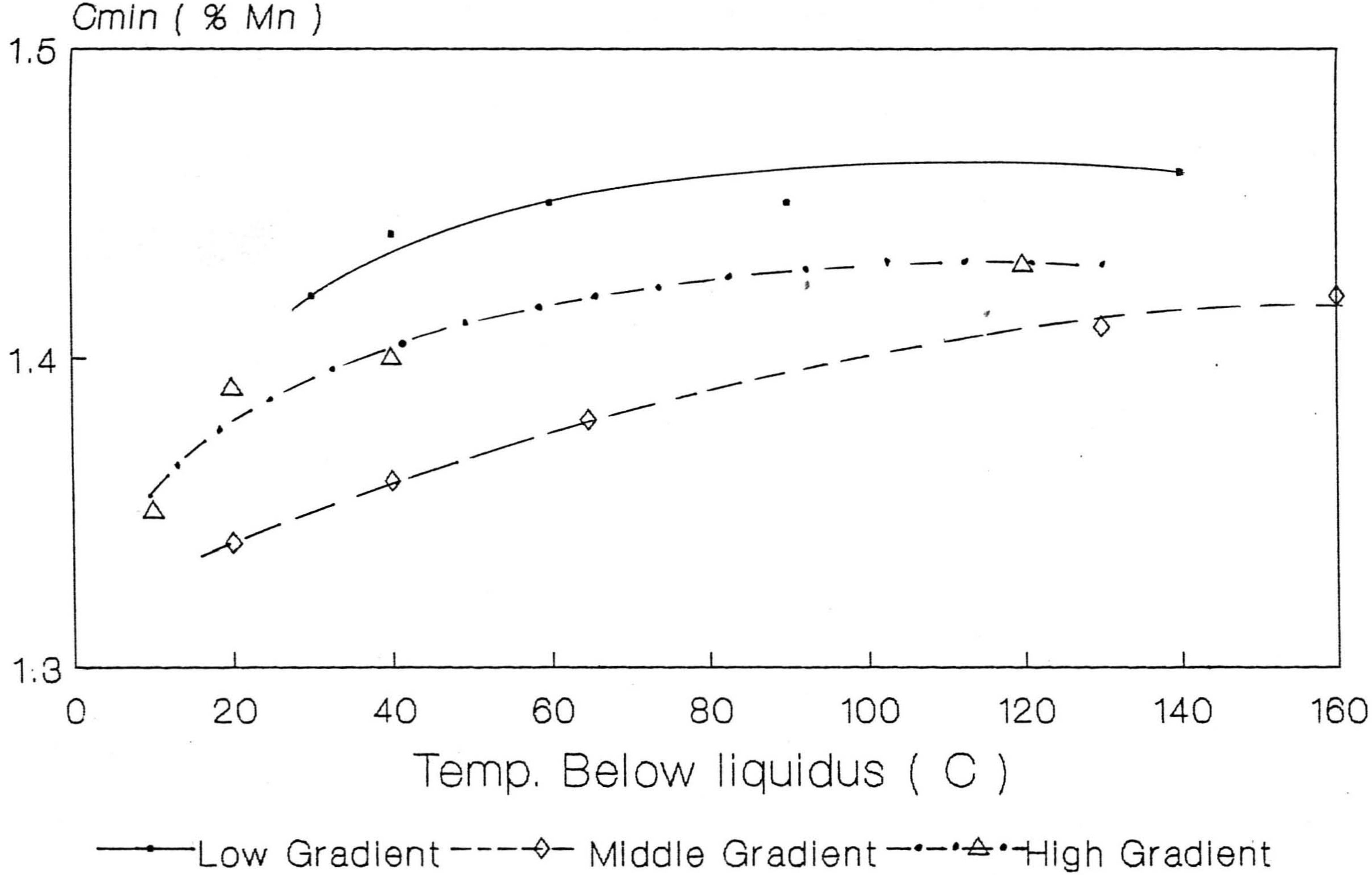

Cmin (% Mn)
1.5
1.4
1.3
0
20
40
60
80
100
120
140
160
Temp. Below liquidus (C)
Low Gradient
Middle Gradient
High Gradient

0.2 % C - 6 mm/min

Figure 59

The change of Cmin as a function of temperature below liquidus and growth rate for 0.4 % C - 1.6 % Mn - Fe alloy

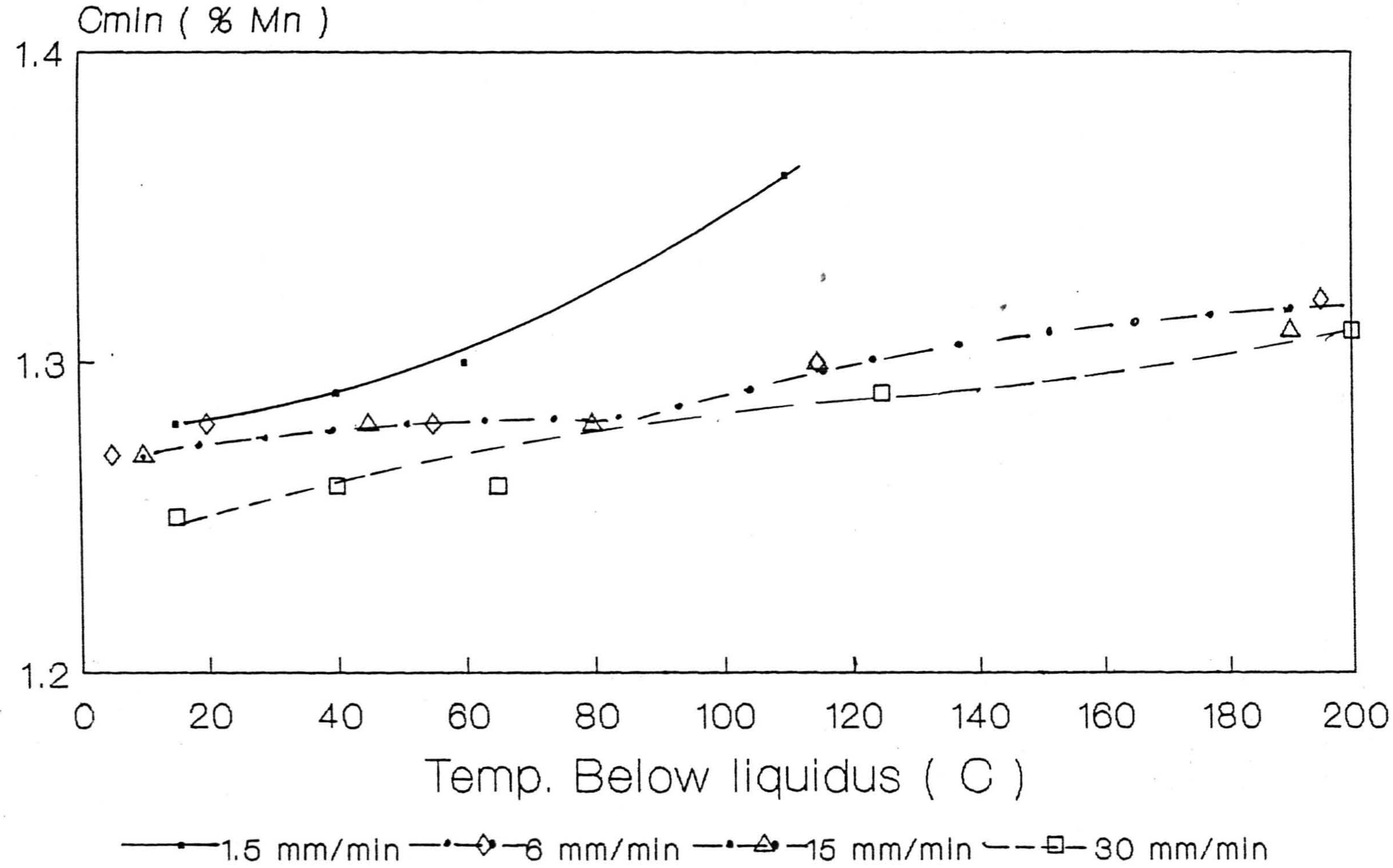
Cmin (% Mn)
1.4
1.3
1.2
0
20
40
60
80
100
120
140
160
180
200
Temp. Below liquidus (C)
1.5 mm/min
6 mm/min
15 mm/min
30 mm/min

0.4 % C

Figure 60

The change of Cmin as a function of temperature below liquidus and growth for 0.8 % C - 1.6 % Mn - Fe alloy

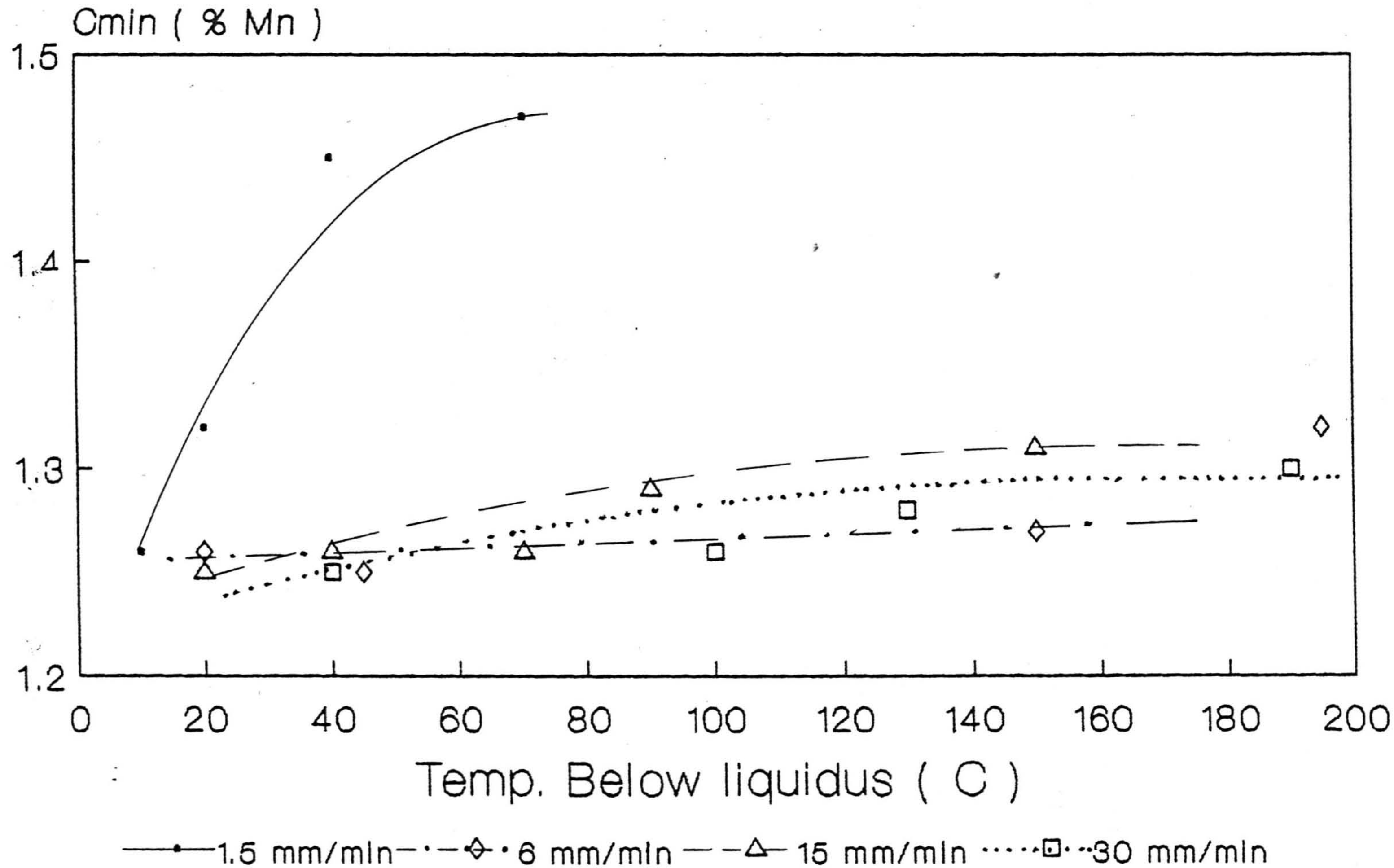

Cmin (% Mn)
1.5
1.4
1.3
1.2
0
20
40
60
80
100
120
140
160
180
200
Temp. Below liquidus (C)
1.5 mm/min
6 mm/min
15 mm/min
30 mm/min

0.8 % C

Figure 61

The change of Cmin as a function of temperature below liquidus and gradient in liquid for 0.4 % C - 1.6 % Mn - Fe alloy at 6 mm/min

Middle Gradient	7.2 C/mm
High Gradient	9.8 C/mm

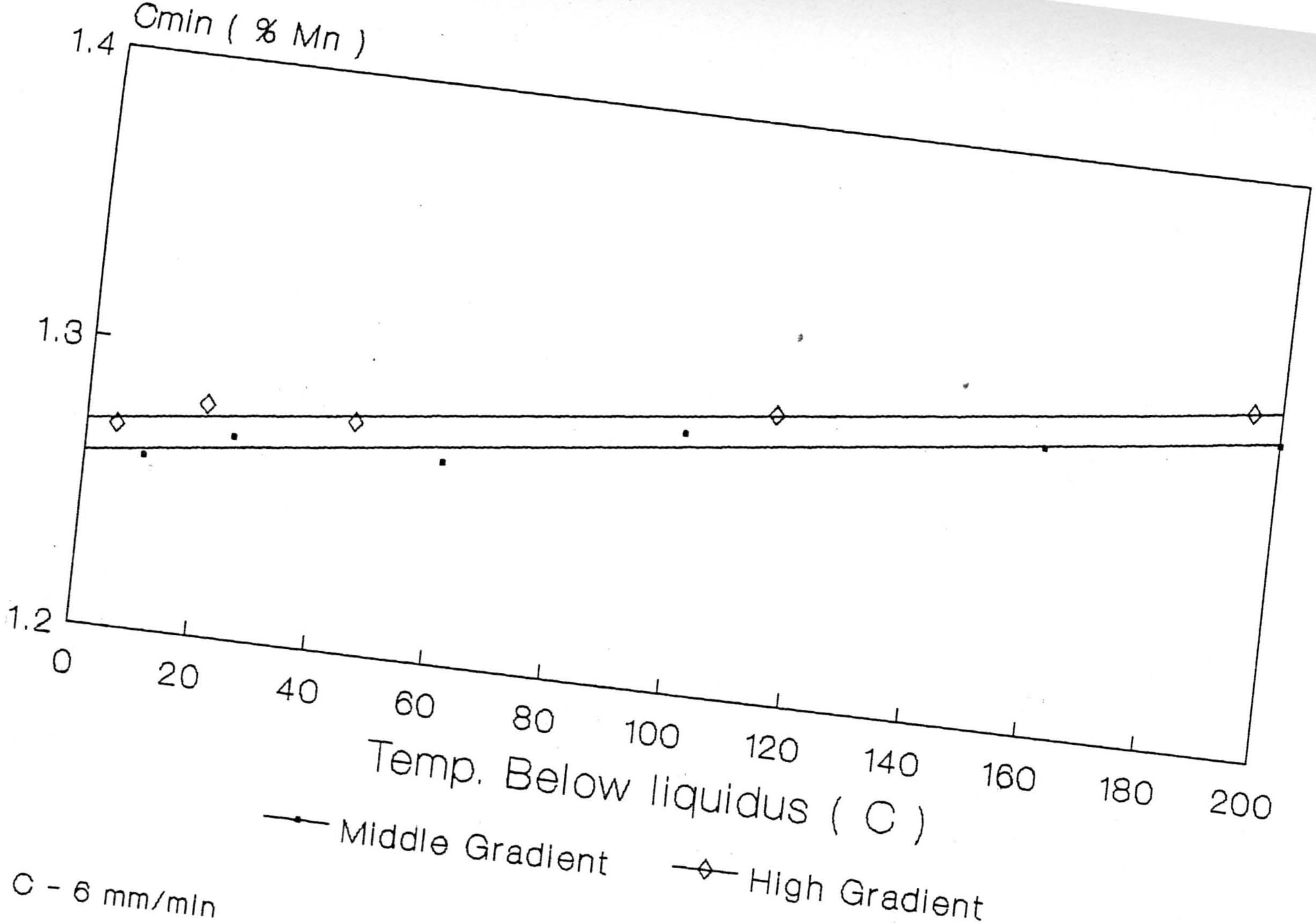

Cmin (% Mn)
1.4
1.3
1.2
0
20
40
60
80
100
120
140
160
180
200
Temp. Below liquidus (C)
Middle Gradient
High Gradient

0.4 % C - 6 mm/min

Figure 62

The change of Cmin as a function of temperature below liquidus and gradient in liquid for 0.8 % C - 1.6 % Mn - Fe alloy at 15 mm/min

Low Gradient	4.8 C/mm
High Gradient	7.6 C/mm

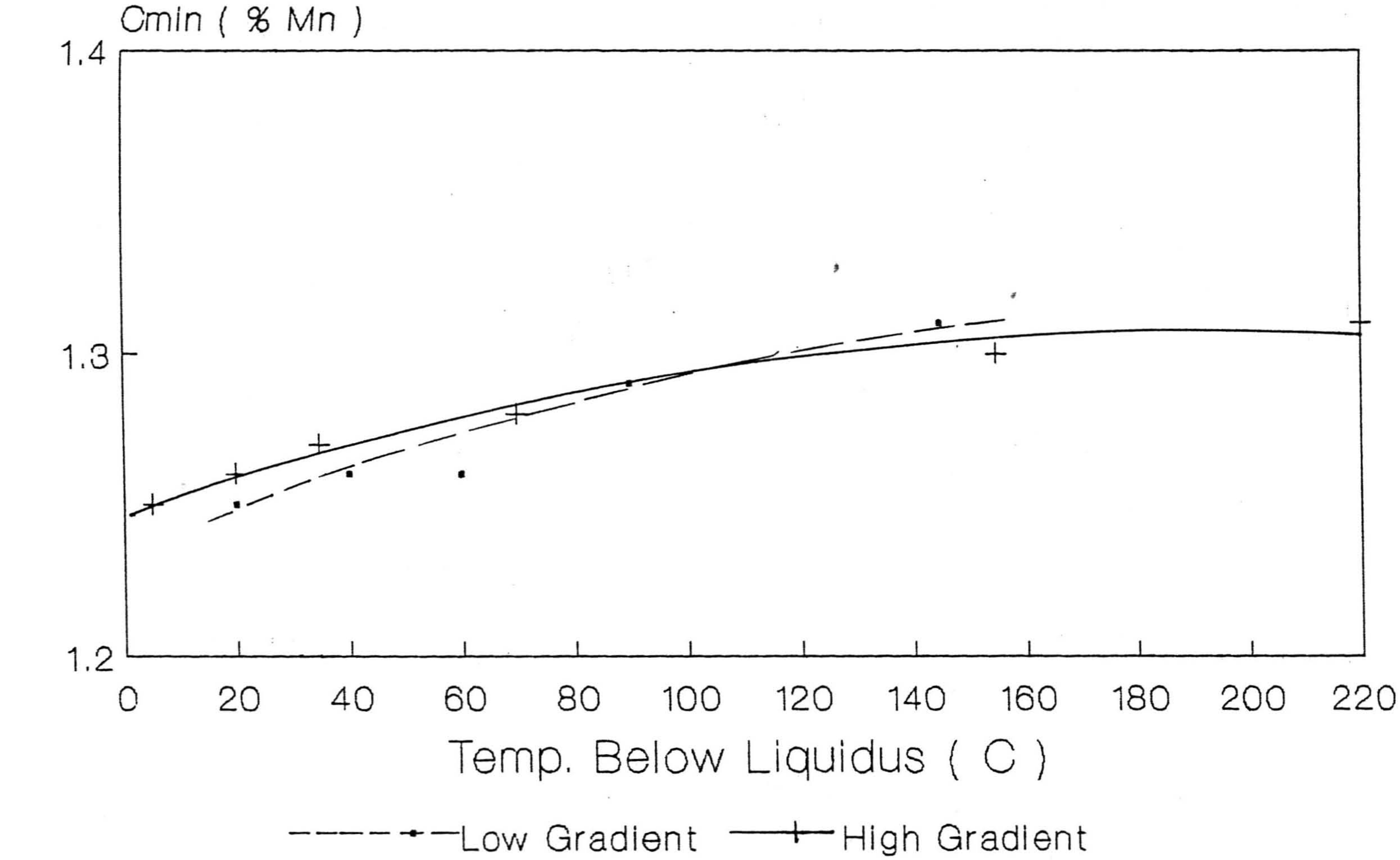

Cmin (% Mn)
1.4
1.3
1.2
0
20
40
60
80
100
120
140
160
180
200
220
Temp. Below Liquidus (C)
Low Gradient
High Gradient

0.8 % C - 15 mm/min

Figure 63

The change of Cmin as a function of temperature below liquidus and carbon content at 6 mm/min under 9.8 C/mm in liquid

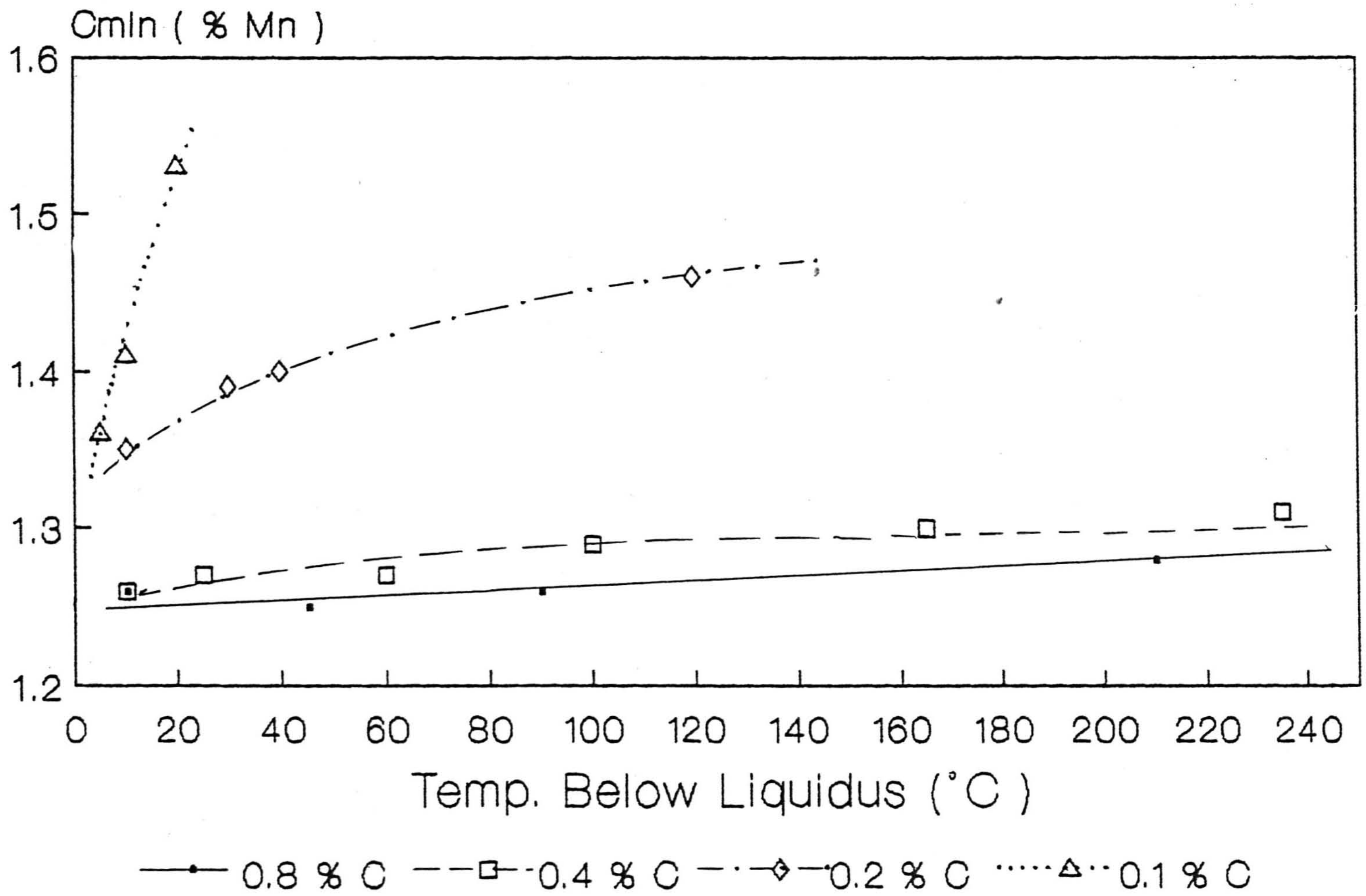

Cmin (% Mn)
1.6
1.5
1.4
1.3
1.2
0
20
40
60
80
100
120
140
160
180
200
220
240
Temp. Below Liquidus (°C)
0.8 % C
0.4 % C
0.2 % C
0.1 % C

6 mm/min

Figure 64

The change in Cmax between secondary arms during growth

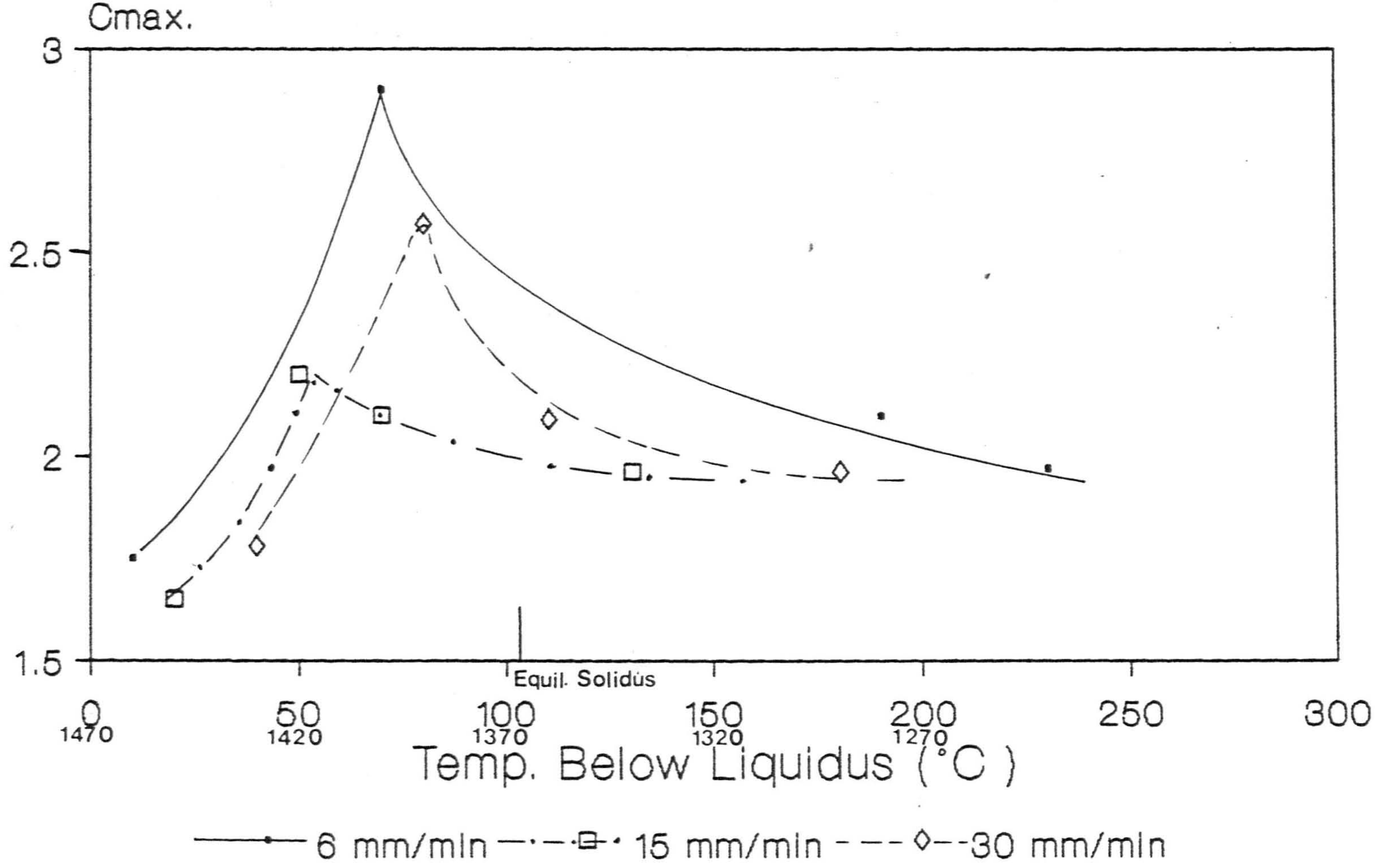

Cmax.
3
2.5
2
1.5
Equil. Solidus
0
1470
50
1420
100
1370
150
1320
200
1270
250
300
Temp. Below Liquidus (°C)
6 mm/min
15 mm/min
30 mm/min

0.8 % C

Figure 65

Cmax and Cmin as a function of cooling rate for 0.4 and 0.8 % C

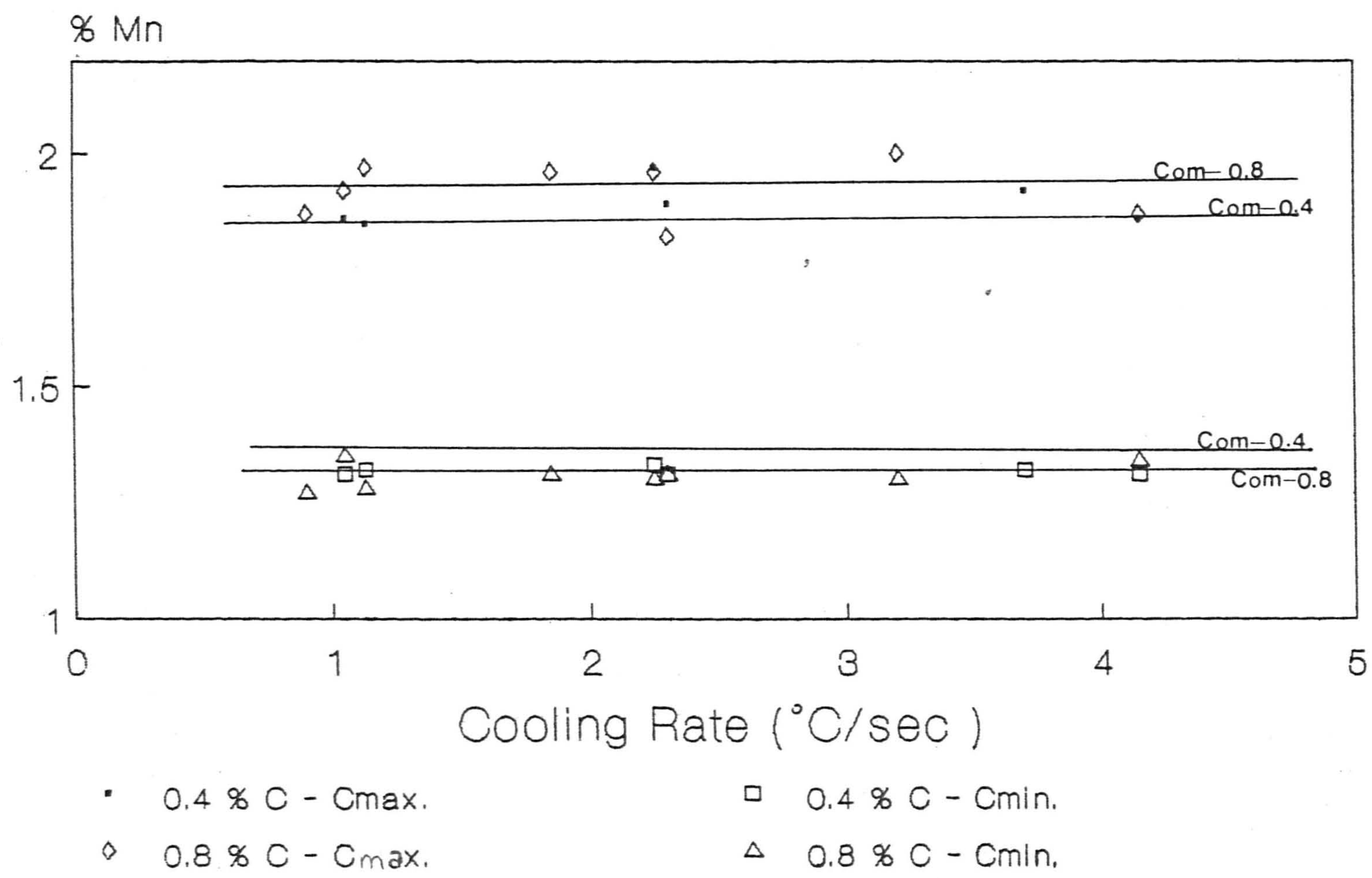
% Mn
2
1.5
1
0
1
2
3
4
5
Com– 0.8
Com–0.4
Com–0.4
Com–0.8
Cooling Rate (°C/sec)
0.4 % C - Cmax.
0.8 % C - Cmax.
0.4 % C - Cmin.
0.8 % C - Cmin.

1200°C

Figure 66

Segregation ratio between secondary arms as a function of cooling rate and carbon content

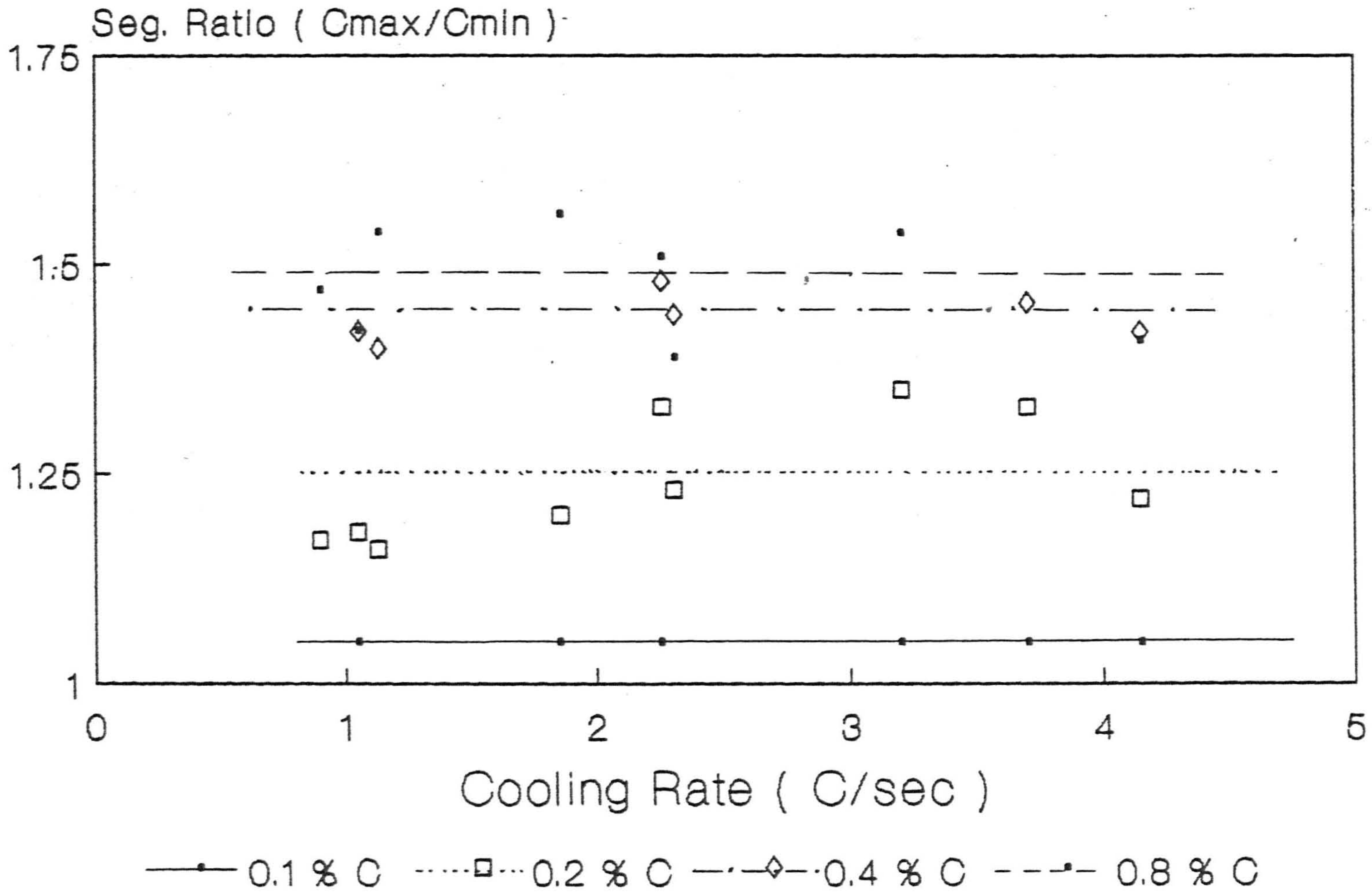

Seg. Ratio (Cmax/Cmin)
1.75
1.5
1.25
1
0
1
2
3
4
5
Cooling Rate (C/sec)
0.1 % C
0.2 % C
0.4 % C
0.8 % C

1200 C

Figure 67

The secondary arm migration distance as a function of growth rate

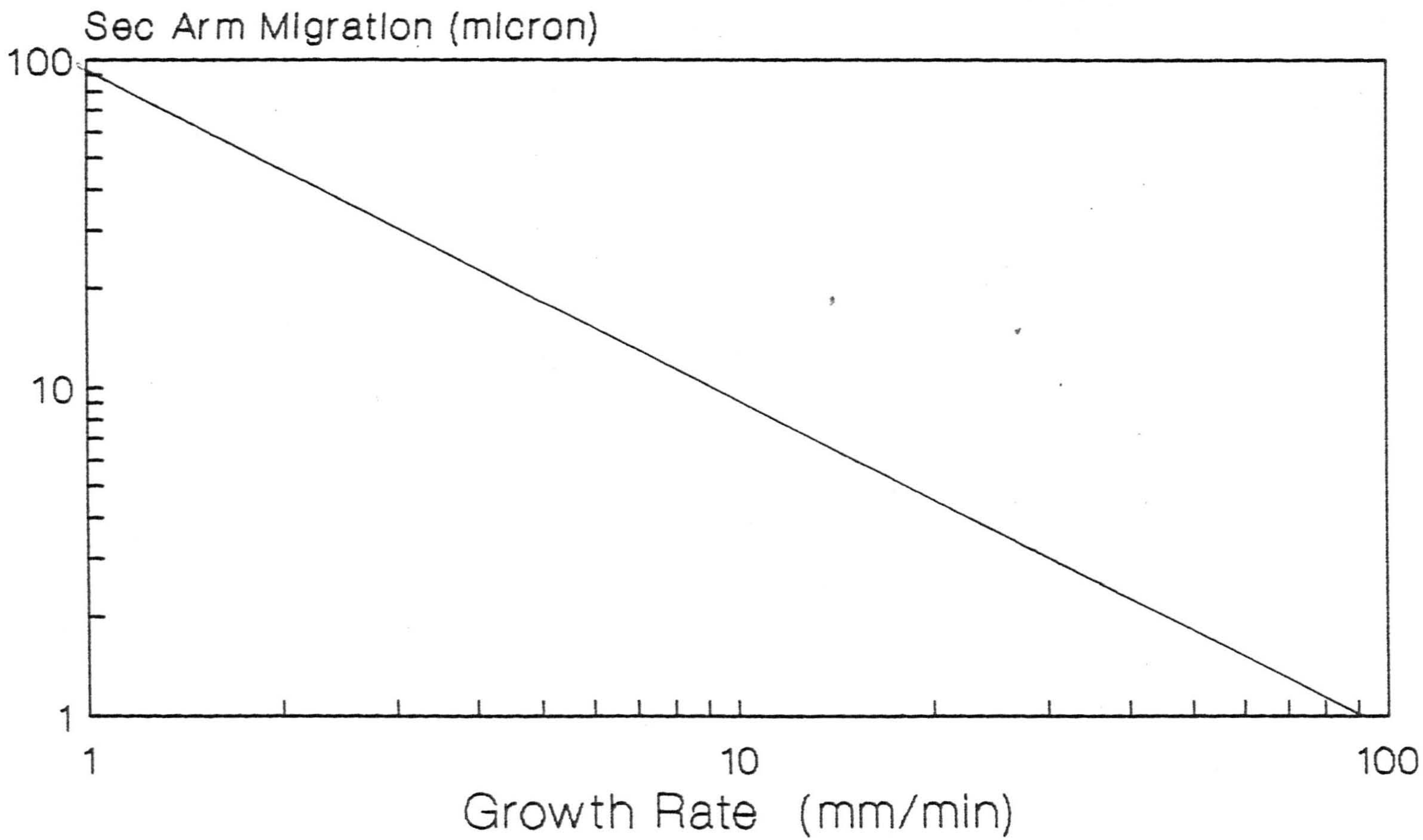
Sec Arm Migration (micron)
100
10
1
1
10
100
Growth Rate (mm/min)

Figure 68

Electron micro probe concentration profiles through the secondary arms (figure 54)

0.8 % C - 1.6 % Mn - Fe

Growth rate 1.5 mm/min

a) 0.93 mm behind tips

b) 2 mm behind tips

c) 3.8 mm behind tips

d) 6 mm behind tips

e) 26 mm behind tips

(A)

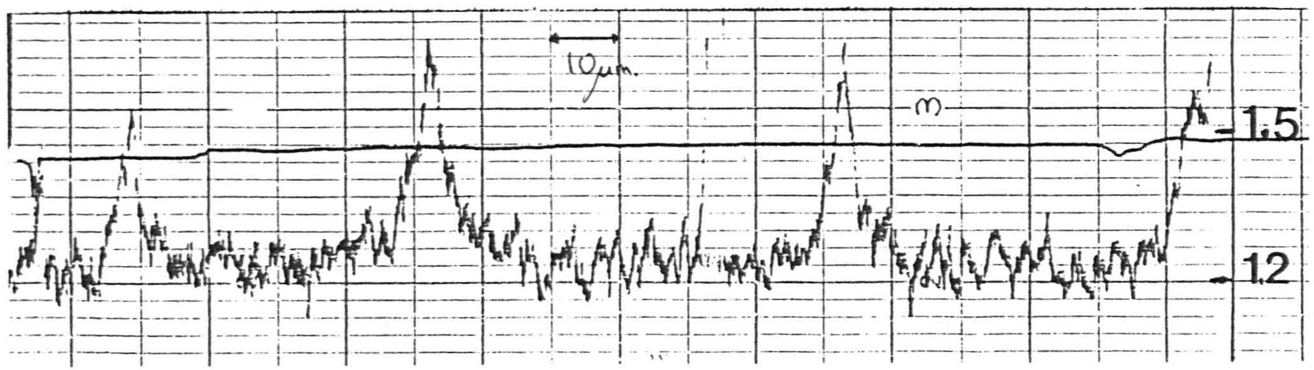

(B)

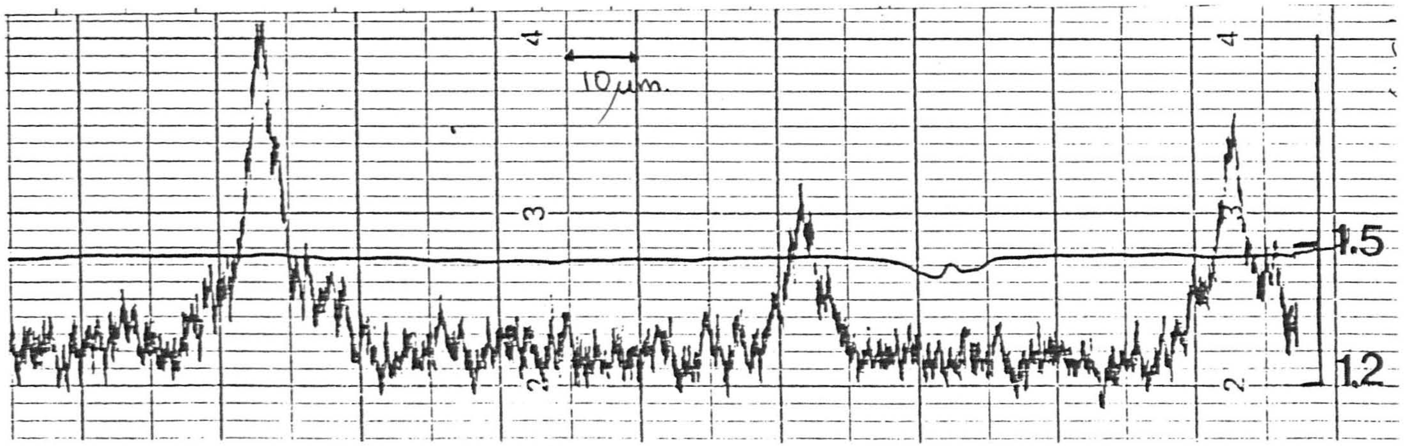

(C)

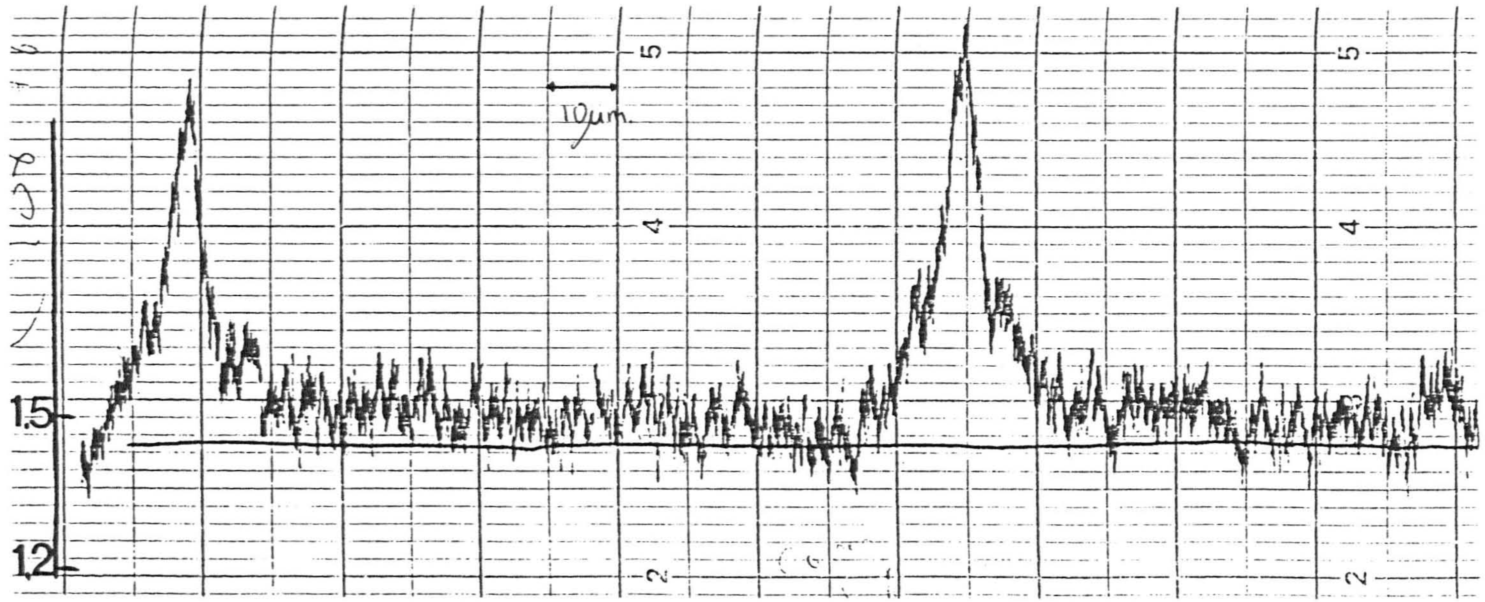

(D)

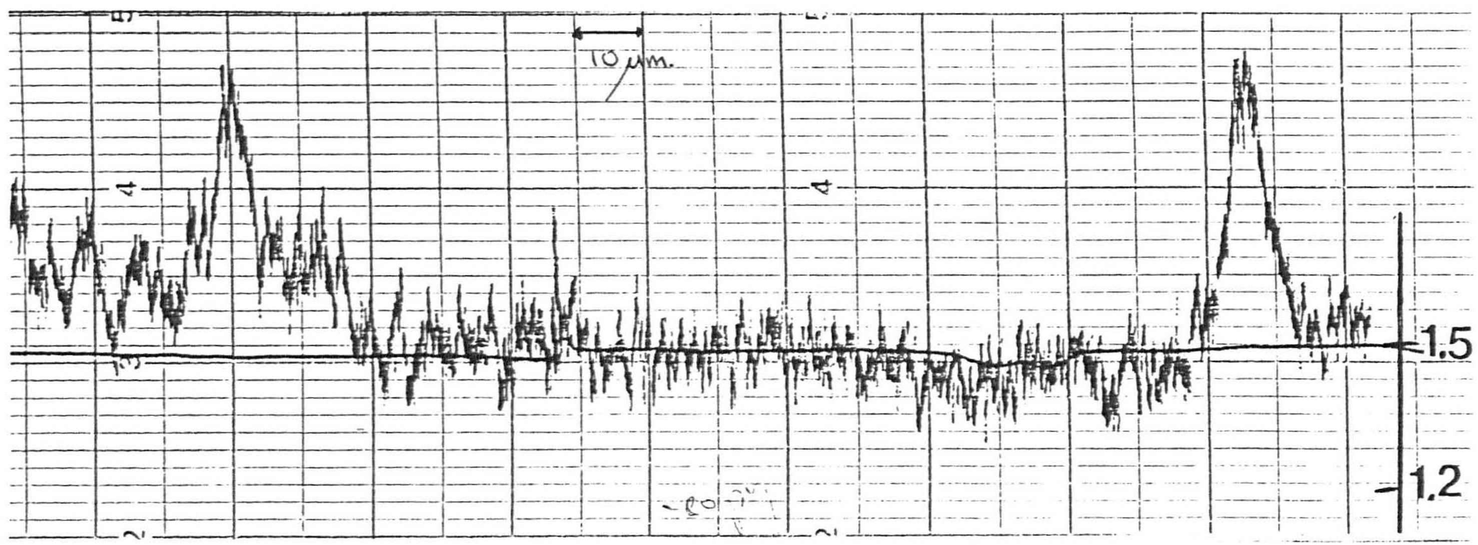

(E)

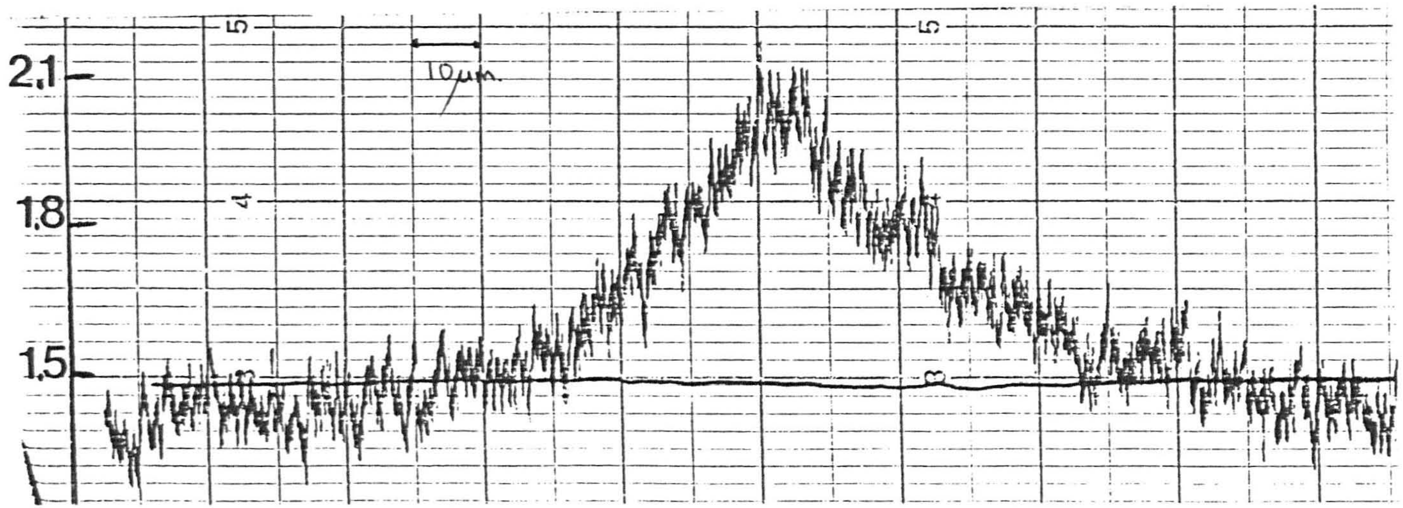

Figure 69

Electron micro probe concentration profiles through the secondary arms showing the TGZM effect (saw-tooth)

0.8 % C - 1.6 % Mn - Fe

Growth rate 6 mm/min

a) 3.2 mm behind tips

b) 5.6 mm behind tips

c) 7.7 mm behind tips

d) 13 mm behind tips

e) after solidification complete

(A)

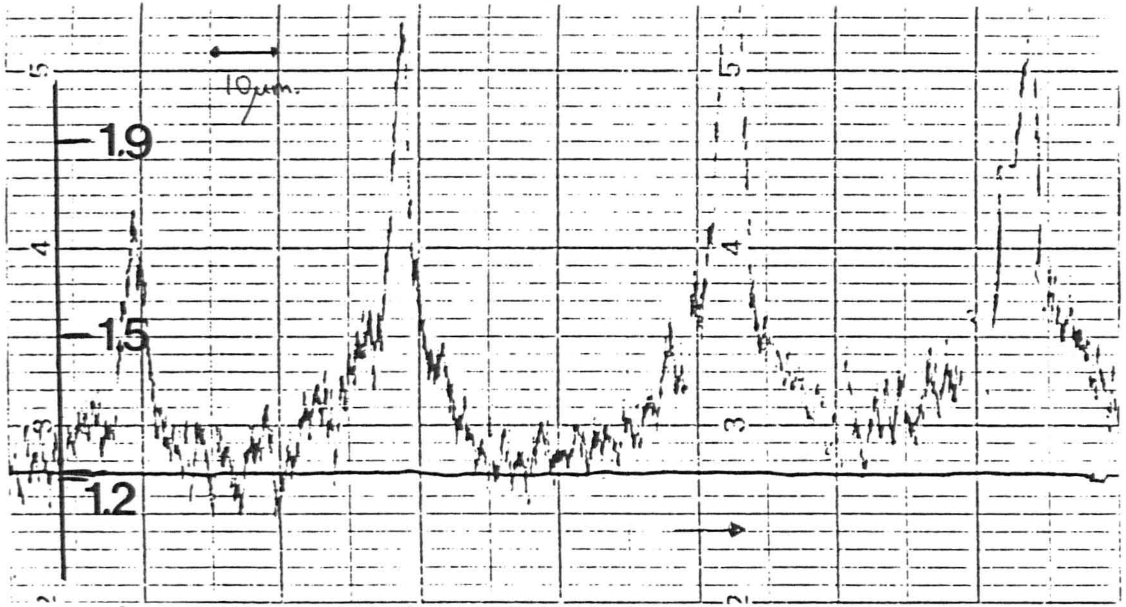

(B)

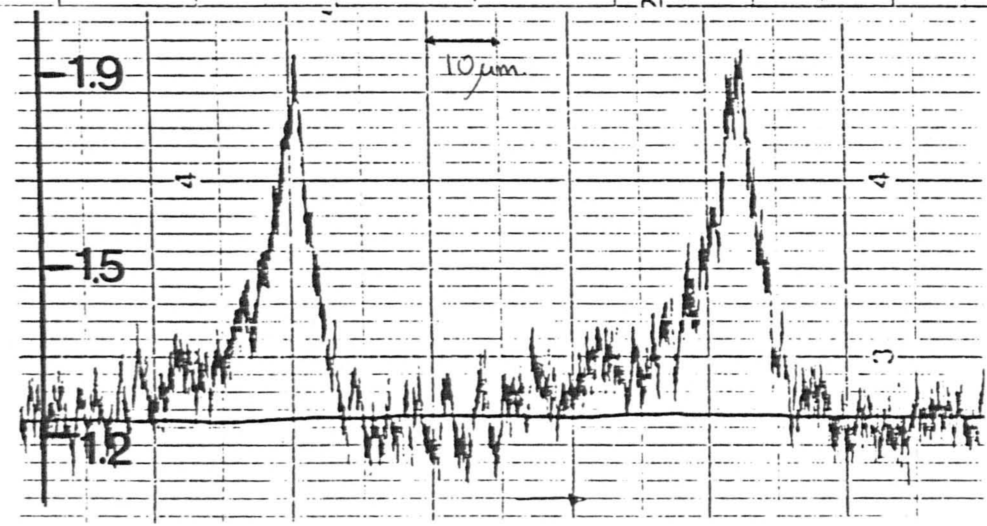

(c)

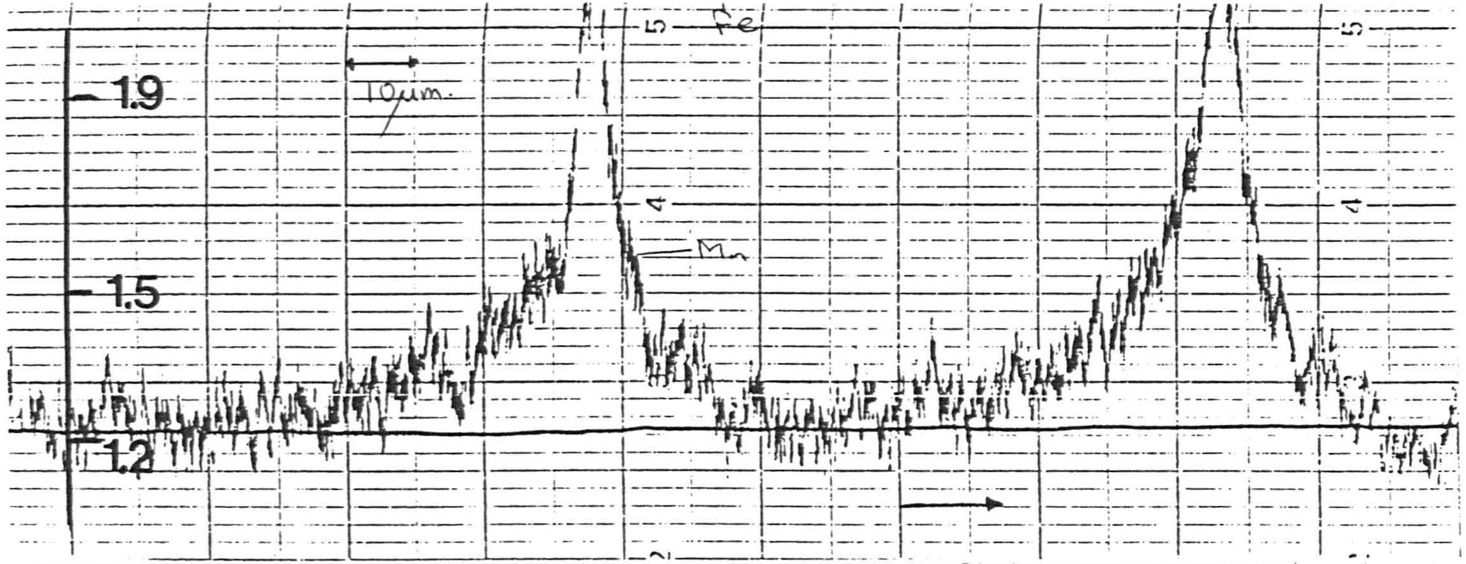

(D)

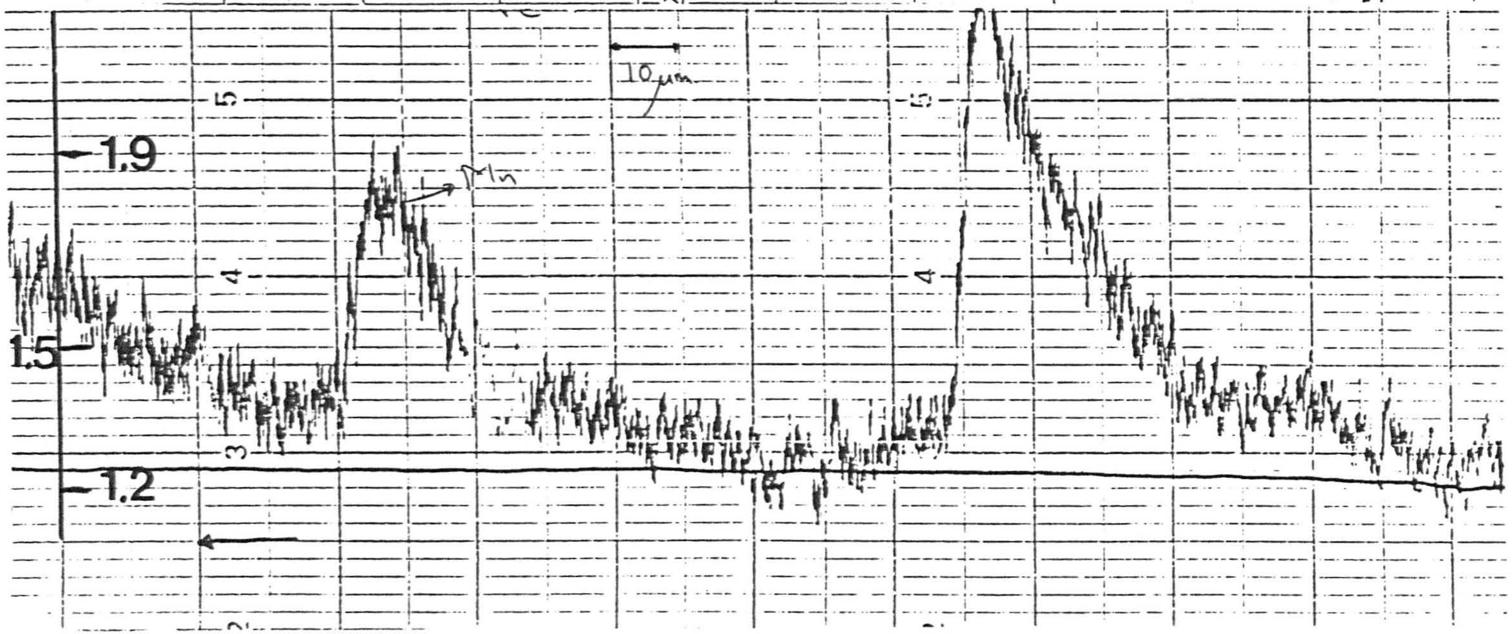

(E)

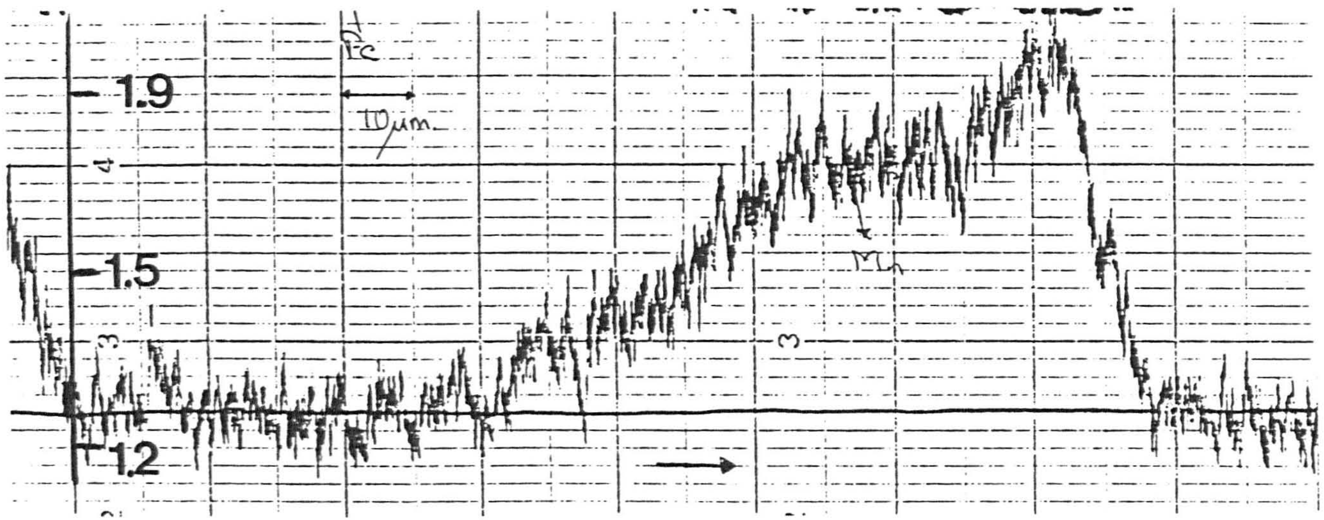

Figure 70

Electron micro probe concentration profiles through the secondary arms showing the TGZM effect (saw-tooth)

0.8 % C - 1.6 % Mn - Fe

Growth rate 15 mm/min

a) 3.25 mm behind tips

b) 15.5 mm behind tips

c) 19 mm behind tips

d) 26.5 mm beind tips

(A)

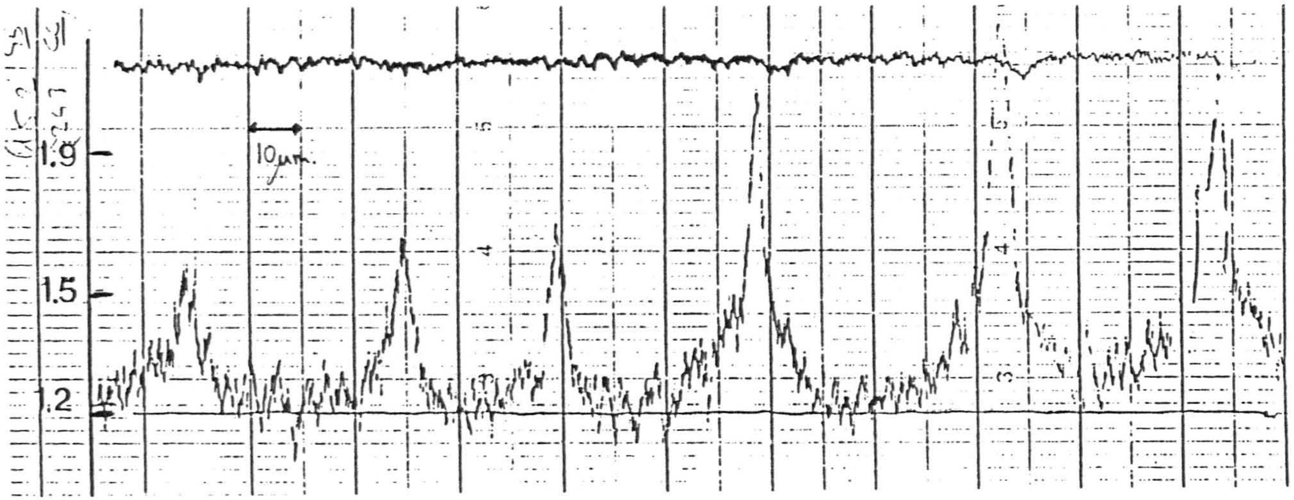

(B)

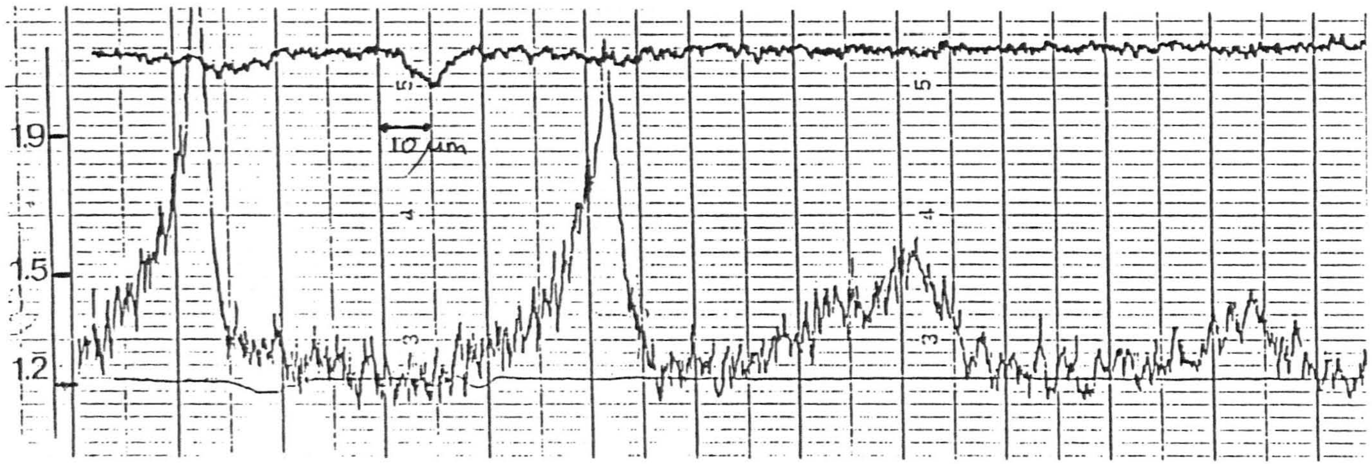

(C)

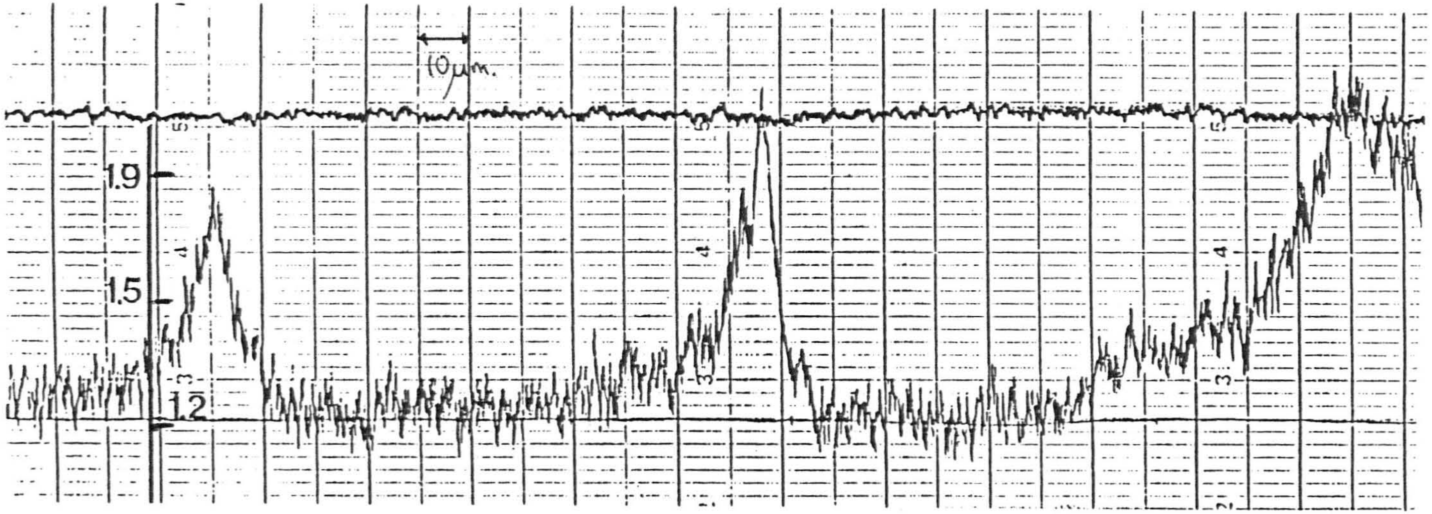

(D)

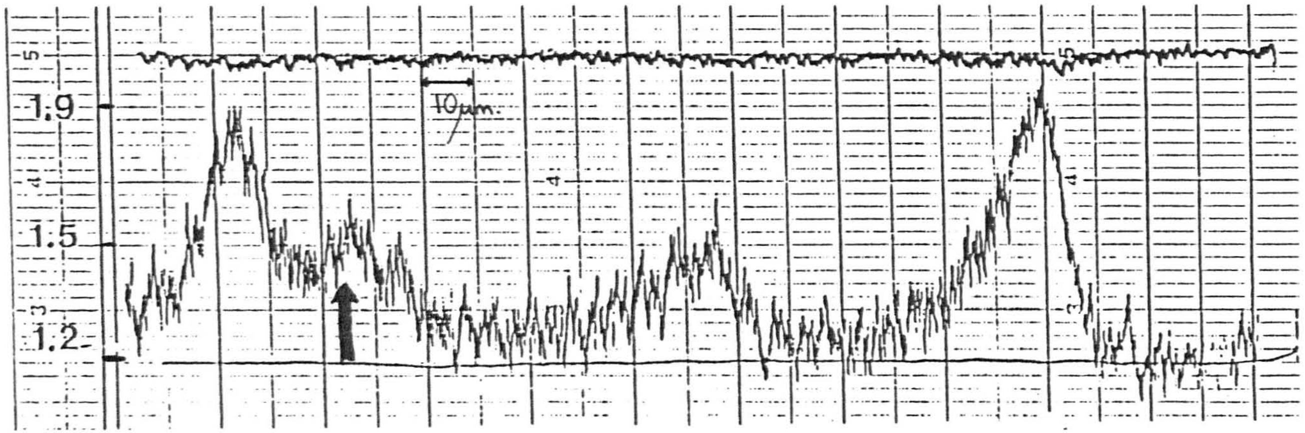

Figure 71

Electron micro probe concentration profiles through the secondary arms showing the TGZM effect (saw-tooth)

0.8 % C - 1.6 % Mn - Fe

Growth rate 30 mm/min

a) 3 mm behind tips

b) 7 mm behind tips

c) 23 mm behind tips

(B)

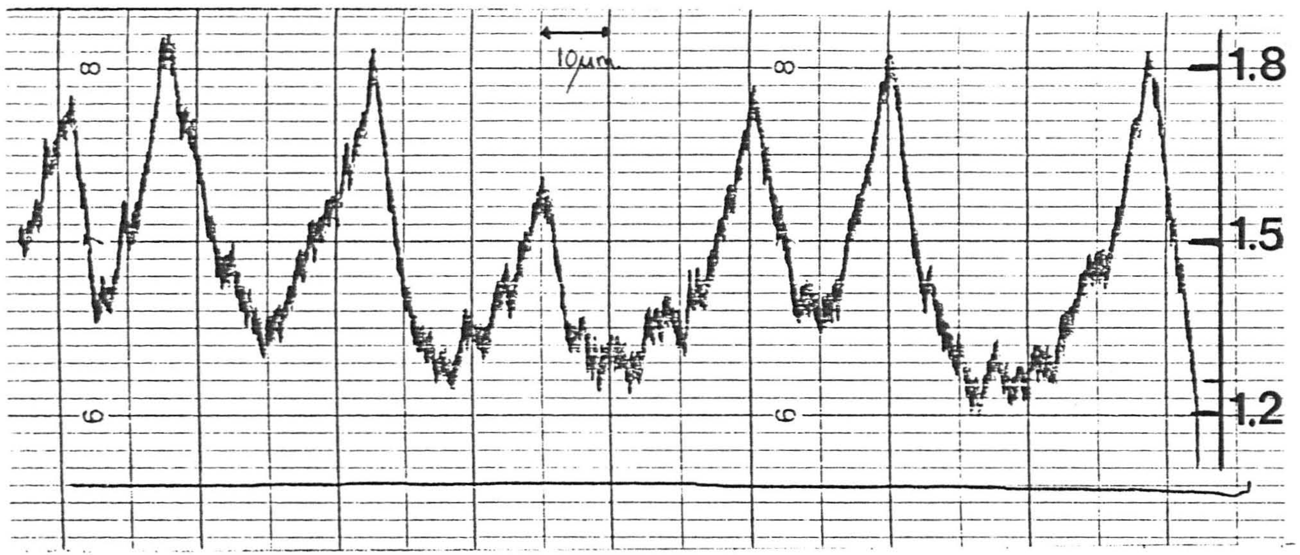

(A)

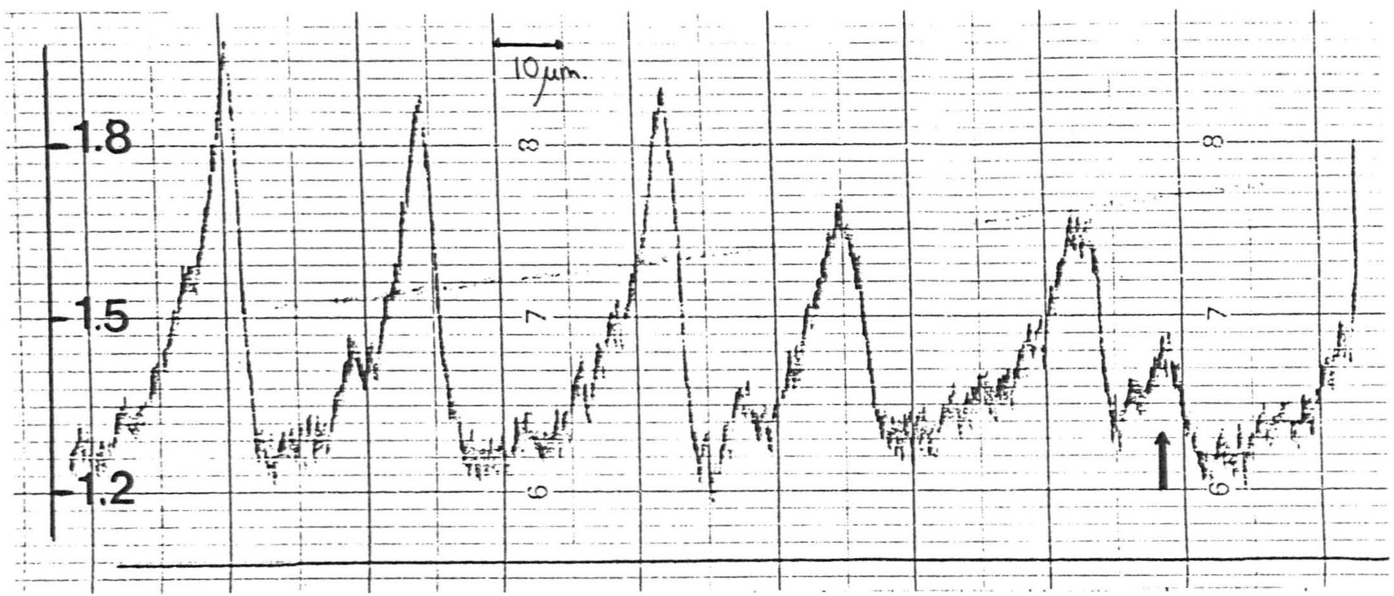

c

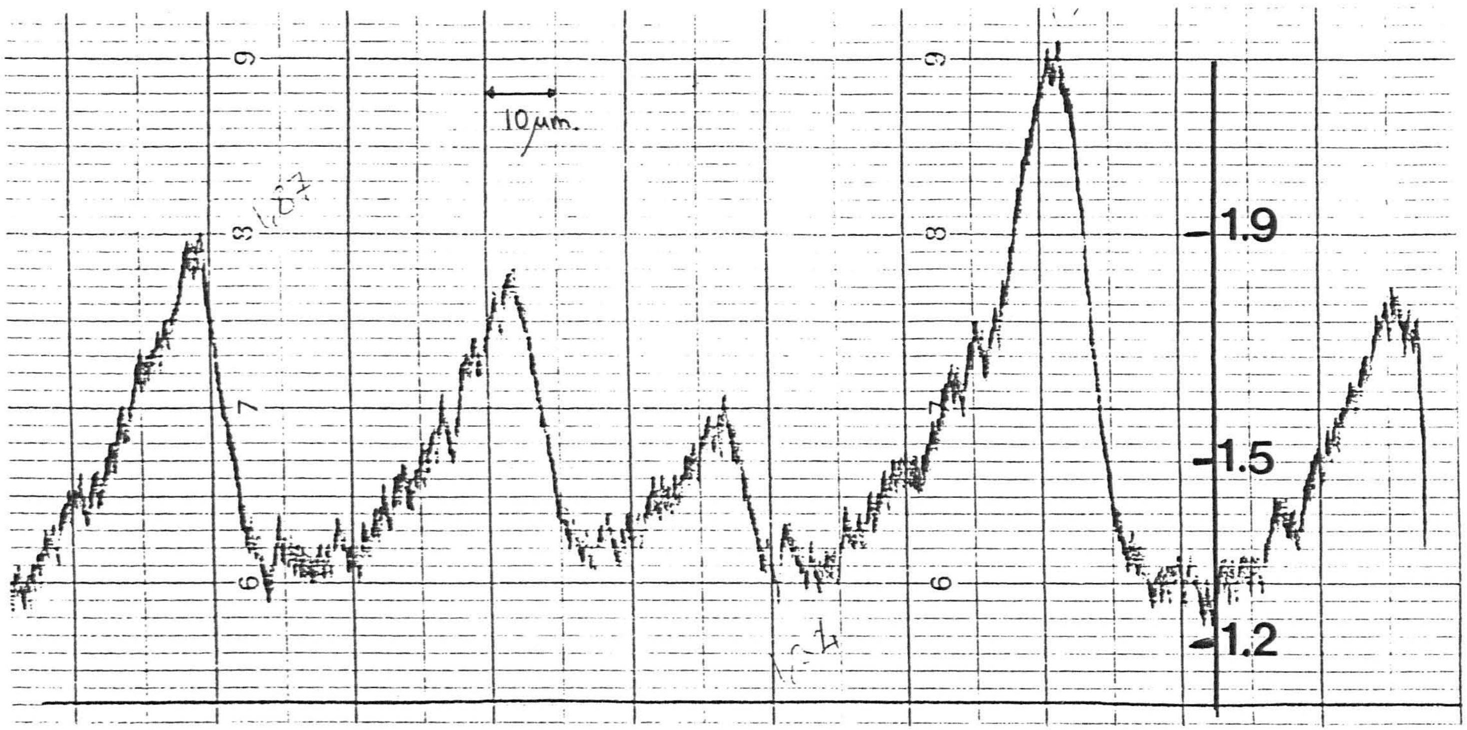

Figure 72

The change of the minimum concentration of manganese as a function of temperature below liquidus for 0.1 % C and 0.2 % C at the 1.5 and 6 mm/min growth rate

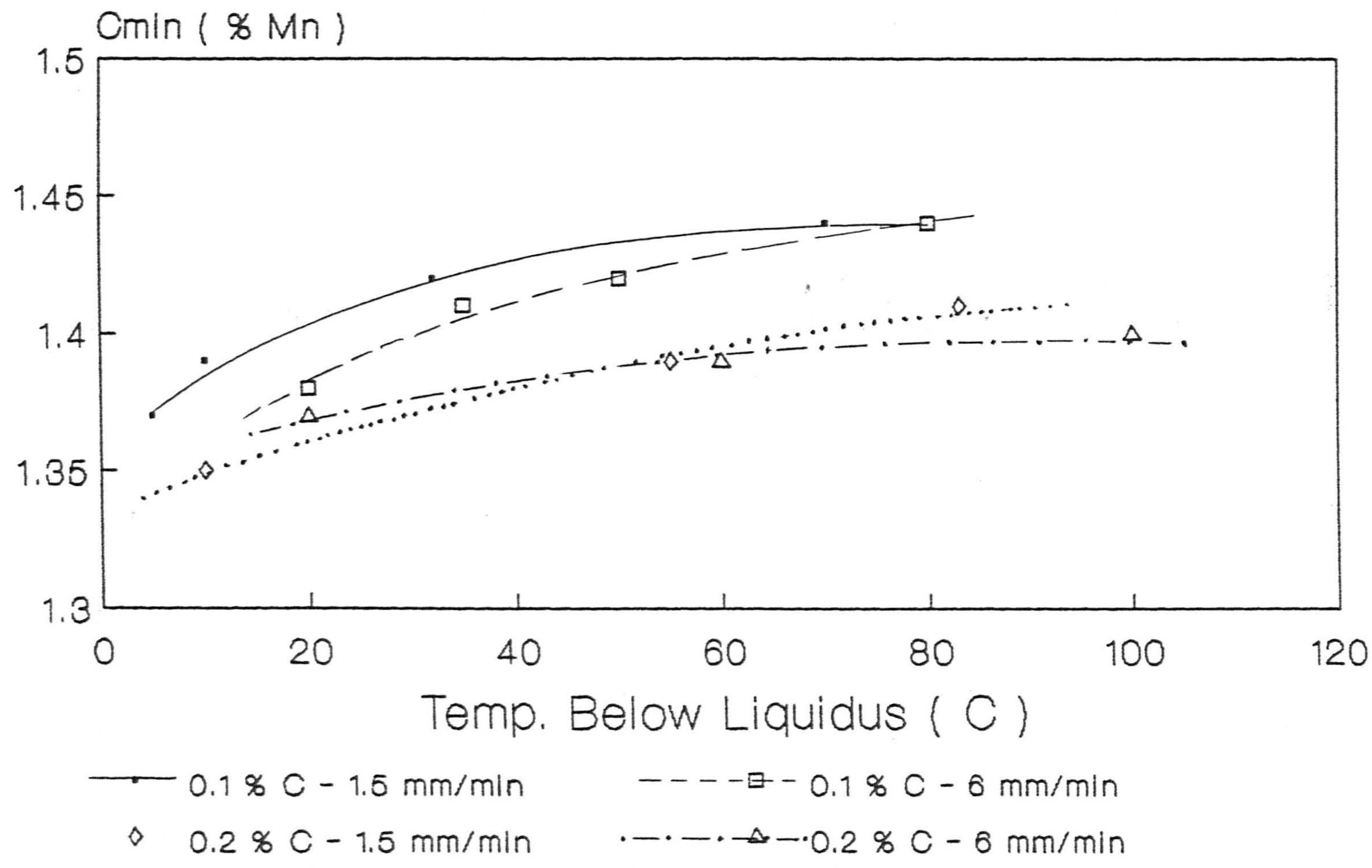

Cmin (% Mn)
1.5
1.45
1.4
1.35
1.3
0
20
40
60
80
100
120
Temp. Below Liquidus (C)
0.1 % C - 1.5 mm/min
0.1 % C - 6 mm/min
0.2 % C - 1.5 mm/min
0.2 % C - 6 mm/min

Figure 73

The minimum concentration of manganese as a function of cooling rate for different carbon contents

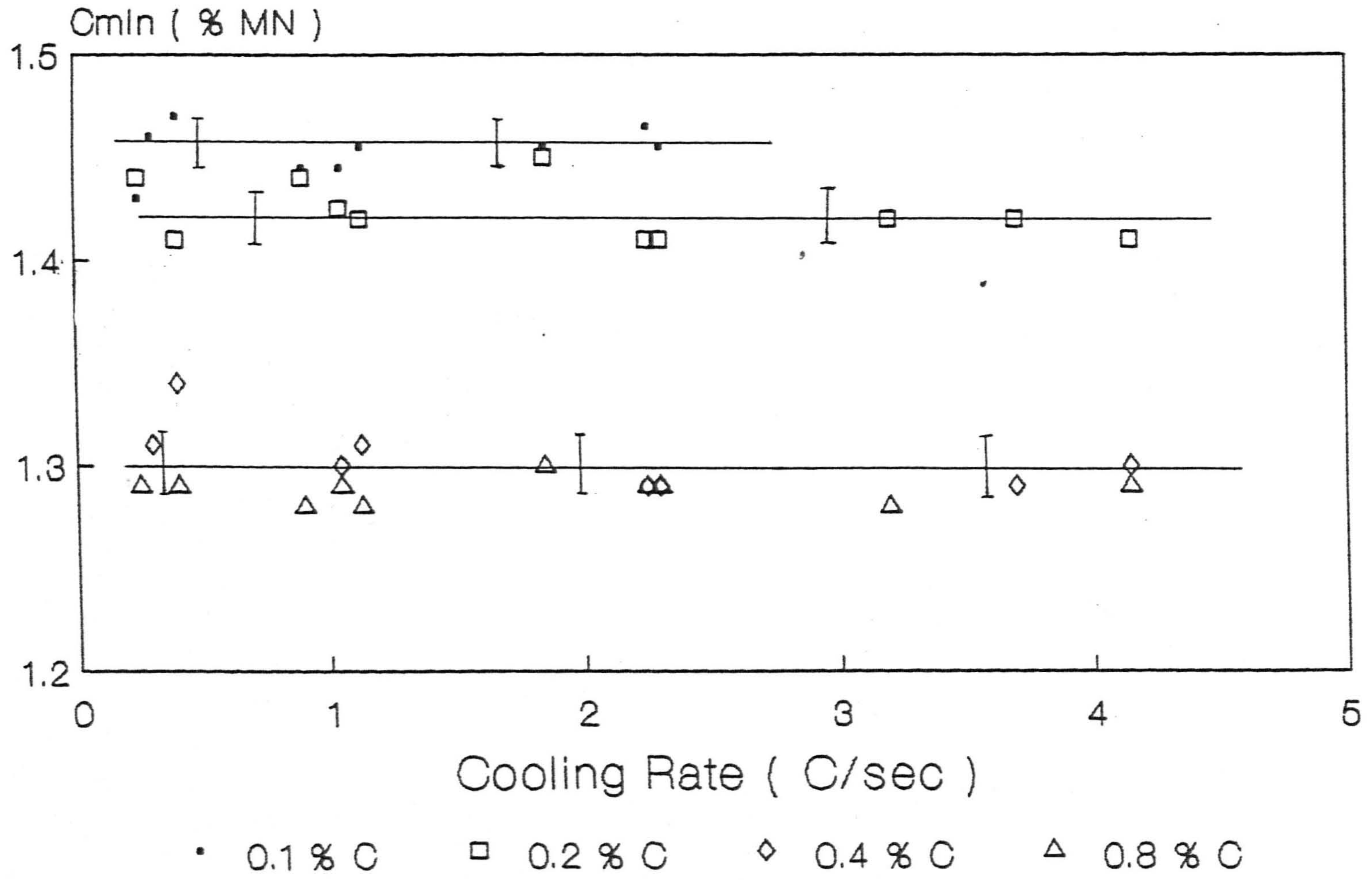

1200 C

Variation of the maximum concentration of manganese and the computer results as a function of cooling rate for

Figure 74 - 0.1 % C

Figure 75 - 0.2 % C

Figure 76 - 0.4 % C

Figure 77 - 0.8 % C

Figure 78 - 0.8 % C , 0.4 % C, 0.2 % C and 0.1 % C

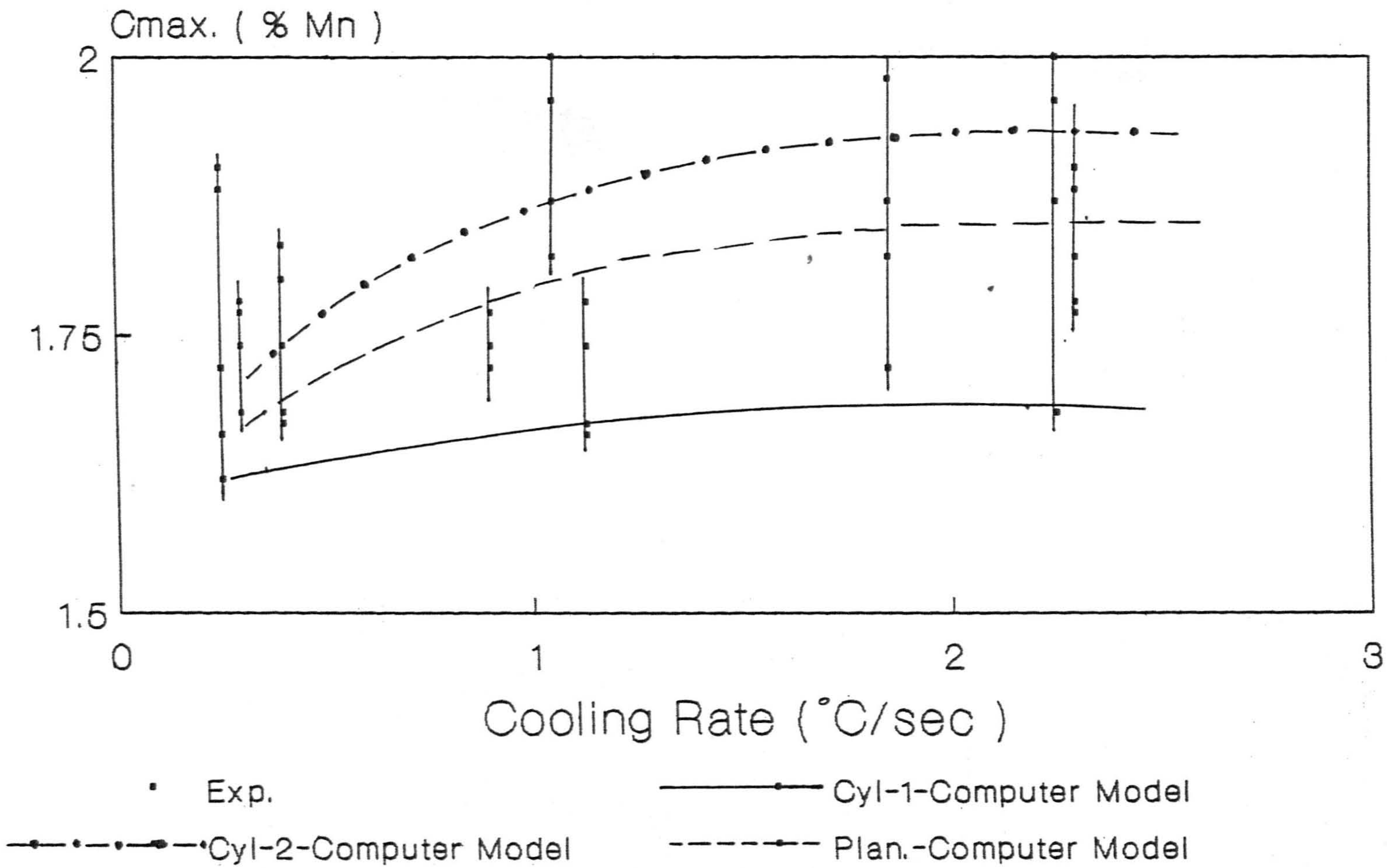

1485°C - 0.1 % C

Figure 74

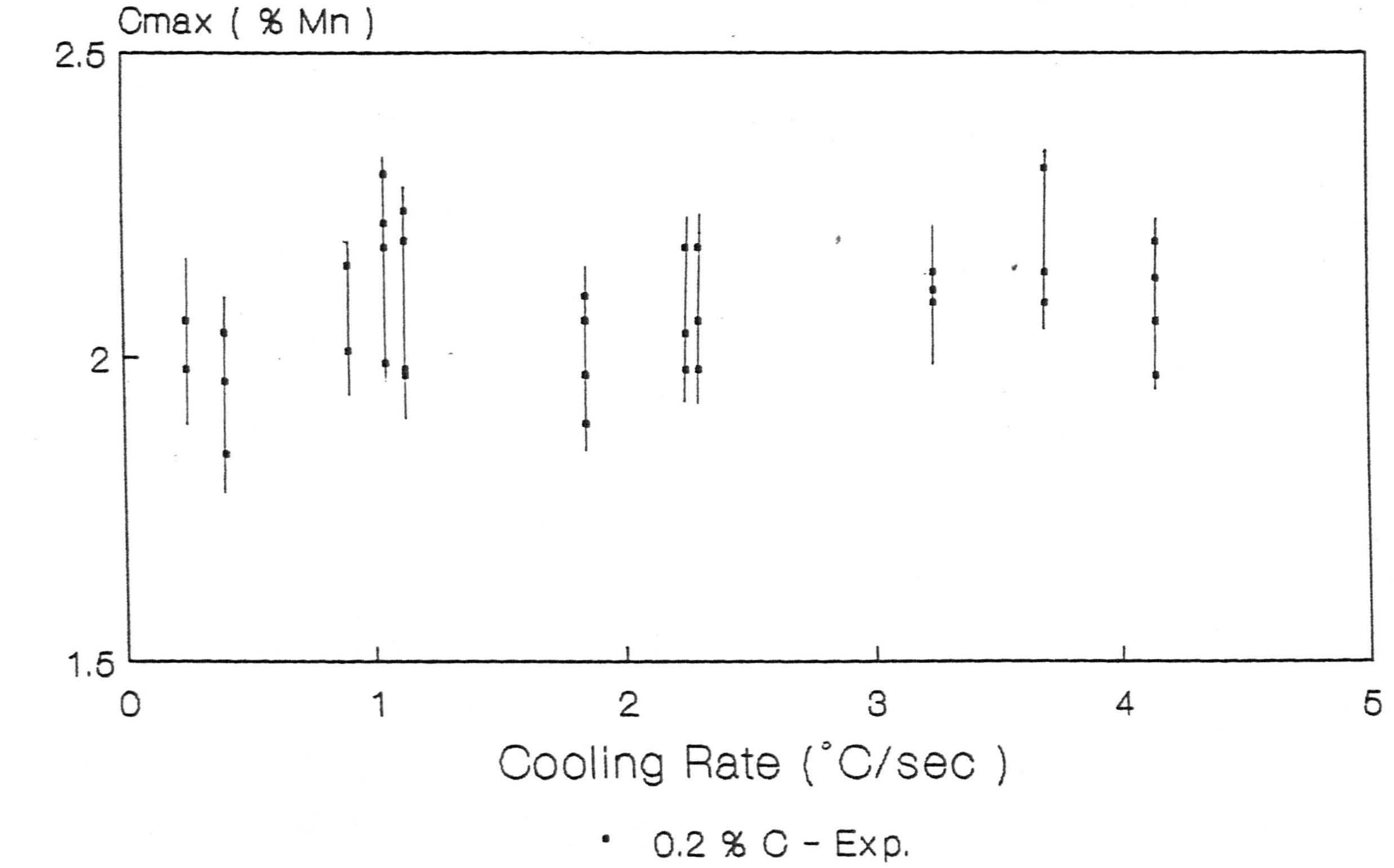

1200°C

Figure 75

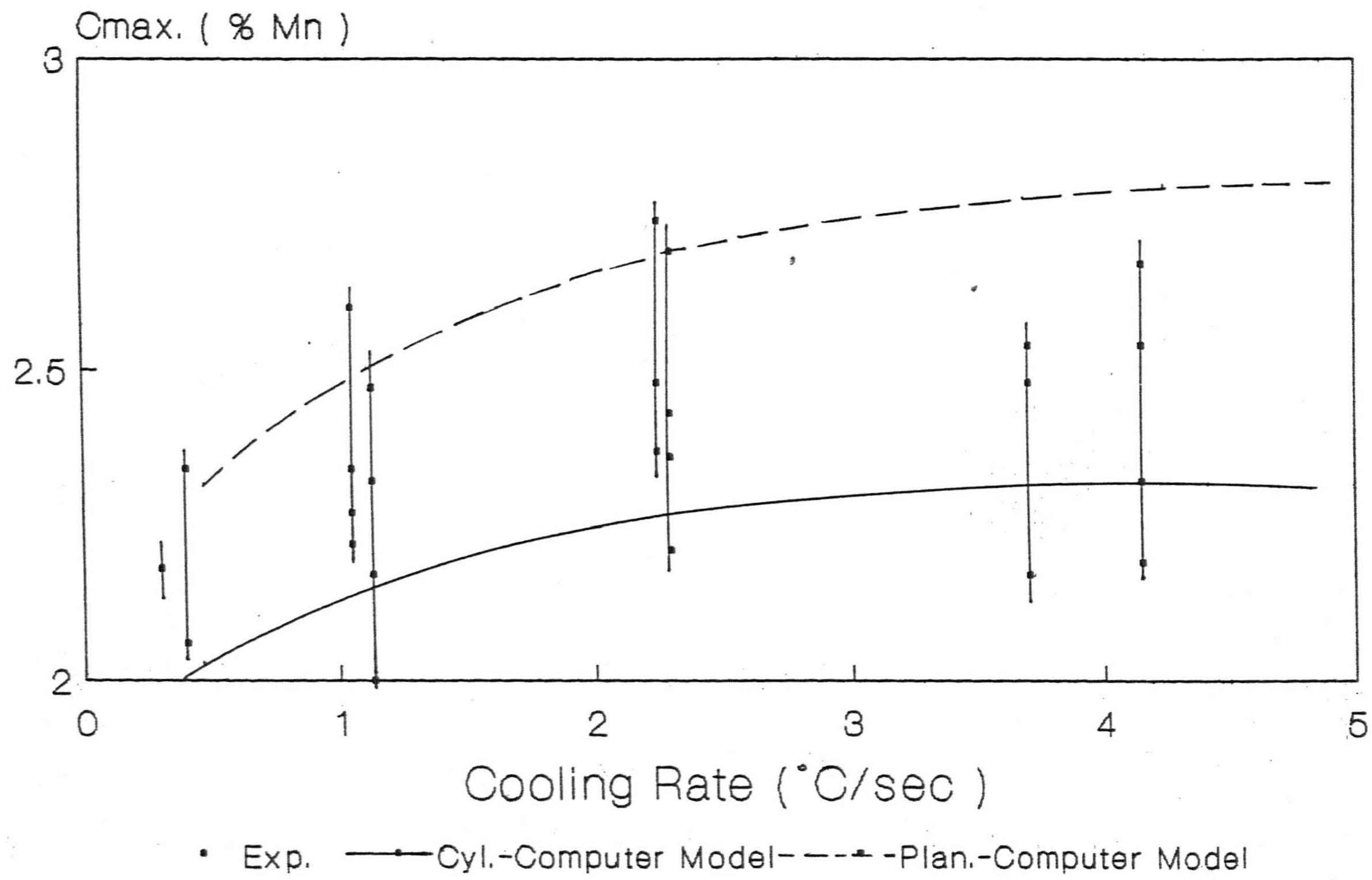

1200˚C - 0.4 % C

Figure 76

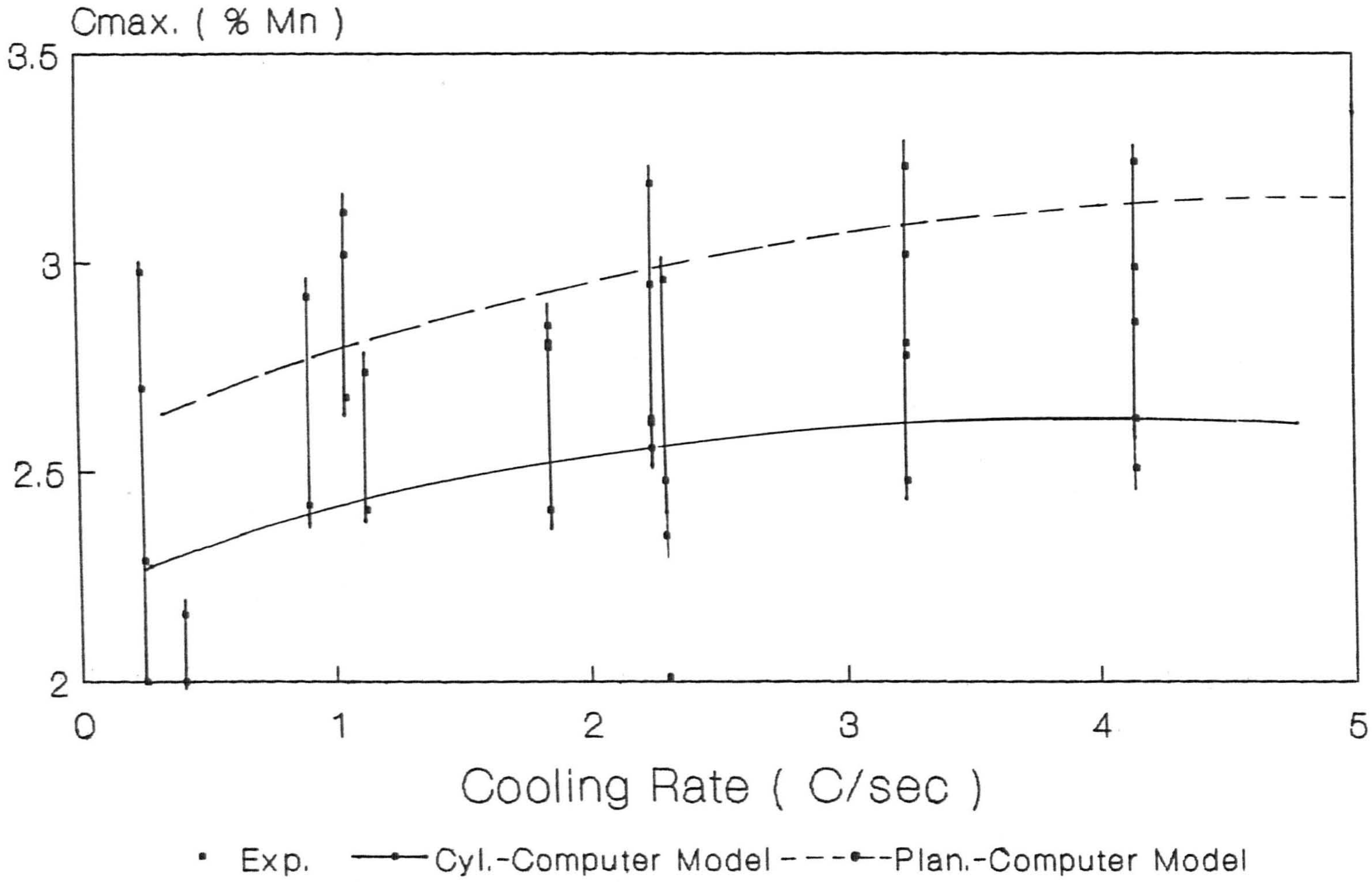

1200 C - 0.8 % C

Figure 77

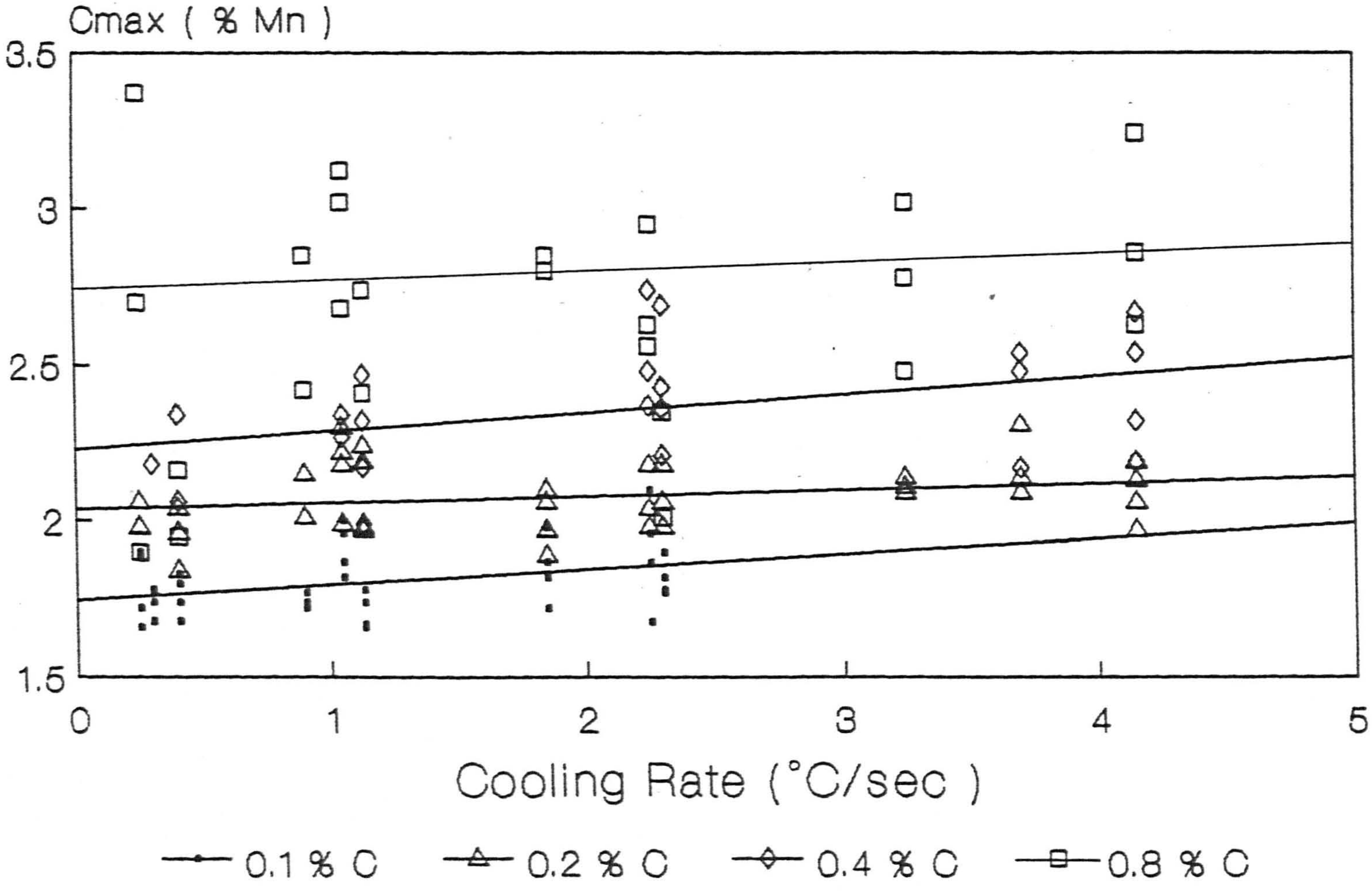

1200°C

Figure 78

Figure 79

The segregation ratio of manganese as a function of cooling rate and carbon content

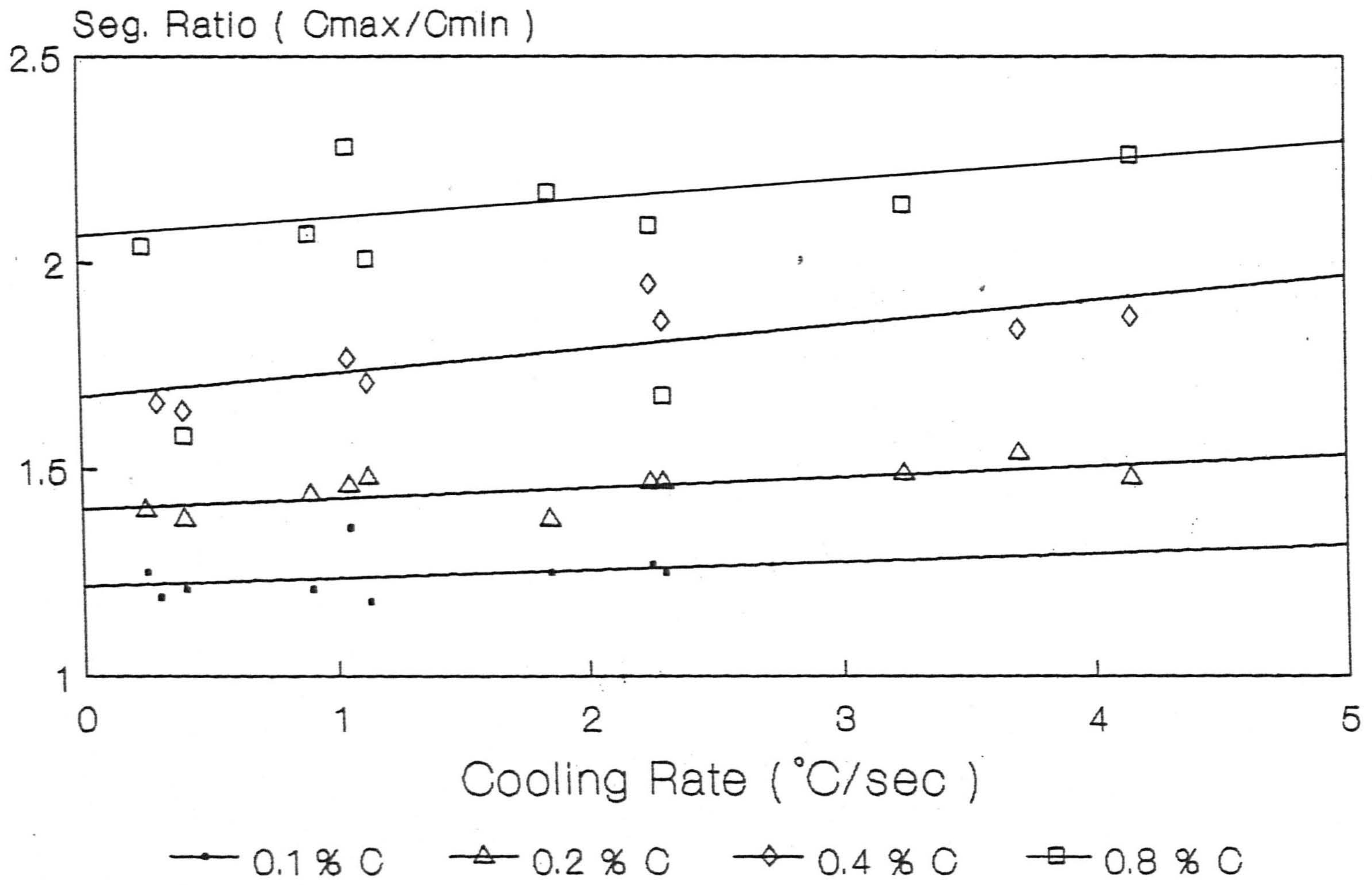
Seg. Ratio (Cmax/Cmin)
2.5
2
1.5
1
0
1
2
3
4
5
Cooling Rate (°C/sec)
0.1 % C
0.2 % C
0.4 % C
0.8 % C

1200°C

Colour concentration maps of primary arms at the different concentration range indicating the concave solidification points

Figure 80

0.8 % C - 1.6 Mn - Fe

Growth rate 1.5 mm/min

a) printed at low concentration range

b) printed at high concentration range

Figure 81

0.1 % C - 1.6 Mn - Fe

Growth rate 1.5 mm/min

a) printed at low concenration range

b) printed at high concentration range

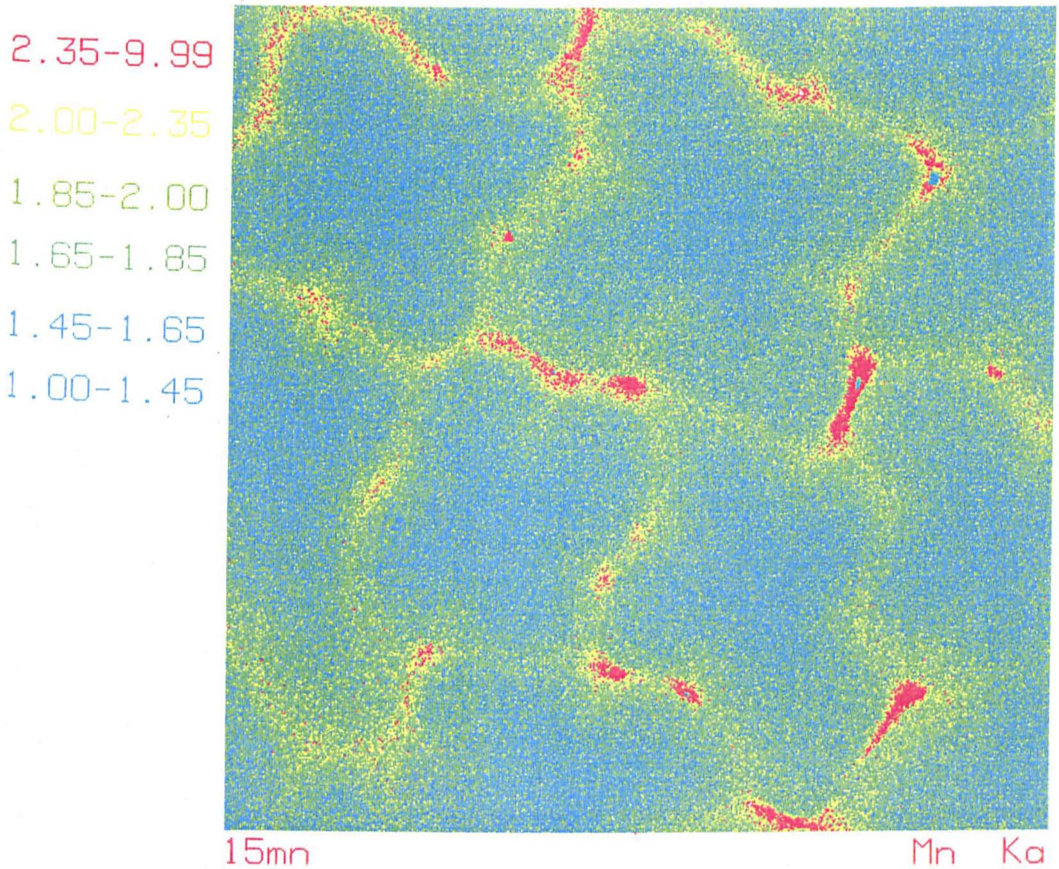
2.35-9.99
2.00-2.35
1.85-2.00
1.65-1.85
1.45-1.65
1.00-1.45
15mn
Mn Ka

(a)

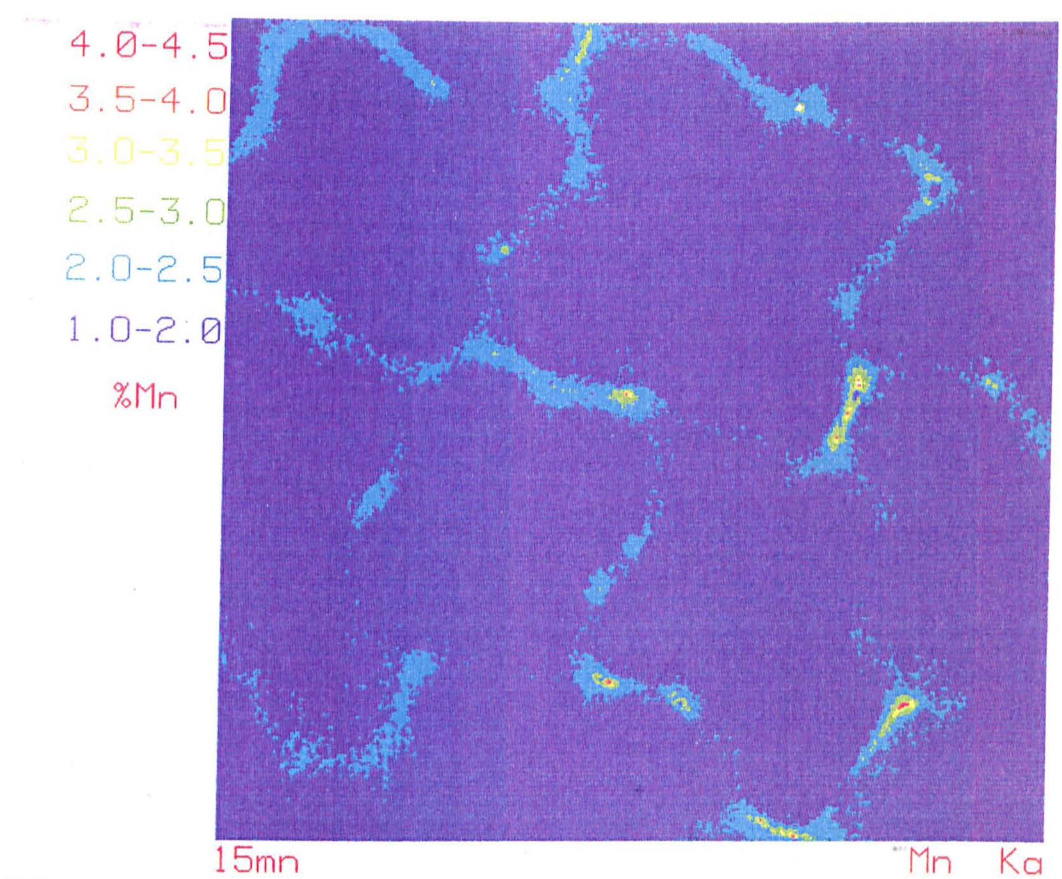
4.0-4.5
3.5-4.0
3.0-3.5
2.5-3.0
2.0-2.5
1.0-2.0
%Mn
15mn
Mn Ka
512x512 PIXELS
001024x001024μ

(b)

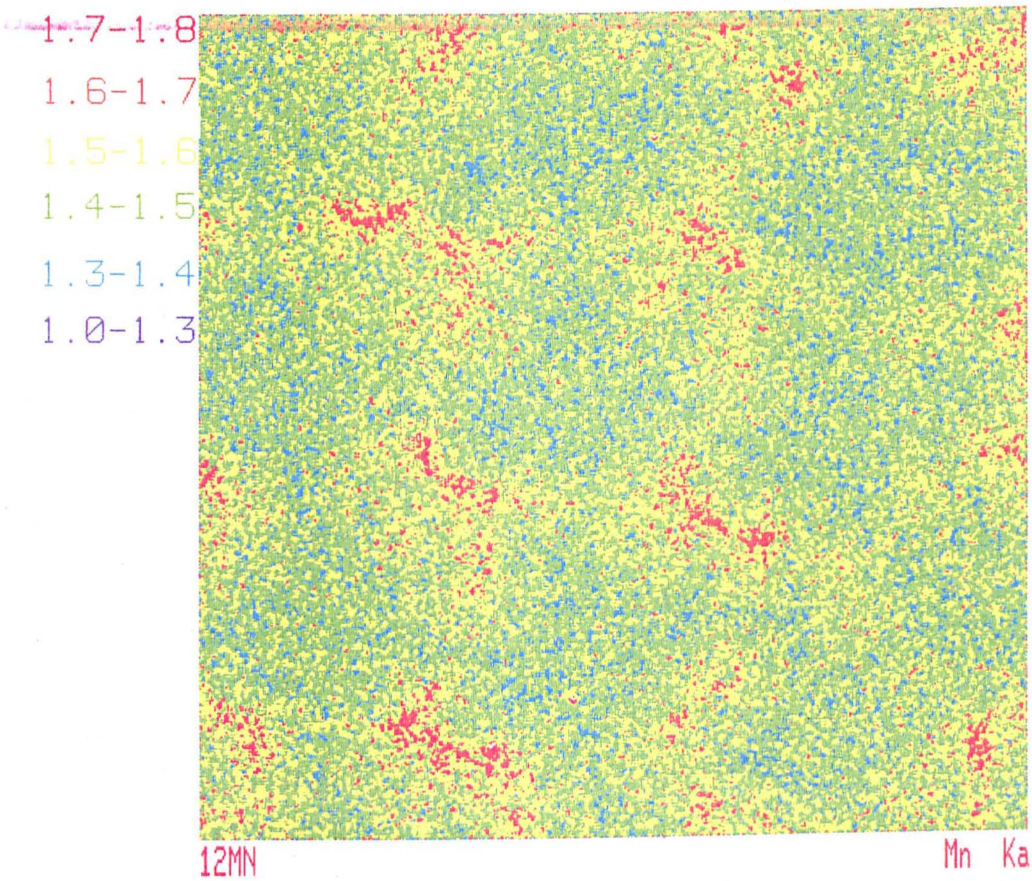
1.7-1.8
1.6-1.7
1.5-1.6
1.4-1.5
1.3-1.4
1.0-1.3
12MN
Mn Ka

(a)

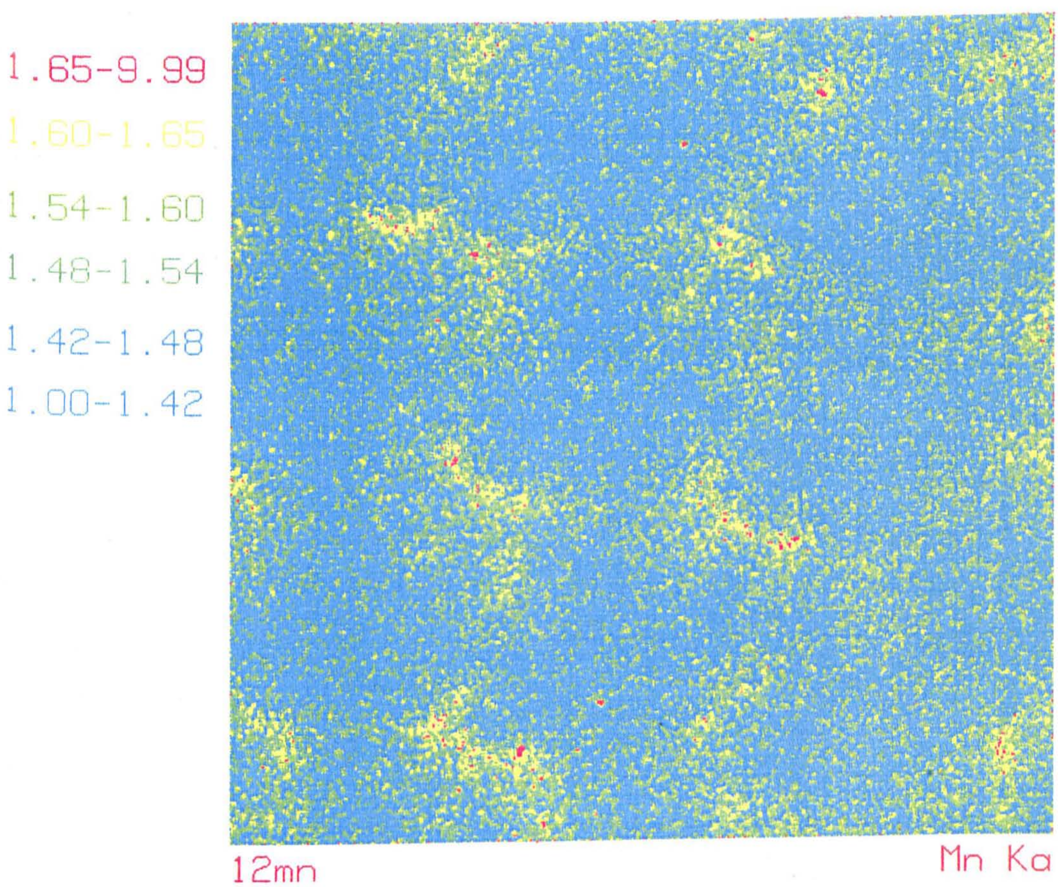
1.65-9.99
1.60-1.65
1.54-1.60
1.48-1.54
1.42-1.48
1.00-1.42
12mn
Mn Ka

(b)

Figure 82

Comparison of predicted maximum concentration of manganese by concave computer model to the experimental results as a function of cooling rate

0.8 % C - 1.6 % Mn - Fe

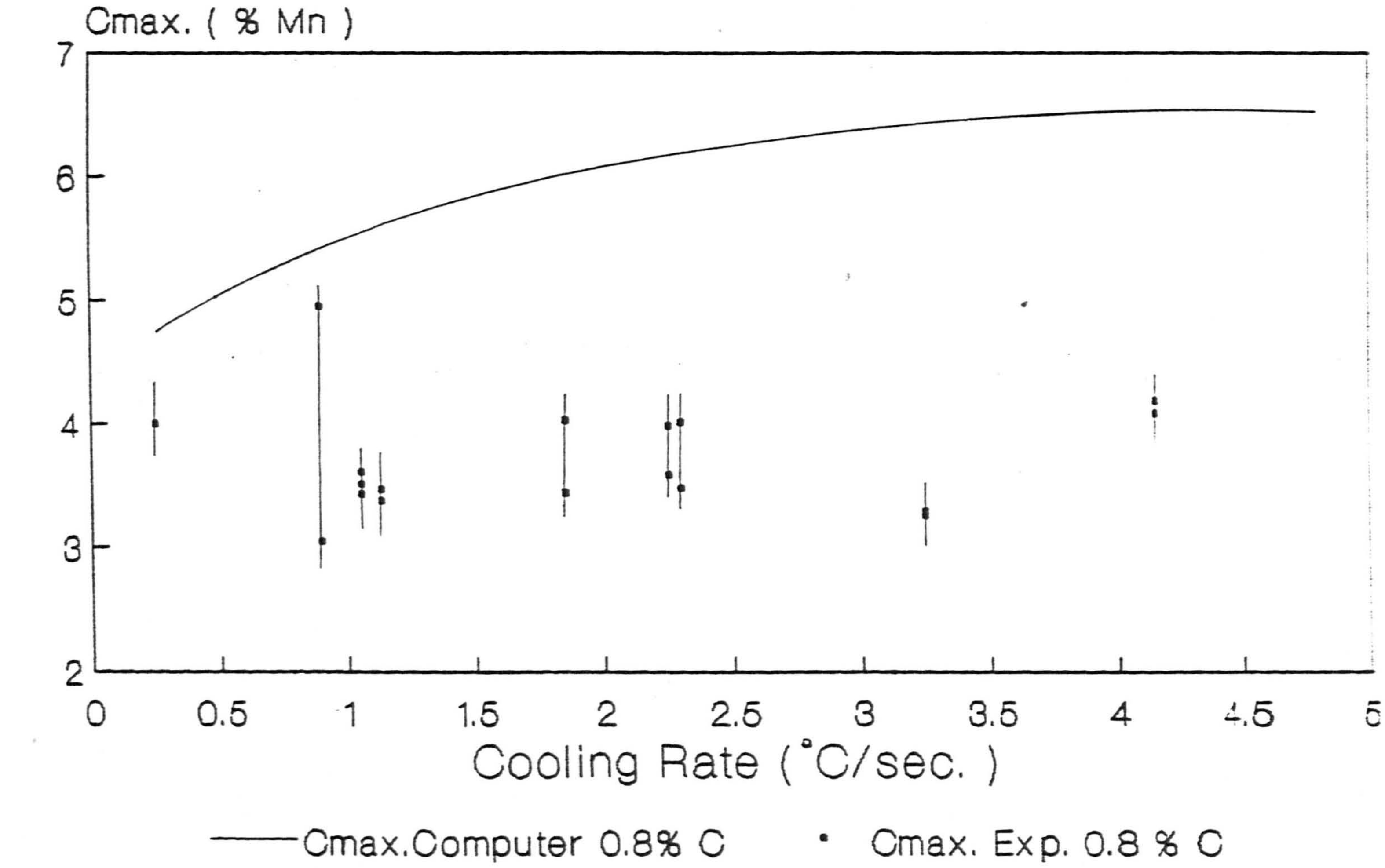
Cmax. (% Mn)
7
6
5
4
3
2
0
0.5
1
1.5
2
2.5
3
3.5
4
4.5
5
Cooling Rate (°C/sec.)
Cmax.Computer 0.8% C
Cmax. Exp. 0.8 % C

1200°C

Figure 83

The maximum concentration of manganese as a function of cooling rate for concave solidification points by comparing between primaries and secondaries

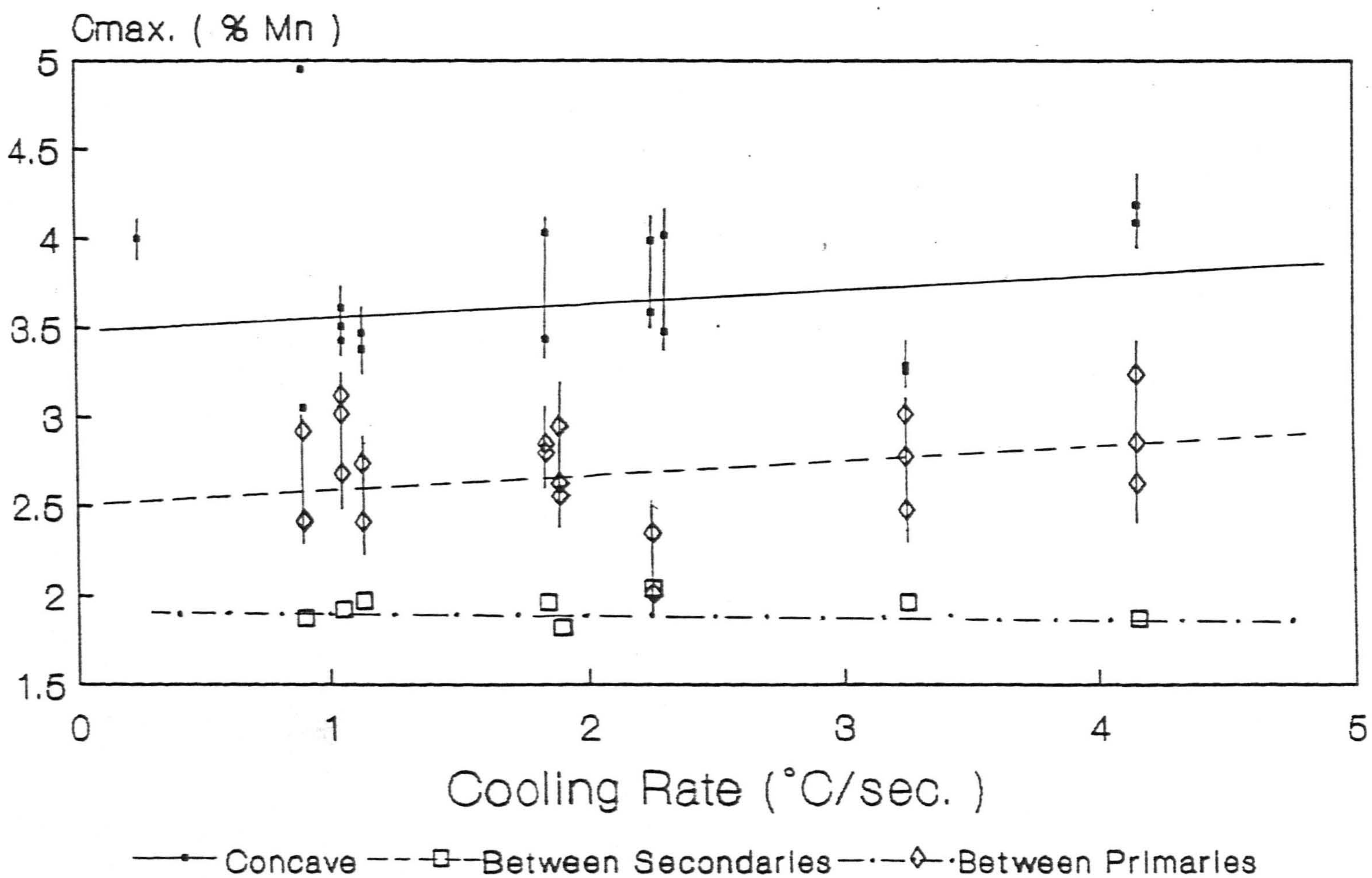

Cmax. (% Mn)
5
4.5
4
3.5
3
2.5
2
1.5
0
1
2
3
4
5
Cooling Rate (°C/sec.)
Concave
Between Secondaries
Between Primaries

0.8 % C - 1200°C

Figure 84

The segregation ratio for concave solidification points by comparing secondaries and primaries

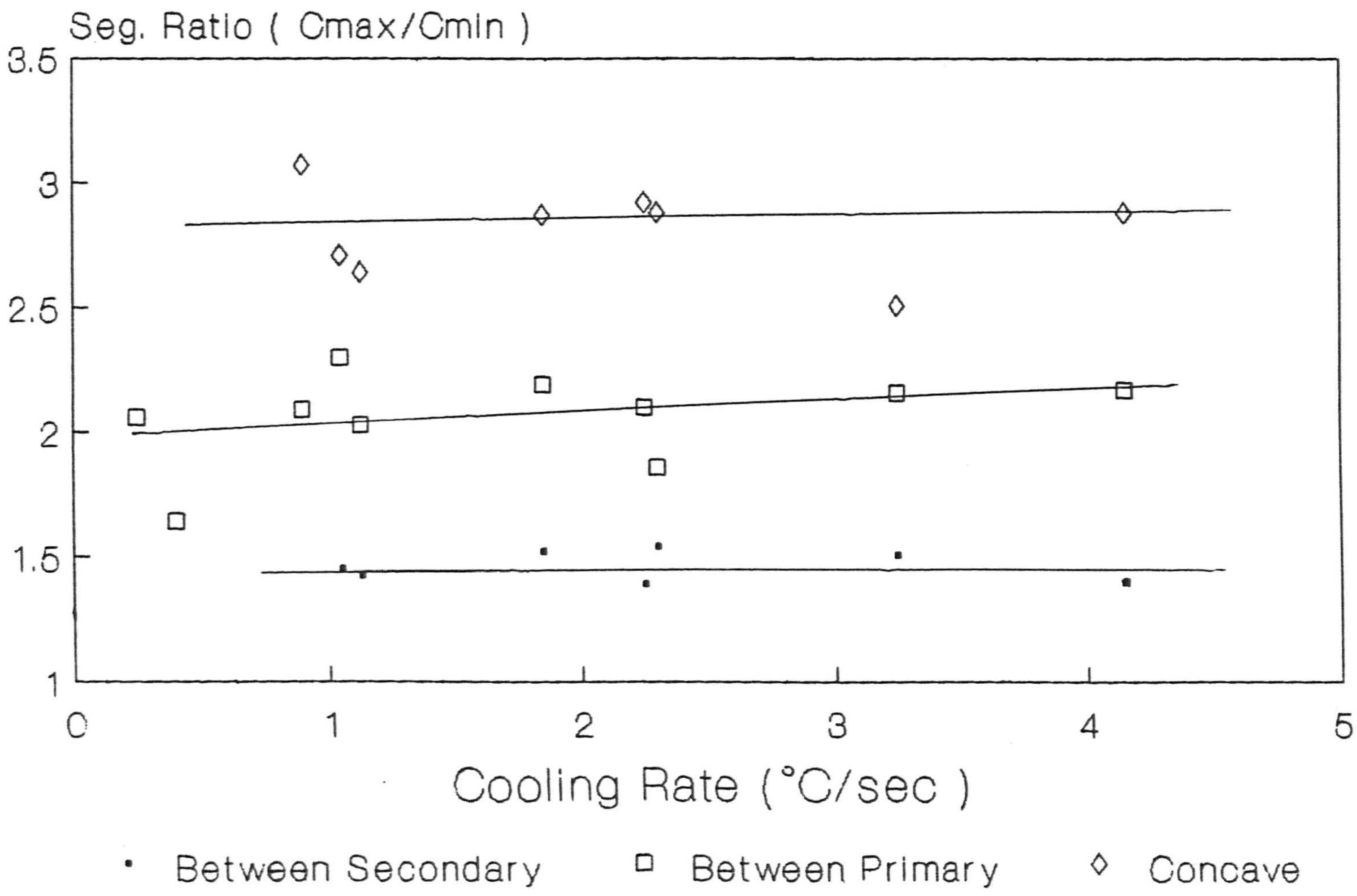
Seg. Ratio (Cmax/Cmin)
3.5
3
2.5
2
1.5
1
0
1
2
3
4
5
Cooling Rate (°C/sec)
Between Secondary
Between Primary
Concave

1200°C

Figure 85

Primary dendrite arm tip shows the beginning of segregation of manganese for 0.8 % C - 1.6 % Mn - Fe at 1.5 mm/min growth rate (mag. X 205)

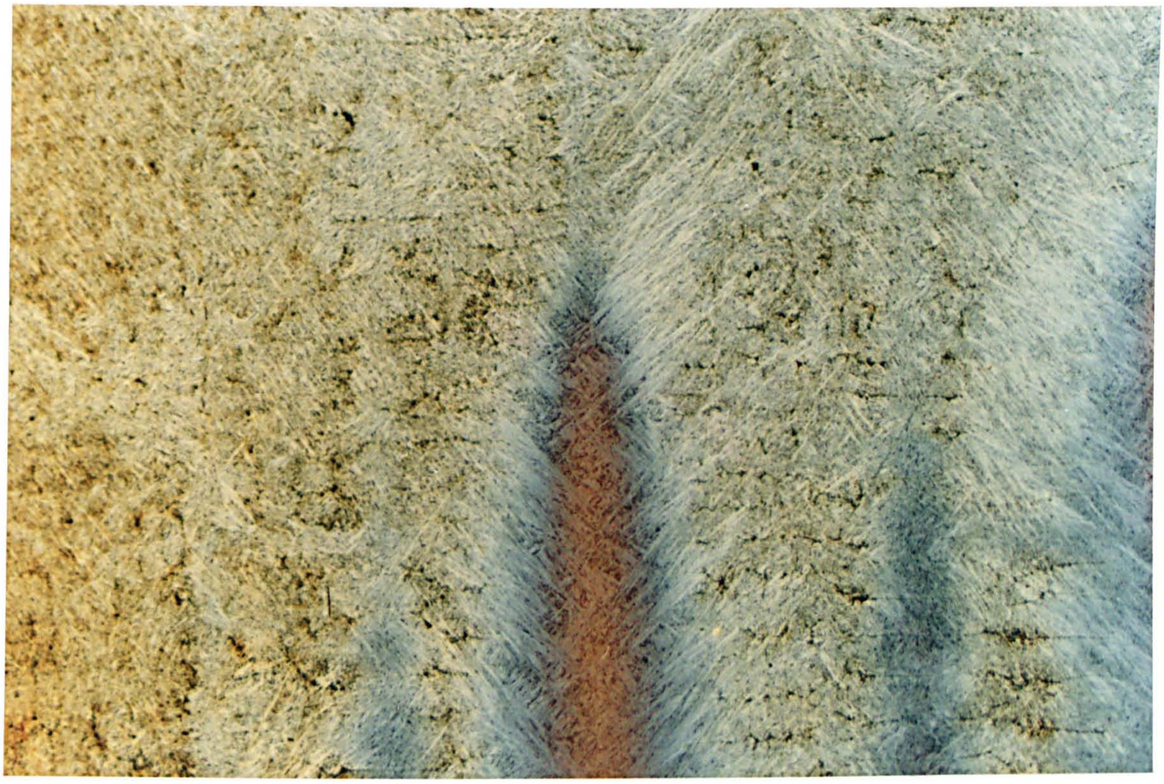

Figure 86

Electron micro probe concentration profile through the centre of primary dendrite tips as shown in the figure 85

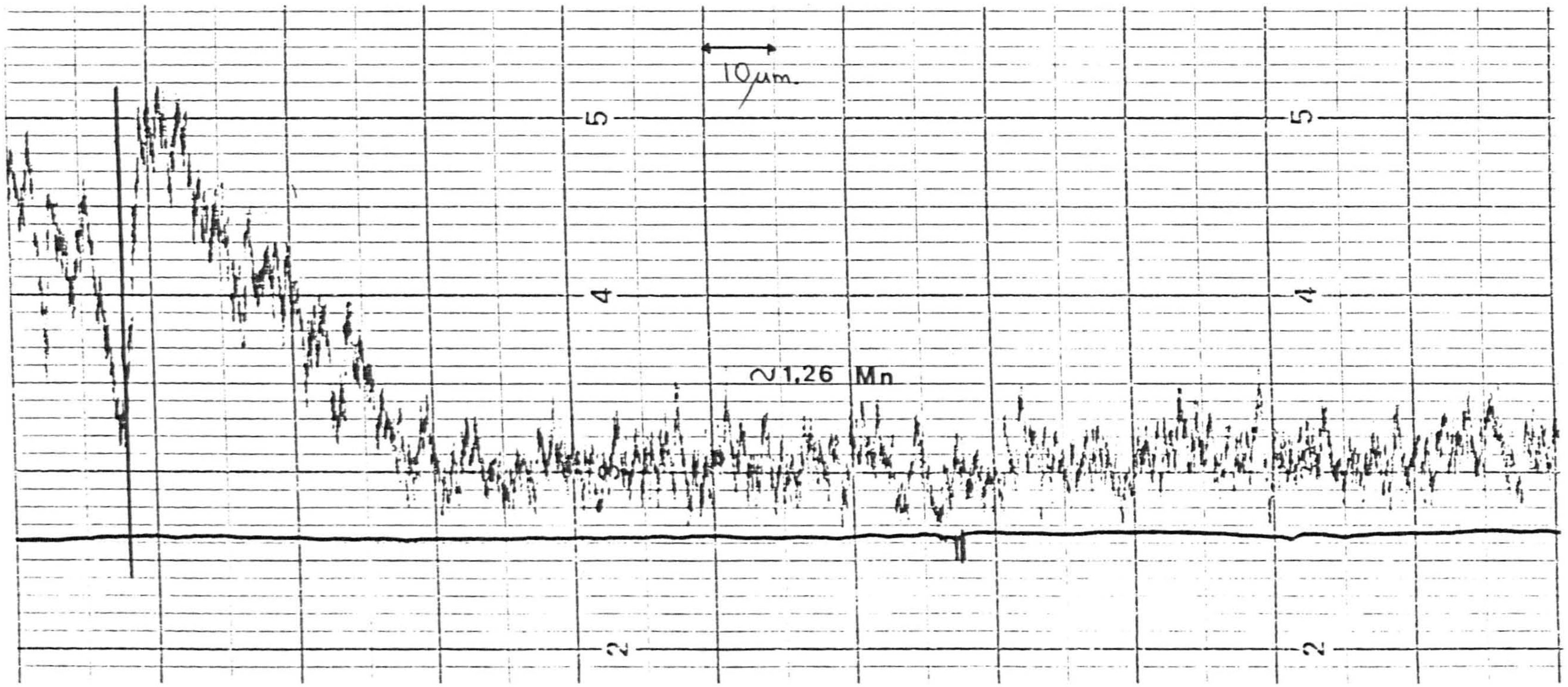

10μm
5
4
∿1,26 Mn
2

Figure 87

The effect of model variables in secondary arm coarsening model

a) effect of coarsening equation exponent

b) effect of coarsening equation pre-exponent

c) effect of diffusion coefficient

d) a comparison between dendrite arm coarsening model and constant arm model

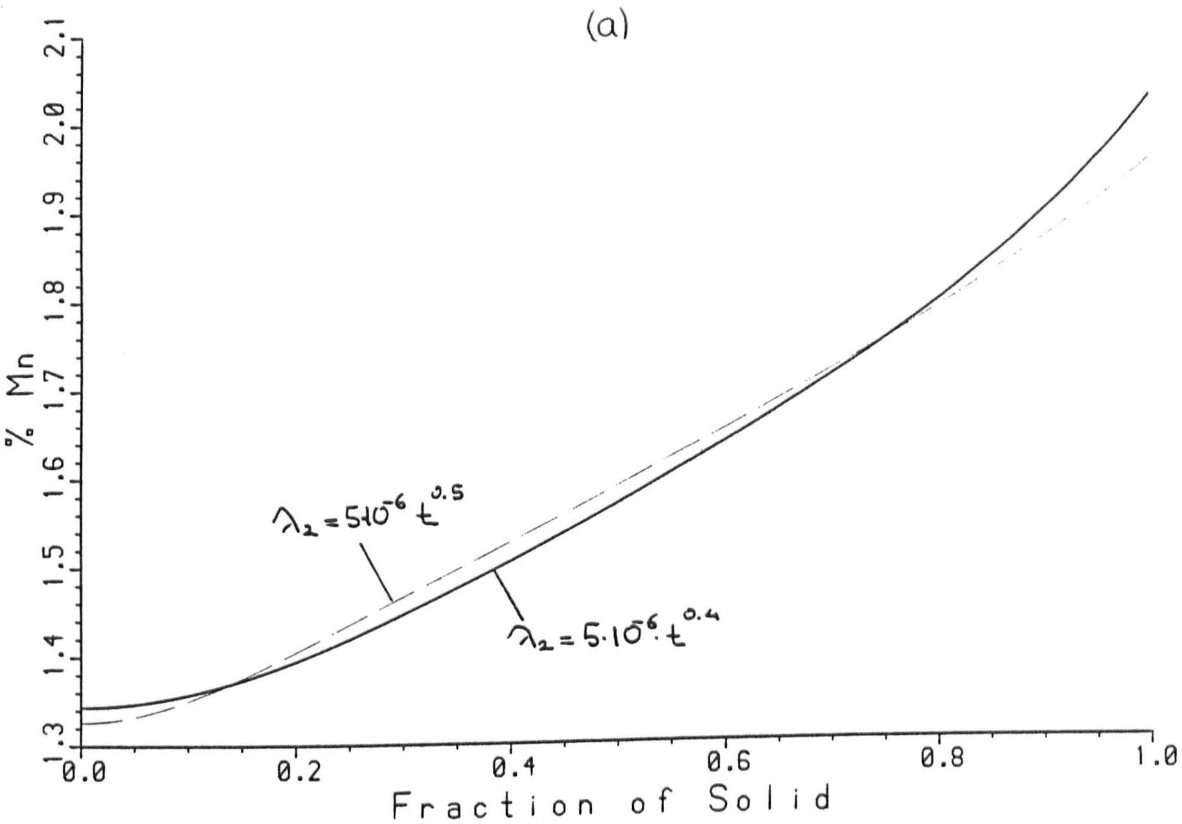
(a)
% Mn
Fraction of Solid
$\lambda_2 = 5\cdot10^{-6}\,t^{0.5}$
$\lambda_2 = 5\cdot10^{-6}\cdot t^{0.4}$

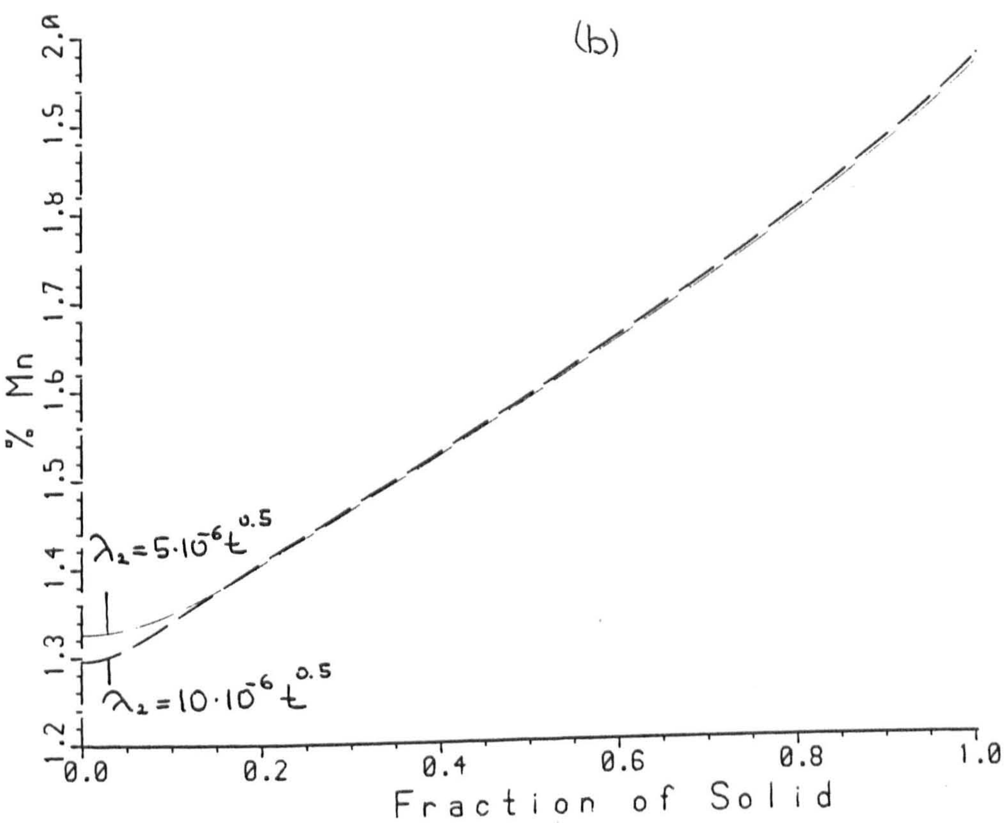
(b)
% Mn
Fraction of Solid
$\lambda_2 = 5\cdot10^{-6}\,t^{0.5}$
$\lambda_2 = 10\cdot10^{-6}\,t^{0.5}$

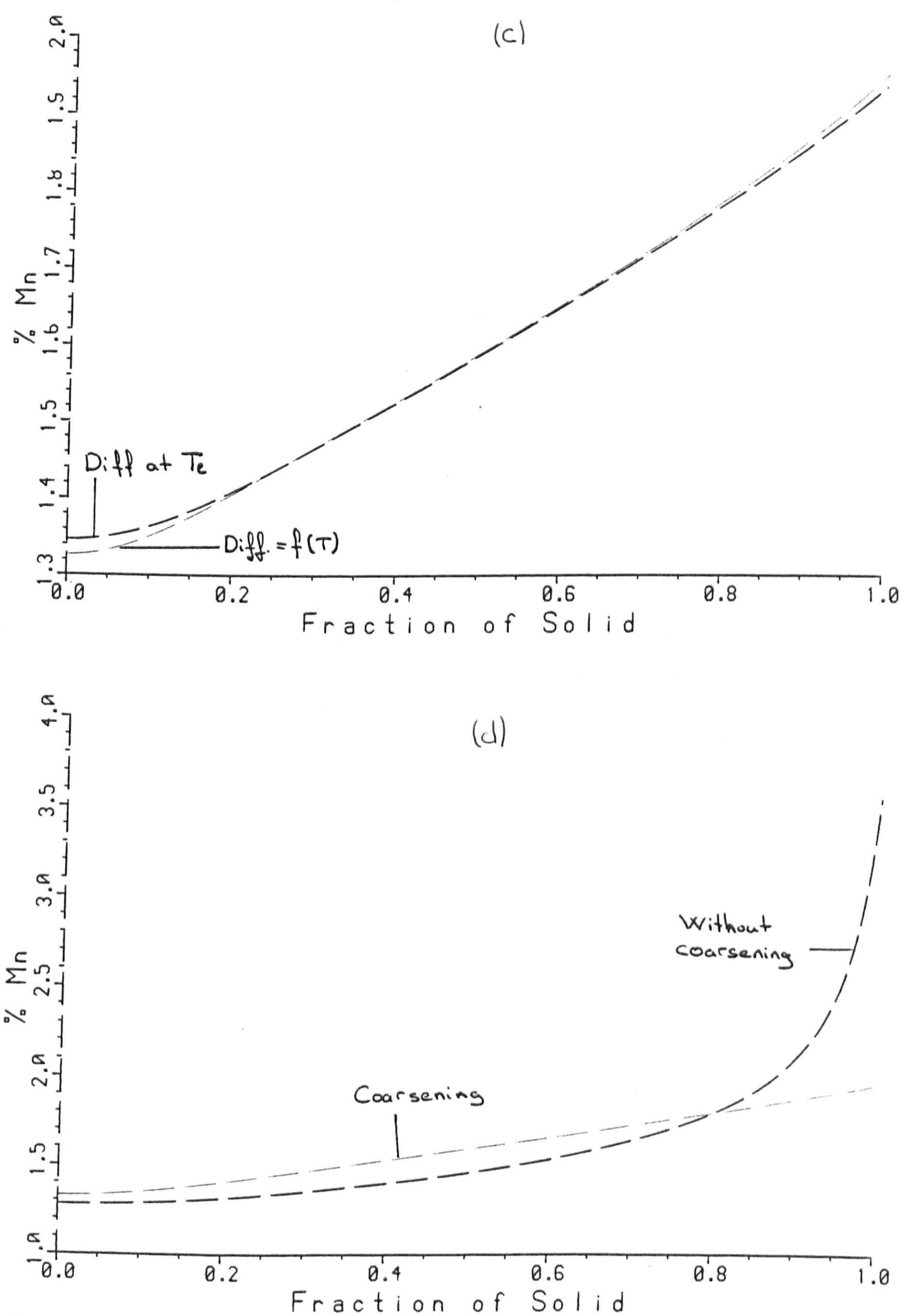

(c)
% Mn
Diff at Te
Diff. = f(T)
Fraction of Solid
0.0
0.2
0.4
0.6
0.8
1.0
(d)
% Mn
Without coarsening
Coarsening
Fraction of Solid
1.0
1.5
2.0
2.5
3.0
3.5
4.0

Figure 88

Secondary arm coarsening computer model prediction for 0.1 % C at the end of solidification for different coarsening rate

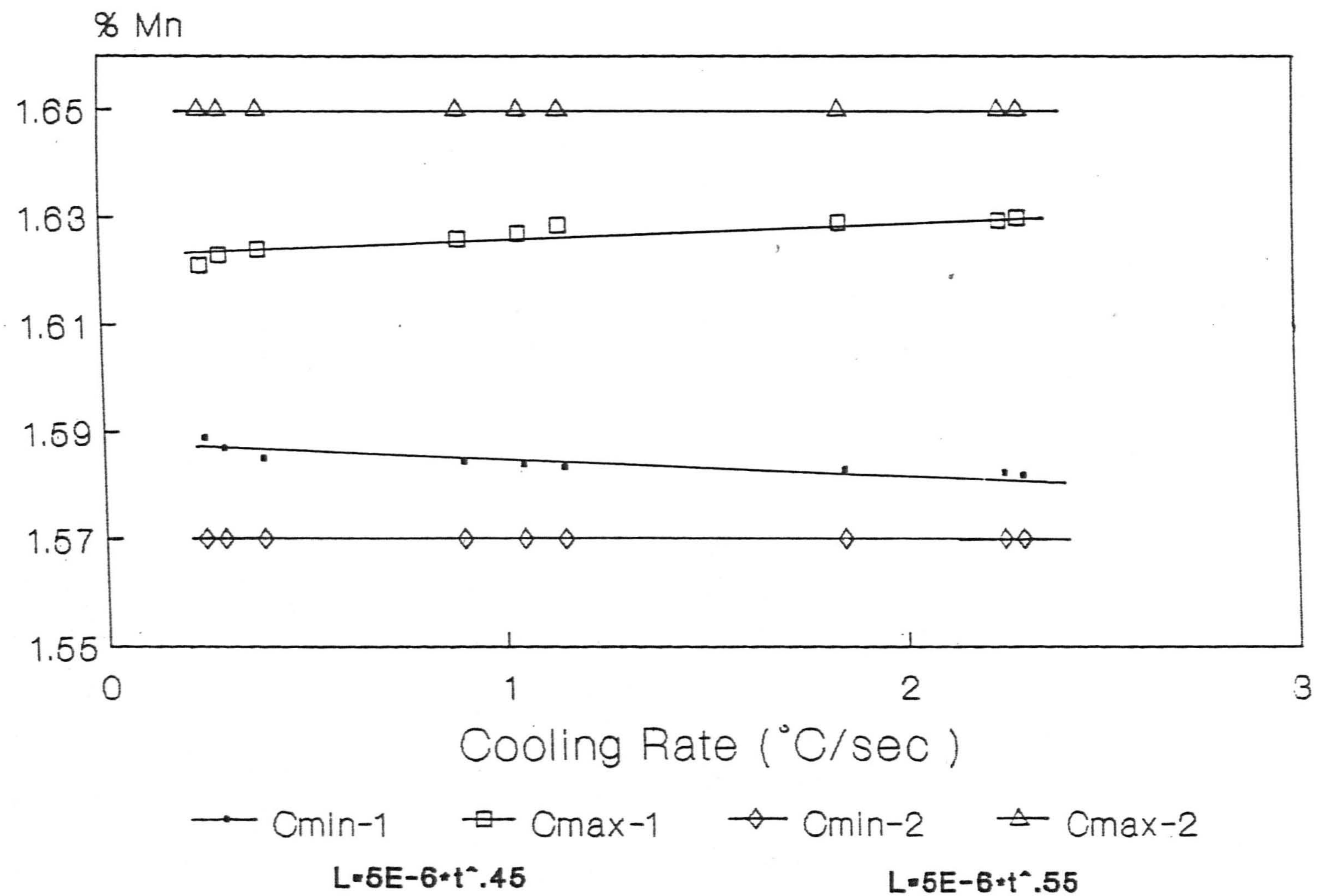
% Mn
1.65
1.63
1.61
1.59
1.57
1.55
0
1
2
3
Cooling Rate (°C/sec)
Cmin-1
Cmax-1
Cmin-2
Cmax-2
L=5E-6*t^.45
L=5E-6*t^.55

1485°C

Figure 89

Comparison of predicted segregation ratio for 0.1 % C at 1485 C and 0.4 % C and 0.8 % C at 1200 C with experimental results

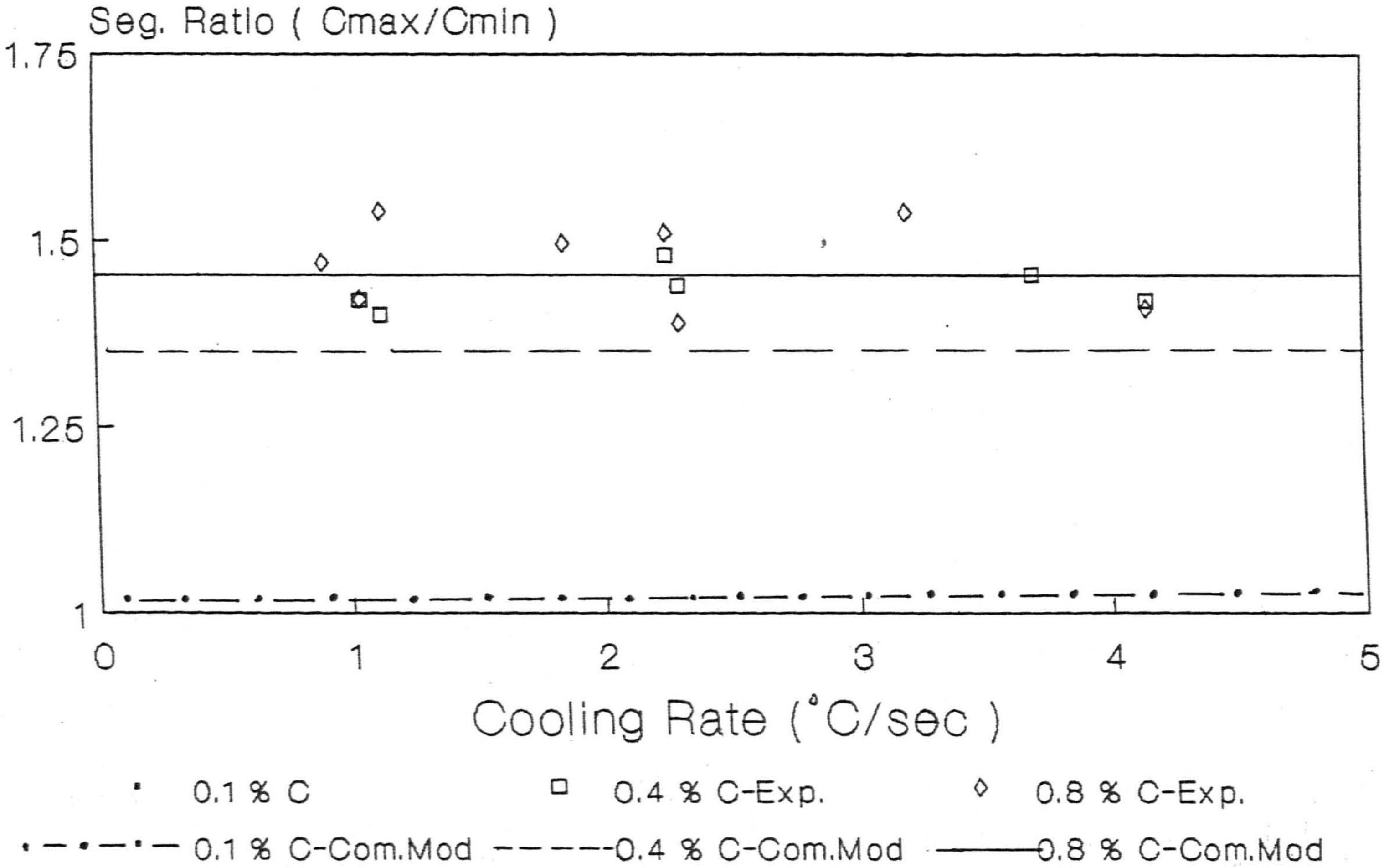
Seg. Ratio (Cmax/Cmin)
1.75
1.5
1.25
1
0
1
2
3
4
5
Cooling Rate (°C/sec)
0.1 % C
0.4 % C-Exp.
0.8 % C-Exp.
0.1 % C-Com.Mod
0.4 % C-Com.Mod
0.8 % C-Com.Mod

1200°C

Comparison of predicted segregation ratio and minimum concentration of manganese of 0.1 at 1485 C for different morphology of primary arms with experimental results

Figure 90 Seg. Ratio

Figure 91 Cmin.

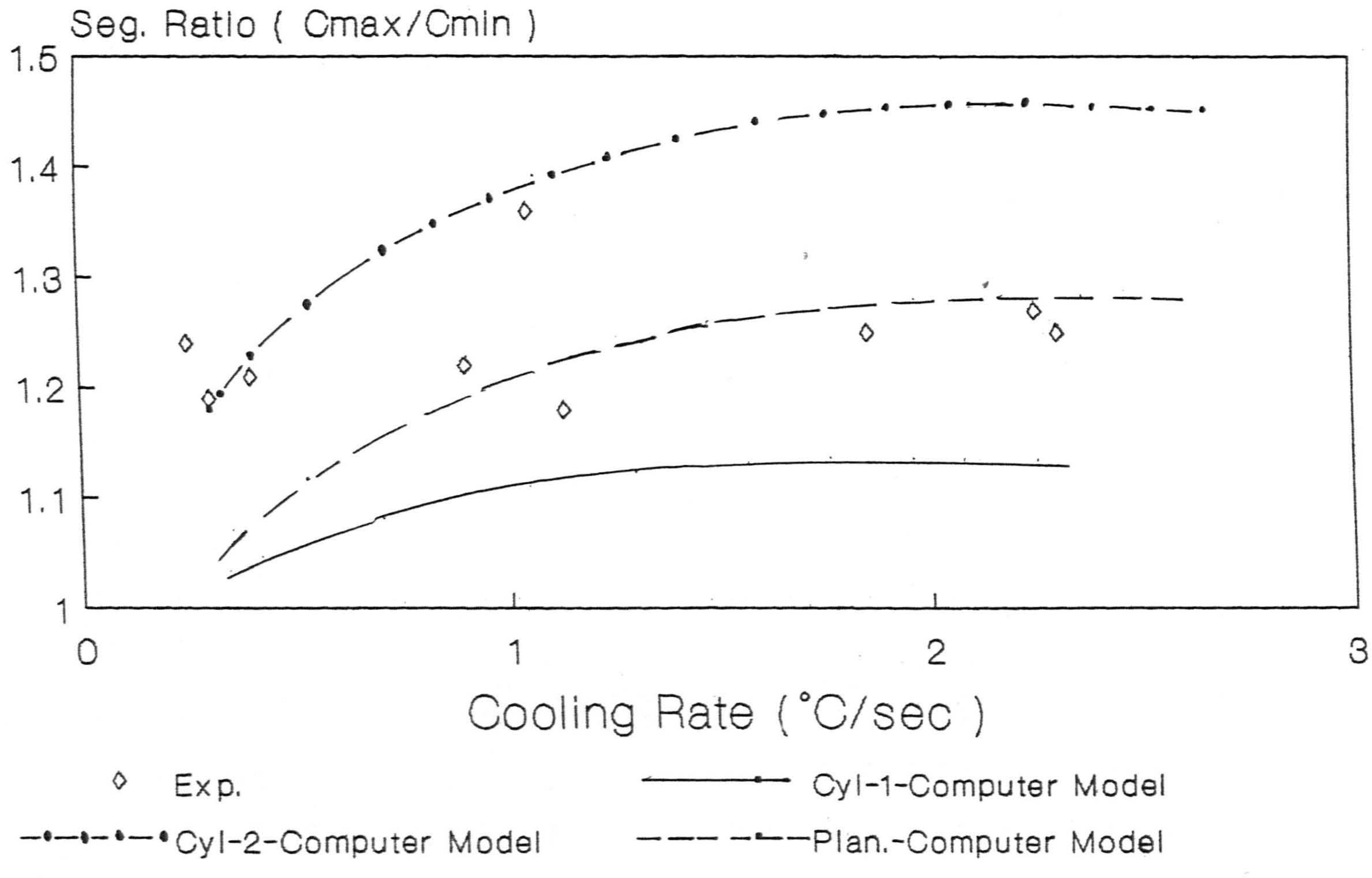
Seg. Ratio (Cmax/Cmin)
1.5
1.4
1.3
1.2
1.1
1
0
1
2
3
Cooling Rate (°C/sec)
Exp.
Cyl-1-Computer Model
Cyl-2-Computer Model
Plan.-Computer Model

1485°C - 0.1 % C

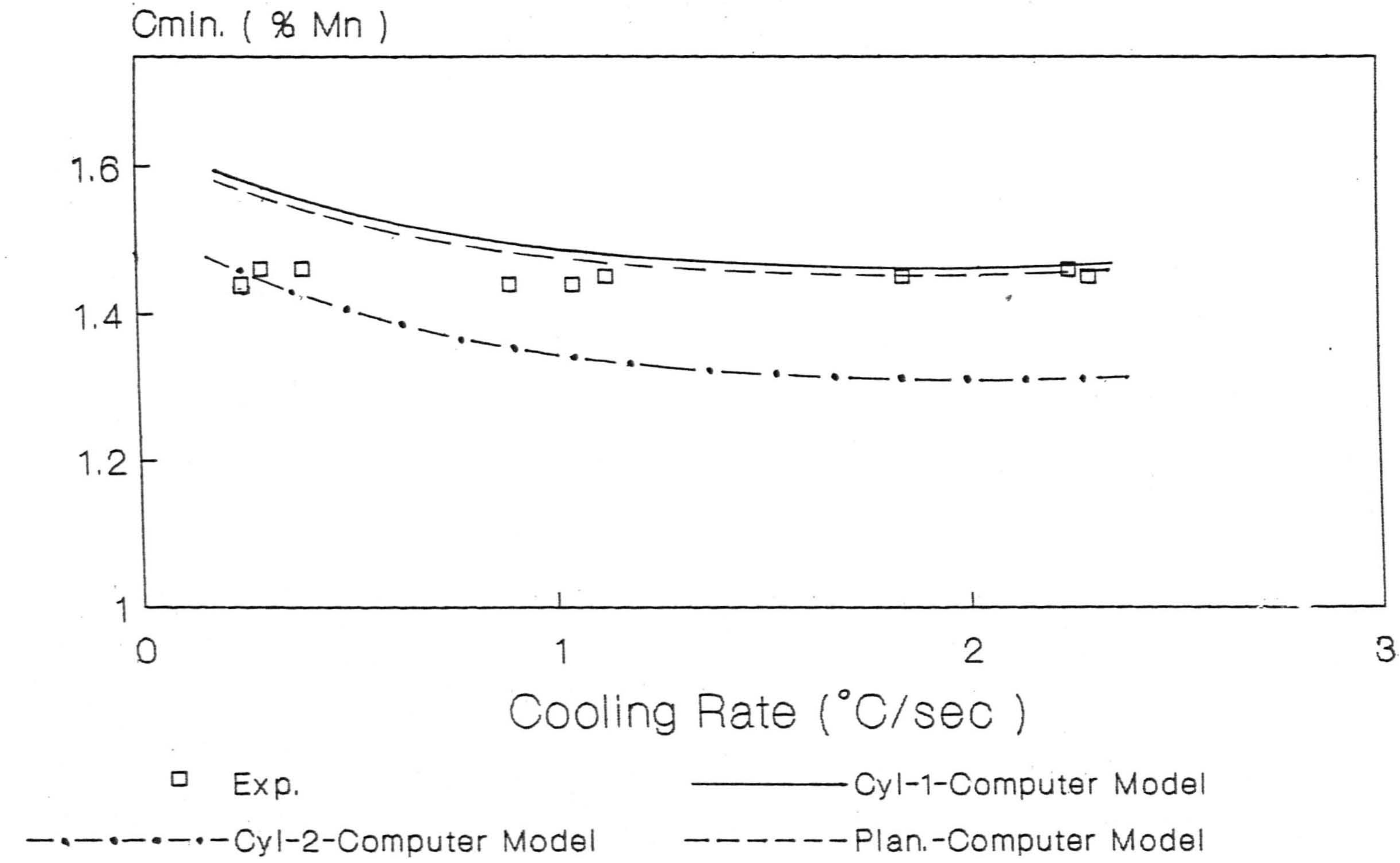
Cmin. (% Mn)
1.6
1.4
1.2
1
0
1
2
3
Cooling Rate (°C/sec)
Exp.
Cyl-1-Computer Model
Cyl-2-Computer Model
Plan.-Computer Model

1485°C - 0.1 % C

Comparison of predicted segregation ratio of different models for 0.4 % C and 0.8 % C at 1200 C with experimental results

Figure 92 for 0.8 % C

Figure 93 for 0.4 % C

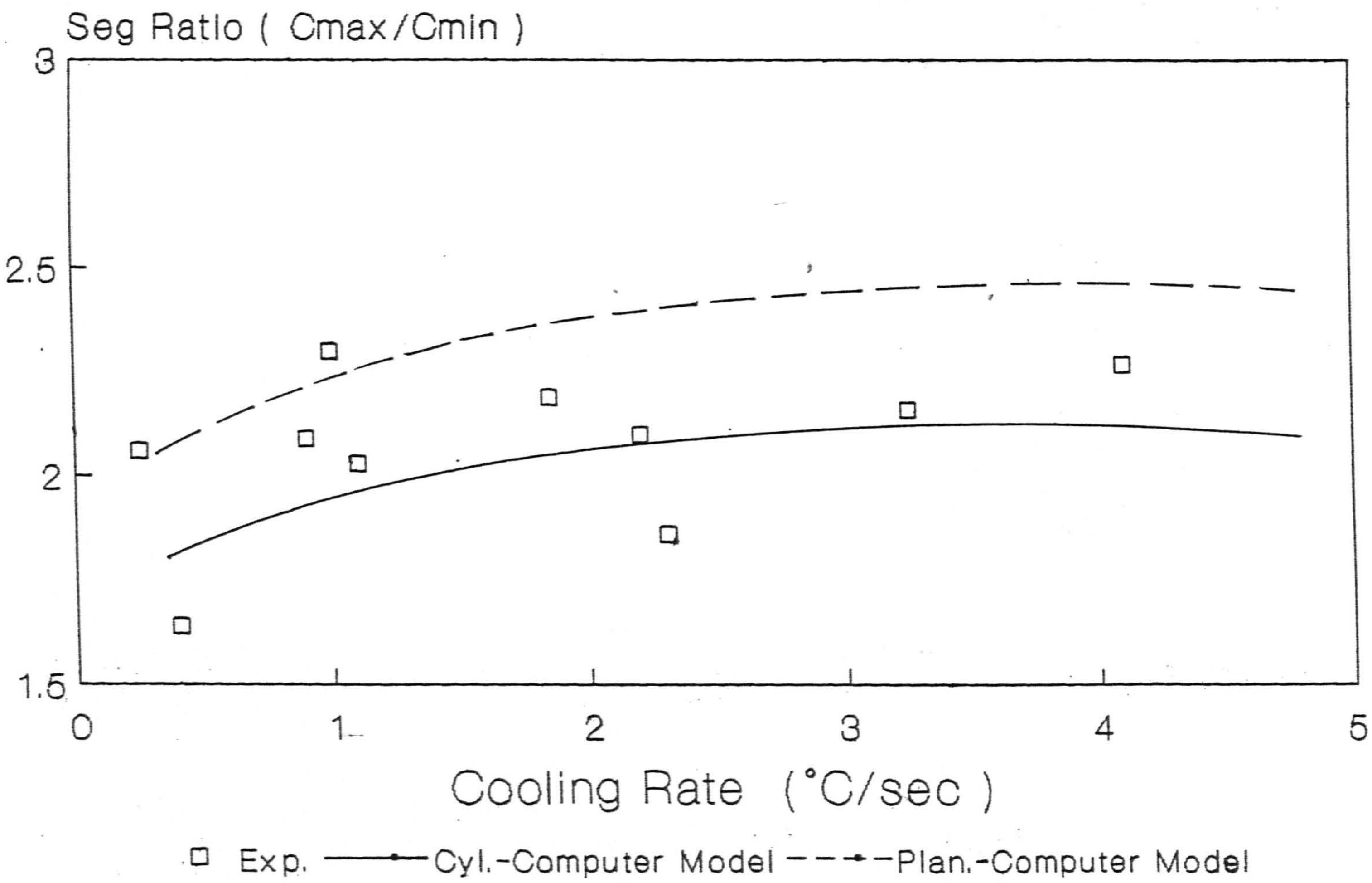

Seg Ratio (Cmax/Cmin)
3
2.5
2
1.5
0
1
2
3
4
5
Cooling Rate (°C/sec)
Exp.
Cyl.-Computer Model
Plan.-Computer Model

1200°C - 0.8 % C

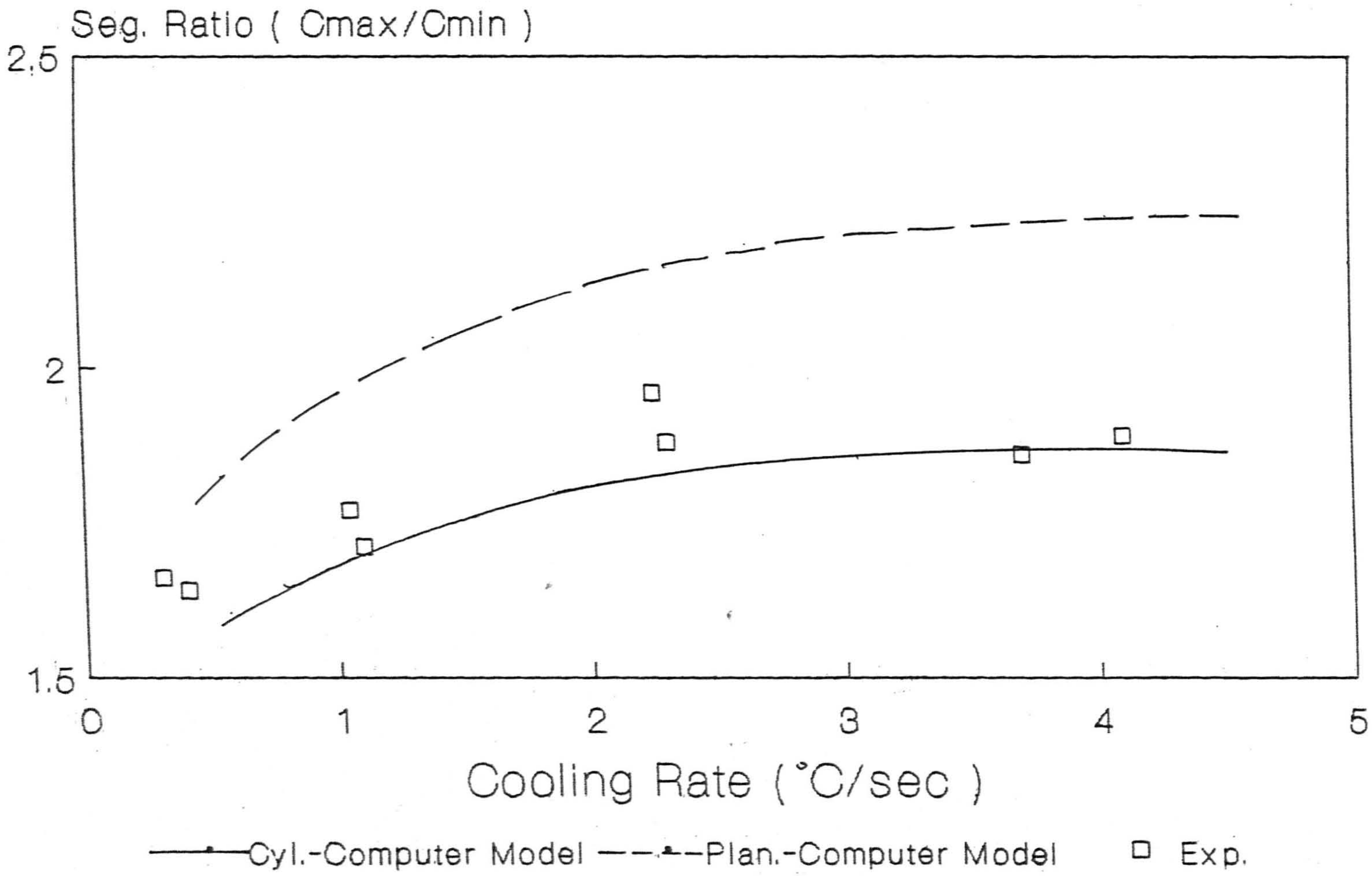

Seg. Ratio (Cmax/Cmin)
2.5
2
1.5
0
1
2
3
4
5
Cooling Rate (°C/sec)
Cyl.-Computer Model
Plan.-Computer Model
Exp.

1200°C - 0.4 % C

Figure 94

The residual segregation index as a function of temperature and time for 0.4 % C - 1.6 % C - Fe at the highest and lowest cooling rates

a) 0.30 C/sec - 0.4 % C

b) 4.15 C/sec - 0.4 % C

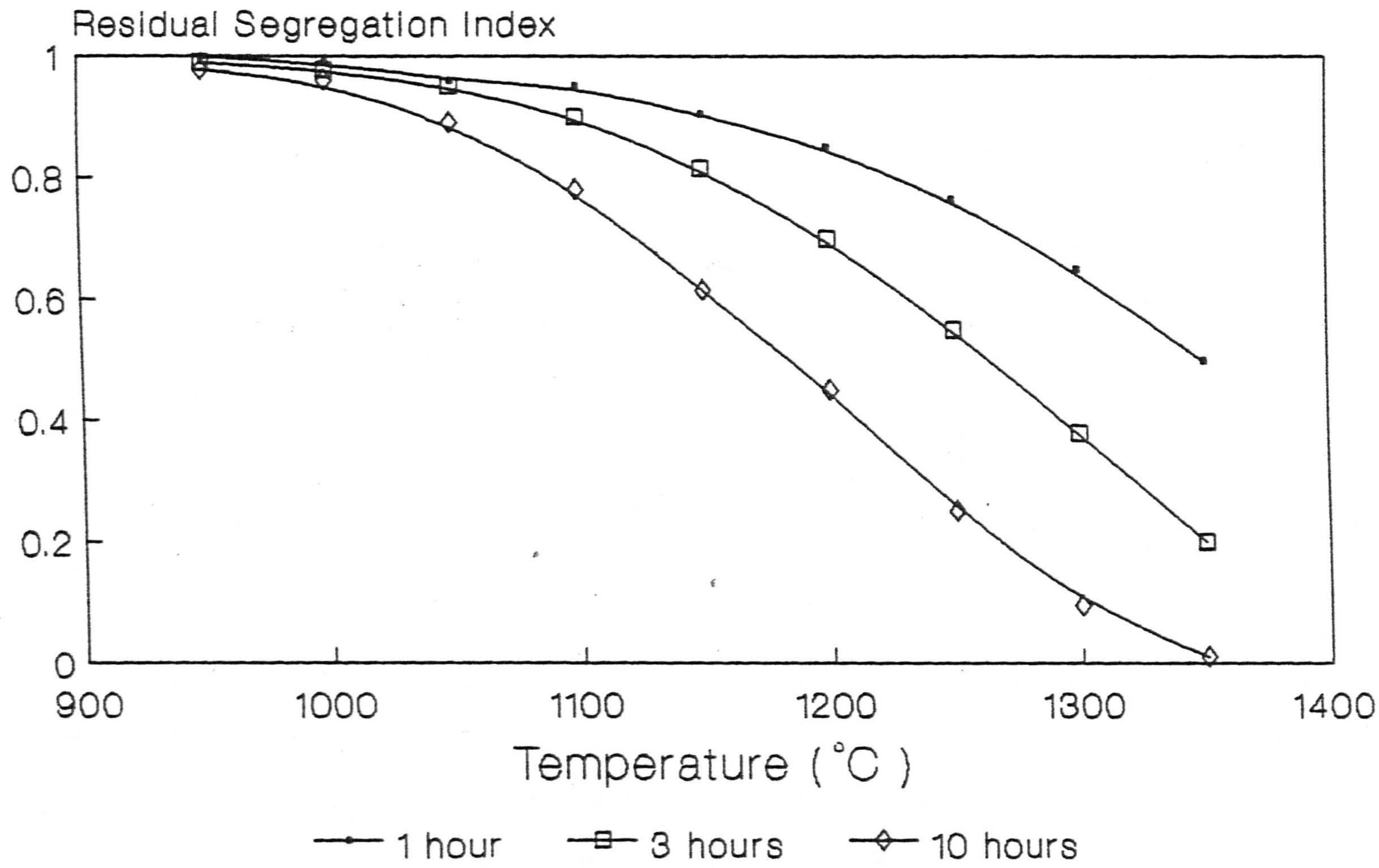

Cooling Rate 0.30°C/sec - 0.4 % C

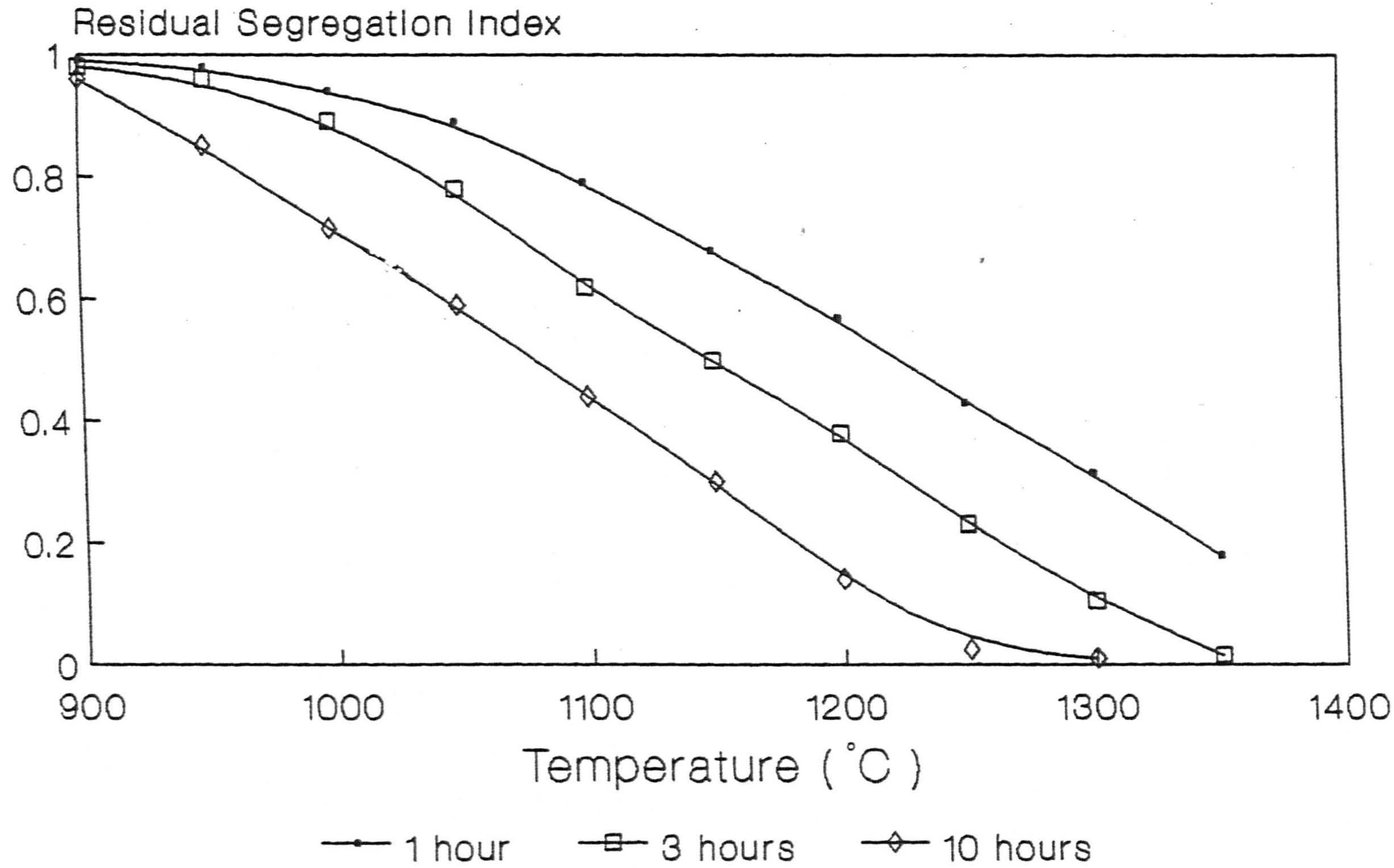

Cooling Rate 4.15 °C/sec - 0.4 % C

Figure 95

The change in the maximum and minimum concentration of manganese as a function of temperature during the solid state cooling at the 1.5 mm/min growth rate (0.25 C/sec cooling rate) for 0.8 % C

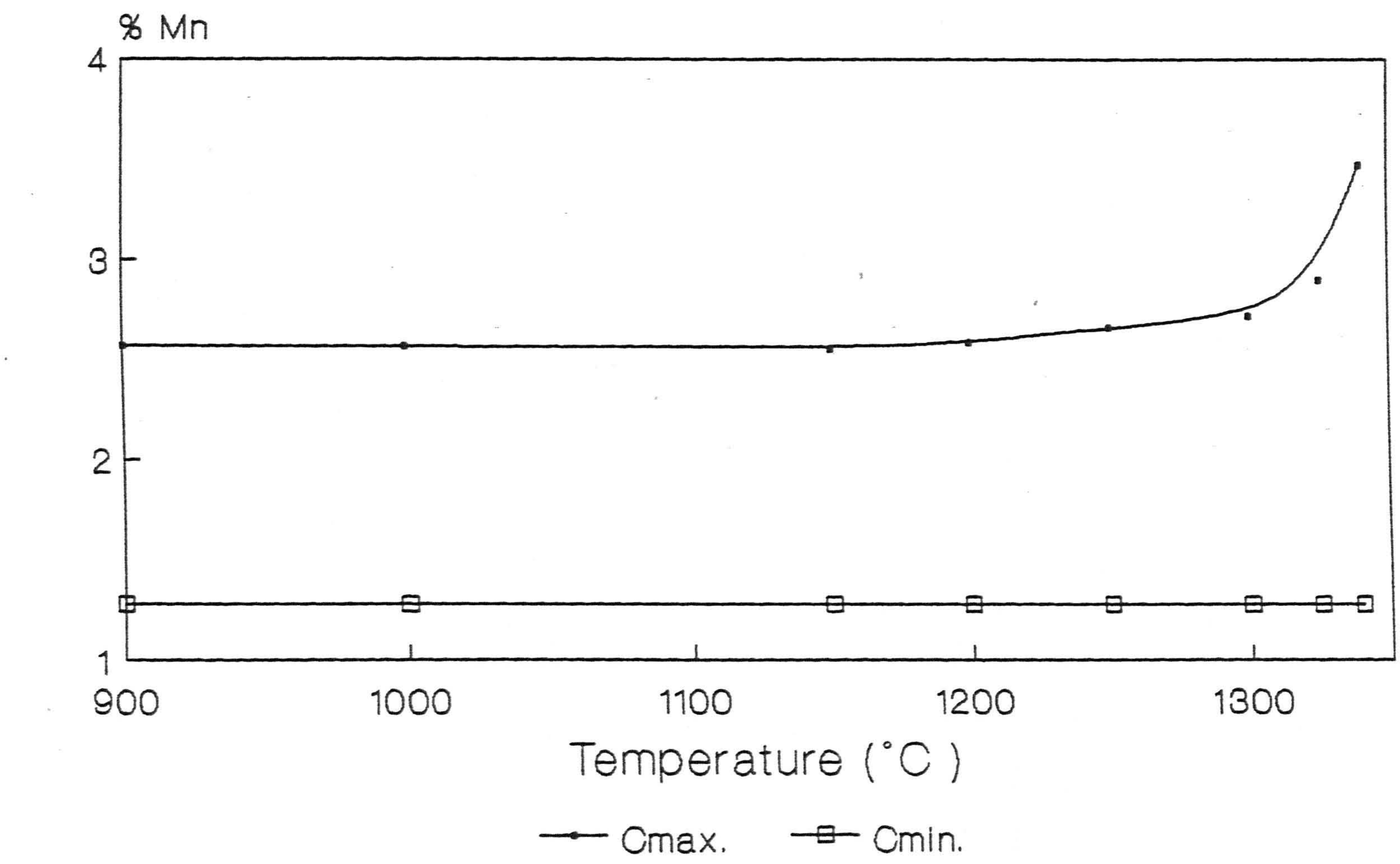

Cooling Rate 0.25°C/sec. - 0.8 % C

Figure 96

Average segregation ratio as a function of carbon content for primary arms and secondary arms

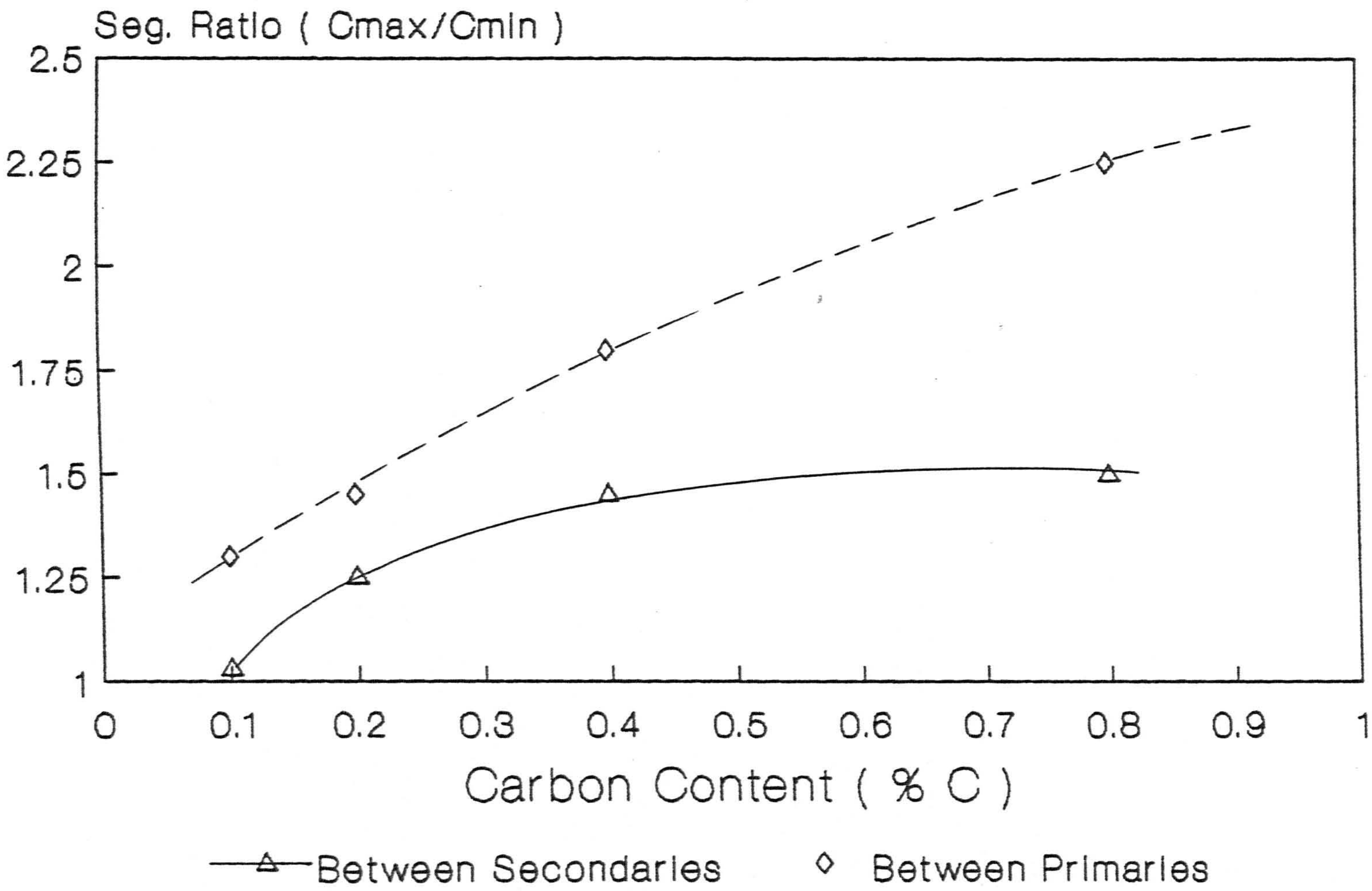

Seg. Ratio (Cmax/Cmin)
2.5
2.25
2
1.75
1.5
1.25
1
0
0.1
0.2
0.3
0.4
0.5
0.6
0.7
0.8
0.9
1
Carbon Content (% C)
Between Secondaries
Between Primaries